Hydrogeology of the Lower Cretaceous Edwards and Trinity Group Formations near Junction (Kimble County) Texas

by

Stephen Robert Allen, B.S.

Thesis

Presented to the Faculty of the Graduate School of
The University of Texas at Austin
in Partial Fulfillment
of the Requirements
for the Degree of

Master of Arts

THE UNIVERSITY OF TEXAS AT AUSTIN

May, 1997

Hydrogeology of the Lower Cretaceous Edwards and Trinity Group Formations near Junction (Kimble County) Texas

Approved by Supervising Committee:

Clark R. Wilson, Co-supervisor

Barry J. Hibbs, Co-supervisor

John M. Sharp

Acknowledgments

I wish to express my appreciation to the many individuals who provided guidance and support to me during this degree program. You have all in your own special way served as facilitators in the unfoldment of my potential. David Hill, Jun Liao, and Bruce Darling checked my answers to homework problems during the coursework phase. Jim Mayer, Jack Sharp, Clark Wilson, and Norman Van Broekhoven helped to clarify field interpretations of structure and stratigraphy. Philip Bennett allowed me to use his ion chromatography lab to perform analyses, and Todd Minehardt assisted by setting up the IC equipment and explaining the use of standards. Alan Fryar and Ian Jones answered questions I had on interpreting chemistry results. Leo Lynch volunteered his help by x-raying sediment samples to determine clay content. Barry Hibbs worked with me to get the numerical model set up and calibrated, and Robert Mace discussed how he resolved problems he encountered while using ground-water flow models. Erica Boghici checked the accuracy of my borehole log cross-sections. I was able to include color graphics in the thesis because I learned to use several software packages under the guidance of Reuben Reyes and Koko Kishi. Clark Wilson, Joel Davidow, Richard Weiland, and Tor Steineke edited the thesis. The final thesis review was performed mainly by Barry Hibbs who directed the research on a day to day basis. Larry Land, Peter Rose, Rene Barker, Jack Sharp, and Keith Young evaluated the proposed thesis goals and scope of work before activities were started. My thanks go to the individual landowners in the Junction, Texas area who allowed me to collect data on their properties. I'm especially indebted to O. C Fisher, former U. S. Congressman who allowed me to stay at his vacation house near London, Texas while I worked in the field.

Abstract

Hydrogeology of the Lower Cretaceous Edwards and Trinity Group Formations near Junction (Kimble County) Texas

by

Stephen Robert Allen, M.A.

The University of Texas at Austin, 1997

Co-supervisors: Clark R. Wilson, Barry J. Hibbs

This study describes ground-water flow in the Lower Cretaceous formations near Junction (Kimble County), Texas. Rock exposures were examined throughout the 150-mile study area to determine the nature and distribution of permeable features. Dominant features include nearly vertical fractures and horizontal bedding planes in carbonate rocks of the Edwards Group formations (Edwards), and coarse-grained fluvial channel deposits in the underlying Hensel Sand Formation (Hensel). Static water levels were measured in over one hundred wells and contoured to reveal the existence of two separate potentiometric surfaces, one overlying the other. Preliminary, but useful estimates of transmissivity, hydraulic conductivity, and ground-water velocity were derived using specific capacities from eighty-three wells completed in both the upper (Edwards) and lower (Hensel) aquifers.

At the edge of the Edwards Plateau where the contact between the Edwards and the Hensel is exposed on the face of the erosional escarpment, ground water discharges from the Edwards aquifer through numerous low volume springs

and seeps. An even greater proportion of ground-water discharge leaks from the Edwards aquifer to the underlying Hensel aquifer across a thin low permeability bed at the base of the Edwards which consists of marly, unfractured, nodular limestone. The sum of these two components of discharge is approximately equal to precipitation recharge to the Edwards.

To gain additional insight into cross-formational flow an analysis of major and minor ions, redox potential, and dissolved oxygen was conducted for twenty-one water wells which were located along three north-south (inferred flow direction) transects. The Edwards waters were found to be a Ca-Mg-HCO_3 facies; the Hensel waters, a mixed facies. This difference in hydrochemical facies was initially thought to be caused by ion evolution along flowpaths, but it more likely reflects the existence of a regional aquifer below a locally constrained aquifer. High values of dissolved oxygen and redox potential in the Edwards aquifer indicate that recharge is predominant; lower values of these parameters in the Hensel aquifer indicate that this water occurs in an intermediate or discharge zone.

To test the conceptual model of steady-state ground-water flow, a numerical model was constructed using the MODFLOW finite-difference computer code. Over one hundred trial and error simulations were executed to calculate leakage through the confining bed, discharge from springs, and discharge to the Llano River. In addition, the distribution and magnitude of focused recharge to the Edwards aquifer was calculated, estimates were made for unknown hydrogeologic parameters, and the Edwards aquifer was demonstrated to be fully perched above the Hensel aquifer.

The increased understanding of the ground-water flow regime resulting from this study will support range management activities and improve the success rate of water well drilling.

Table of Contents

Acknowledgments		iii
Abstract		iv
Table of Contents		vi
Introduction and Geology		1
Methods and Data		36
Results of Field Observations and Water Chemistry Analyses		43
Conceptual Model of Ground-Water Flow		73
Mathematical Model of Ground-Water Flow		81
Conclusions		110
Appendices		114
Appendix A	Water chemistry sampling and analysis procedures	115
Appendix B	Rainfall record	119
Appendix C	Descriptions of soil types	121
Appendix D	Table of water levels in wells	123
Appendix E	Specific capacity and transmissivity calculations	128
Appendix F	Aquifer recharge calculation	132
Appendix G	Table of water chemistry values	136
Bibliography		145
Vita		155

Introduction and Geology

Research objectives and scope of work

This study describes the ground-water flow regime in a 390 square km (150-square mile) area at the edge of the Edwards Plateau in Kimble County, Texas. Along this escarpment the Lower Cretaceous Fort Terrett and Segovia Formations of the Edwards Group (Edwards) and the underlying Hensel Sand Formation (Hensel) of the Trinity Group are exposed. The study resulted in the development of a conceptual model which describes recharge, discharge, head-dependent flux through a thin low-permeability bed between two aquifers, and flow within the saturated zone. The model explains how hydrogeologic inputs, throughputs, and outputs are controlled by stratigraphy, structure, and topography.

Fieldwork consisted, first, in measuring the water levels in 112 wells to produce potentiometric surface maps. Next, the water from twenty-one of the wells was analyzed for major ions, minor ions, unstable indicator parameters. These two sources of data guided the mapping of recharge and discharge areas, and supported the hypothesis of two separate aquifers.

The finite-difference program MODFLOW (McDonald and Harbaugh, 1984) was used to create a quasi three-dimensional, steady-state model for the purposes of visualizing the ground-water flow regime, testing the validity of assumptions used to construct the conceptual model, and verifying and adjusting estimated hydrogeologic parameter values.

Location and physiography

The study area lies between north latitudes 30° 30' and 30° 42' 30", and west latitudes 99° 35' and 99° 50', at the eastern edge of the Edwards Plateau in Kimble County, Texas (Figure 1). It is located 210 km (130 miles) west of Austin and 177 km (110 miles) northwest of San Antonio. Surface geology and major physiographic features are shown in Figure 2. The edge of the plateau is represented by an erosional escarpment having an average relief of approximately 60 meters (200 feet) (Figures 3 and 4). This escarpment extends across the center of the study area and strongly influences the ground-water flow regime. Its existence has the effect of separating the study area into two distinct physiographic regions: a highly dissected, horizontally bedded carbonate upland composed of the Lower Cretaceous Edwards (Figures 5 and 6); and, the Llano River floodplain, which is veneered with alluvium atop the siltstone, sandstone, and conglomerate of the Lower Cretaceous Hensel (Figure 7). Relief ranges from 713 meters (2,340 feet) at the topographic divide to 475 meters (1,560 feet) at the lower (eastern) end of the Llano River.

Significance of the study

This study investigates the physical and chemical hydrogeology in the Junction, Texas area. It provides a framework from which to understand cross-formational flow and the origin and distribution of solutes. The increased knowledge of aquifer quality, storage and capacity can also be used by landowners to exploit this limited resource more effectively.

Physical hydrogeology

Two separate potentiometric surfaces were drawn from water levels measured in wells that were located throughout the study area. These potentiometric surface maps, when overlayed by the topographic map, will establish depths to the

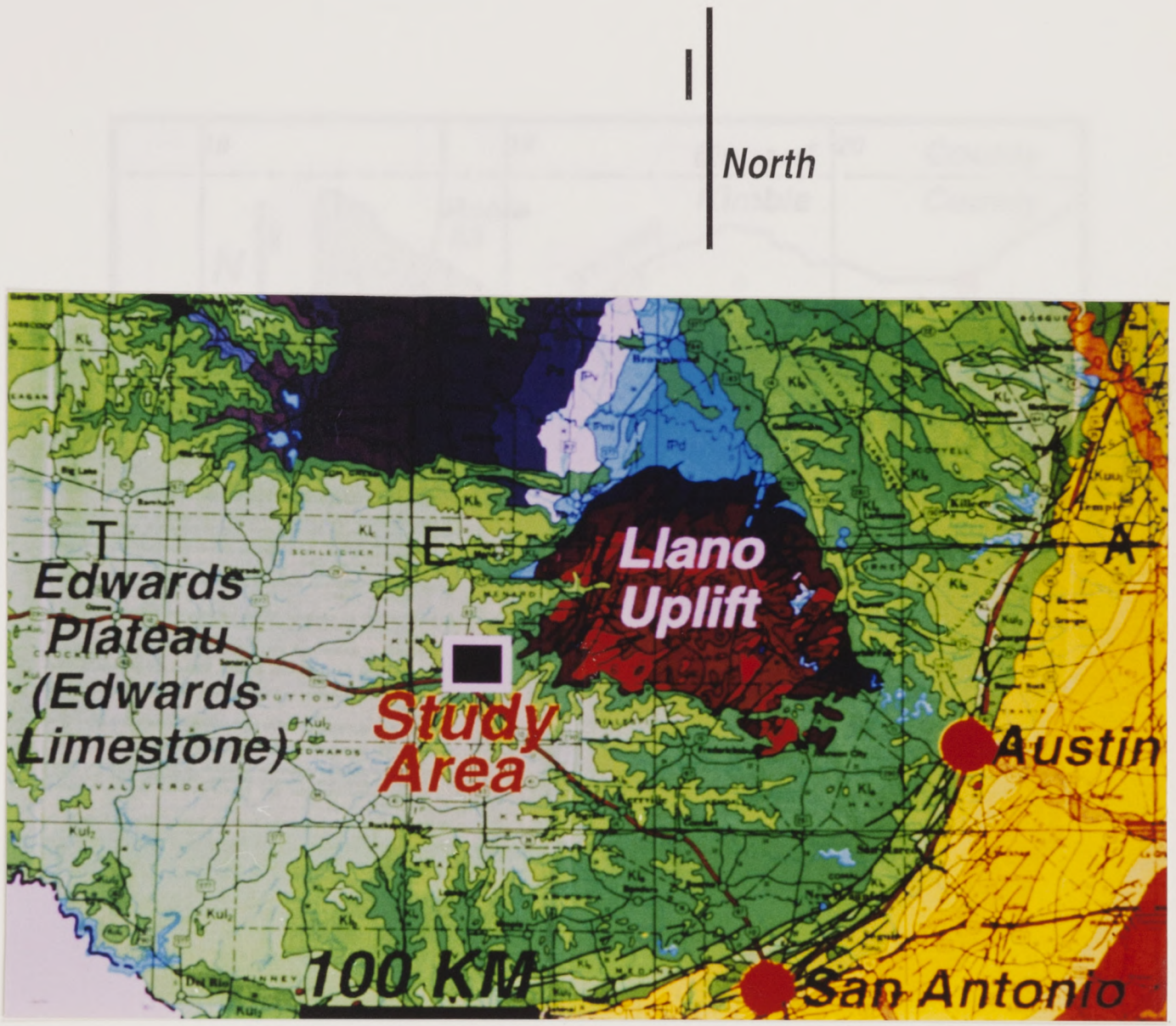

Figure 1. Map of regional geology in central Texas. The study area is located in part, at the dissected edge of the Edwards Plateau; and in part, on the Llano River floodplain (modified from American Association of Petroleum Geologists, 1973).

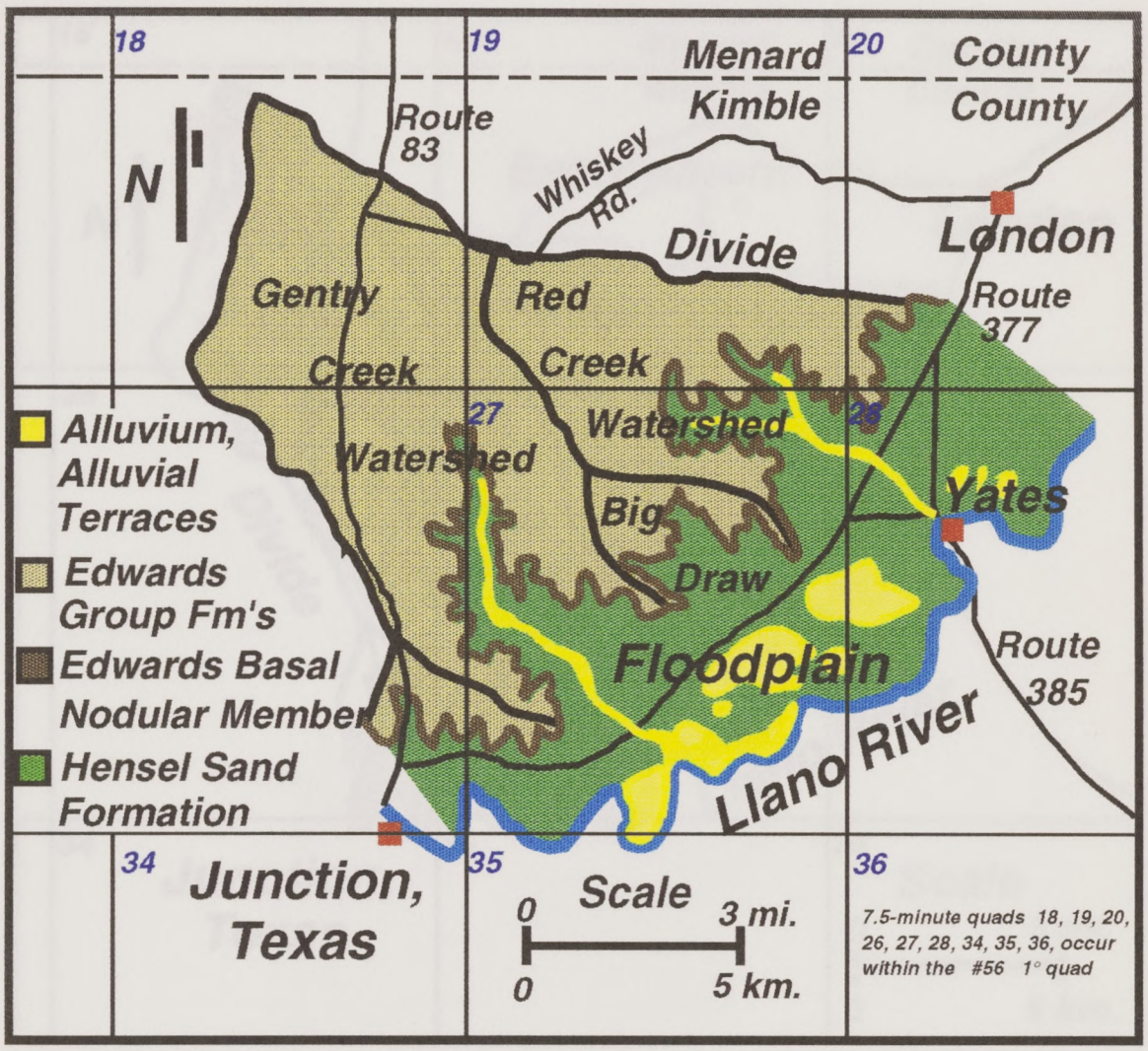

Figure 2. Base map of the study area showing surface geology, watersheds, the Edwards Plateau escarpment, and the Llano River floodplain. The exact distribution of alluvium in the study area has not been established (modified from Barnes, 1981).

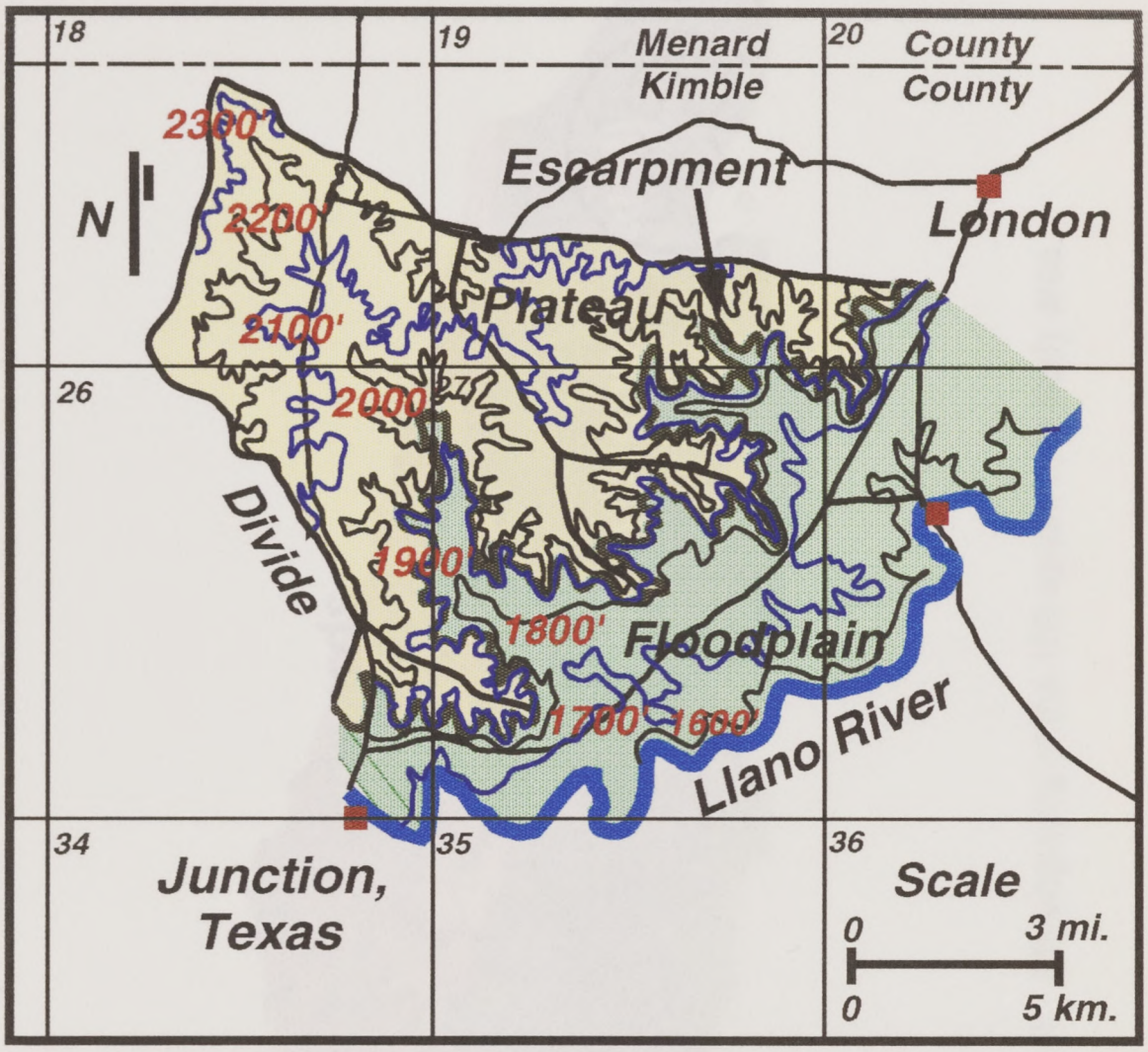

Figure 3. Topography in the study area. Elevations range from 475 meters (1,560 feet) at the eastern end of the Llano River to 713 meters (2,340 feet) at the highest topographic divide (modified from Barnes, 1981).

Figure 4. Physiography of the 150-square mile study area.

Figure 5. Boundary between the flat top of the Edwards Plateau and one of the many deeply incised tributaries that originate at the edge of the plateau.

Figure 6. A steep-walled tributary valley close to its head at the edge of the Edwards Plateau. Vertical fractures and horizontal bedding planes in the carbonate rocks serve as outlets for ephemeral discharge of rainwater that has infiltrated the Edwards Group Formations via its flat upland surface.

Figure 7. Floodplain of the underfit Llano River near Junction, Texas. The floodplain is underlain by the Hensel Sand Formation which is veneered with alluvium (seen here along the banks of the river). The erosional escarpment of the Edwards Plateau looms in the background.

saturated zone at potential drilling locations. In the past, drillers have not understood the nature of ground-water occurrence in this region. The relationship between relief and water-table depth in the highly dissected region at the edge of the Edwards has not been recognized. This has resulted in the drilling of non-productive wells in places where the saturated zone is thin or non-existent.

Numerical flow simulation assisted in evaluating the distribution of recharge. Spatially variable recharge was assigned to the model grid, and the simulated water-table contours were compared to hand-drawn contours. The recharge pattern leading to the best match was used to calibrate the model and to derive estimates of rate and spatial variability of recharge.

Observations of springs and seeps, and aerial photos of tree line patterns were used to identify areas of ground-water discharge. A comparison of present and historical tree coverage (as seen in photographs provided by landowners) shows that an increase in the number of mesquite and juniper trees since earlier in the century correlates with a reduction in ground-water discharge from Edwards aquifer springs. The spread of opportunistic vegetation over time (Figure 8), and the related loss of grass cover, are likely to be responsible for a reduction in aquifer recharge, and a concomitant reduction in spring discharge. This observation suggests it may be of benefit to remove these species of trees to increase the throughput of water. A study by Dugas and Hicks (1994) in the Seco Creek watershed in Texas concluded that spring discharge increased after junipers were removed from a selected area.

Chemical hydrogeology

The analysis of major ions and indicator parameters (DO, pH, Eh, temperature, and alkalinity as bicarbonate) in twenty-one wells establishes a water quality baseline. Ion concentration data were used to determine the spatial distribution of hydrochemical facies, and to map the locations of aquifer recharge and discharge zones. Variations of hydrochemical facies correlated mostly to transitions

Figure 8. Opportunistic species such as Mesquite and Juniper have increased in spatial coverage since earlier in the century.

in lithofacies and, to a much lesser extent, to hydrochemical evolution along flowpaths.

Environmental setting

Land use and economics

The economy of the study area is based primarily on ranching, outdoor recreation, and interstate travel. Limited withdrawals are made from the Llano River to irrigate hay fields and pecan orchards near the river. Deer, turkey, and numerous exotic species graze on private property where they are harvested by hunters who lease the land. Ground water contributes directly to the economy as water supply and, indirectly, as a scenic feature, with springs and spring-fed streams contributing to the recreational value of the area.

Climate and weather

The study area is located in a subtropical subhumid climatic region characterized by hot humid summers and dry winters (Larkin and Bomar, 1983). Onshore flow of tropical maritime air from the Gulf of Mexico is the dominant control of regional climate. Intermittent seasonal intrusions of continental air, exert secondary influences on the climate.

Droughts and floods occur in Texas on a regular basis. Floods are caused by thunderstorms in the spring and tropical storms in late summer. Spring thunderstorms occur along the line of contact between cold fronts and overtopping warm, moist air from the Gulf of Mexico. In late summer, tropical cyclones originate in weather systems that have their beginnings in the Caribbean Sea or the Gulf of Mexico. Droughts are caused mainly by the extensive subtropical high pressure cell (the Bermuda High) that drifts latitudinally with the passing of the seasons. When the Bermuda High is entrenched over the southern United States the possibility of drought becomes more likely (U. S. Geological Survey, 1989).

In the Junction, Texas area the average annual precipitation for the period 1939-1993 (Dunk, 1994; Appendix A) was 61.34 cm (24.15 inches). Two graphs of precipitation are shown in Figure 9. One shows the average monthly precipitation for this period; and the other, the total rainfall for each year in the period of record. Monthly rainfall maxima occur in late spring and early fall; minima occur in midwinter and early summer (Dunk, 1994).

The monthly gross lake evaporation rate during the period 1951-1980 ranged from an average of 6.60 cm (2.60 inches) during January to an average of 25.40 cm (10.0 inches) during August for an annual average of 177.80 cm (70.0 inches) (Larkin and Bomar,1983).

Vegetation

A variety of vegetation is present on the Edwards Plateau. Prairie grasses, live oak and Spanish oak, and "cedar" (scrub juniper) grow on the limestone upland and marly dissected zones. Lining the banks of the creeks and rivers are cypress trees. Terraces support growths of live and post oak, juniper, elm, hackberry, cottonwood, sycamore, and willow. Natural grasses include little bluestem, indian grass, sideoats grama, and Texas winter grass. Introduced grasses include coastal Bermuda, plains lovegrass, Klein grass, and King ranch bluestem (Cuyler, 1931).

Trees, such as the juniper, are wasteful water users compared to grasses because they release moisture to the atmosphere through their stomatas twenty-four hours a day. Some landowners report that where junipers have been removed, creeks and springs on their property have increased in discharge. It is hypothesized that excessive growth of juniper and other opportunistic trees have caused a reduction in aquifer recharge, and a concomitant reduction in spring discharge.

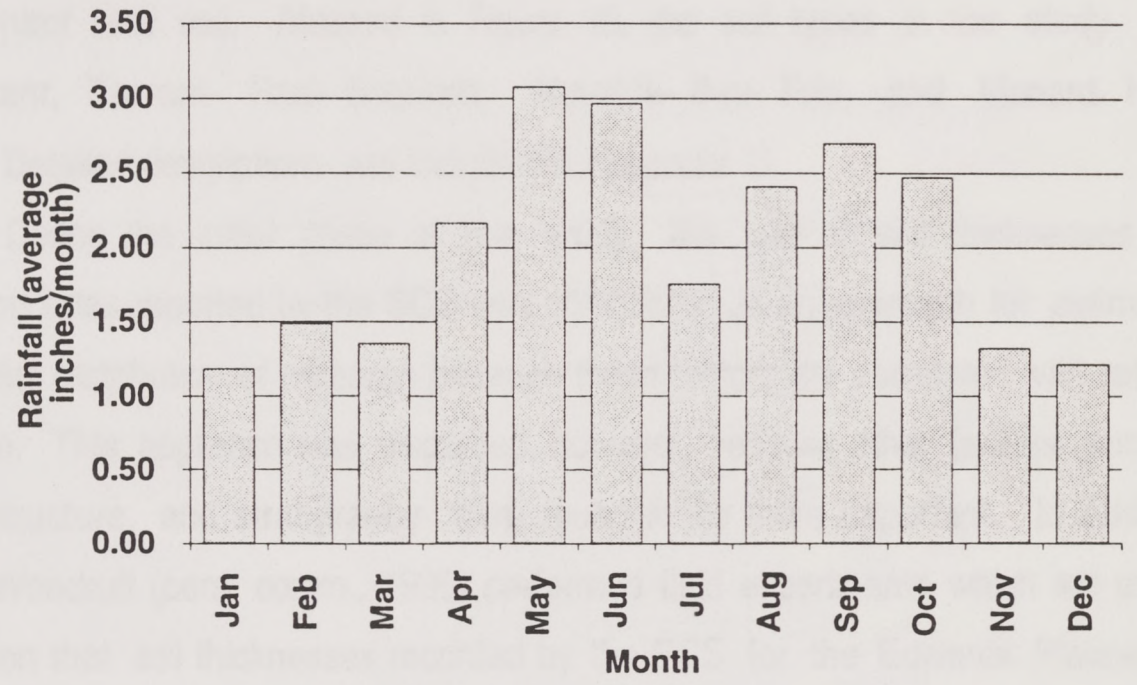

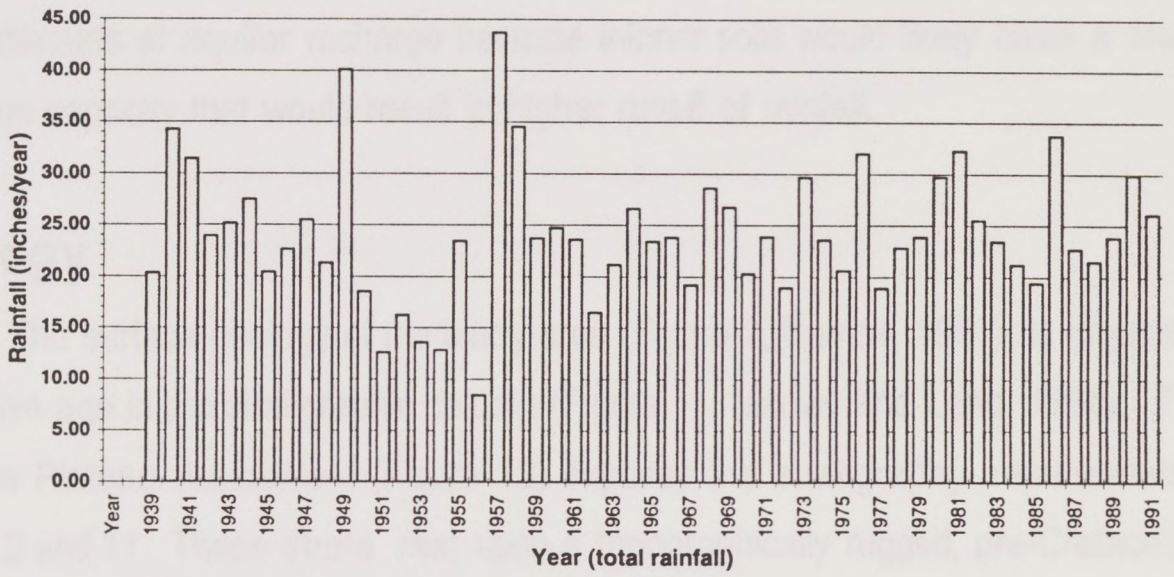

Figure 9. Histograms of rainfall in Junction, Texas from 1939 to 1991. The upper histogram shows average monthly rainfall; the lower, total annual rainfall (Dunk, 1994).

Soils

Soils in the study area are divided into four types by the Soil Conservation Service (SCS) (Blum, 1982). This division is based on sets of physical properties that control land use. Mapped in Figure 10, the soil types in the study area areTarrant, Tarrant- Real- Brackett, Nuvalde- Dev- Frio, and Menard- Hext- Latom. Detailed descriptions are included in Appendix C.

During the initial phase of this study, the use of soil thicknesses and infiltration rates reported by the SCS was considered as an approach for estimating the spatial distribution of recharge because these factors are correlated with rate of recharge. This approach was discarded, however, because other factors such as relief, structure, and stratigraphy were found to be more important. In addition, Chock Woodruff (pers. comm., 1995) performed field experiments which led to the conclusion that soil thicknesses recorded by the SCS for the Edwards Plateau-Hill Country area were underestimated because they had been measured with handtools rather than backhoes. These underestimates of soil thicknesses could lead to underestimates of aquifer recharge because thinner soils would likely have a lower infiltration capacity that would result in higher runoff of rainfall.

Geology

The surface geology of the study area (Figure 2, Barnes, 1981), is organized by relative age in the stratigraphic column (Figure 11; Maclay and Land, 1984). The Edwards Plateau escarpment (Figure 12) exposes the stratigraphy represented in Figures 2 and 11. These strata rest upon a topographically rugged, pre-Cretaceous unconformity named as the Wichita Paleoplain (Hill, 1898). Strata were deposited in conjunction with the eustatic rise and northwestward transgression of the Lower Cretaceous Comanchean Sea. Referring to Figure 12, the lower strata is the Hensel Sand Formation (Hensel) of the Trinity Group, and the upper is the Fort Terrett

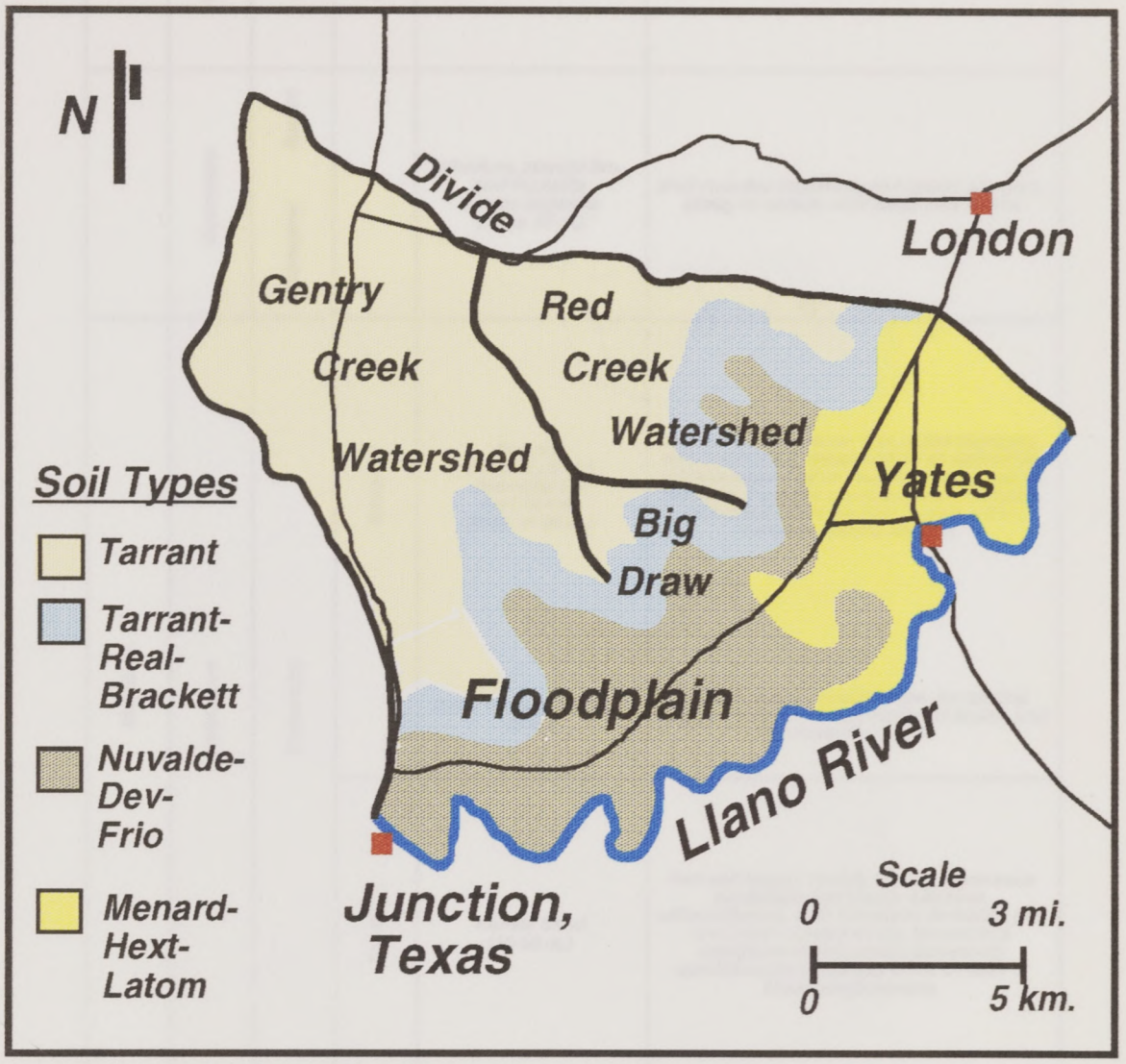

Figure 10. Distribution of soil types in the study area (Blum, 1982).

ERA	SYSTEM	SERIES	GROUP	FORMATION	CHARACTER OF ROCKS
	Quaternary	Pleistocene Recent		Alluvium, alluvial fan, and fluviatile terrace deposits (up to 15 m.)	Well-rounded limestone and cherty alluvium, sandy to cobbly, with limey clay matrix
Mesozoic	Cretaceous	Comanche	Edwards	Segovia (max. of 38 m.) overlying the Fort Terrett (max. of 58 m.)	Carbonate grainstone, and rudist bioherms and biostromes, deposited on an extensive, shallow-water, low to medium energy marine platform. Contains abundant chert nodules, and at the top of the Fort Terrett, a thin collapse breccia horizon.
				Basal Nodular Member (5 m.)	Massive nodular wackestone, containing Exogyra texana, lunatid, turritellid snails, and protocardid clams.
			Trinity	Hensel Sand (15-60 m.)	Red and brown, mostly friable, calcareous sandstone and clayey siltstone, unfossiliferous, with limestone in middle part and basal conglomerate, formed in a nearshore environment. Commonly calichified, hematite and silica cement in basal conglomerate.
Wichita Paleoplain Unconformity(base of Cretaceous aquifer system)					
Paleozoic	Permian(?)			Unknown with any certainty directly under study area	Low permeabilty sediments whose structural complexity compartmentalizes and hydrologically isolates small aquifers

Figure 11. Generalized stratigraphic column in the Junction, Texas area (modified from Maclay and Land, 1984).

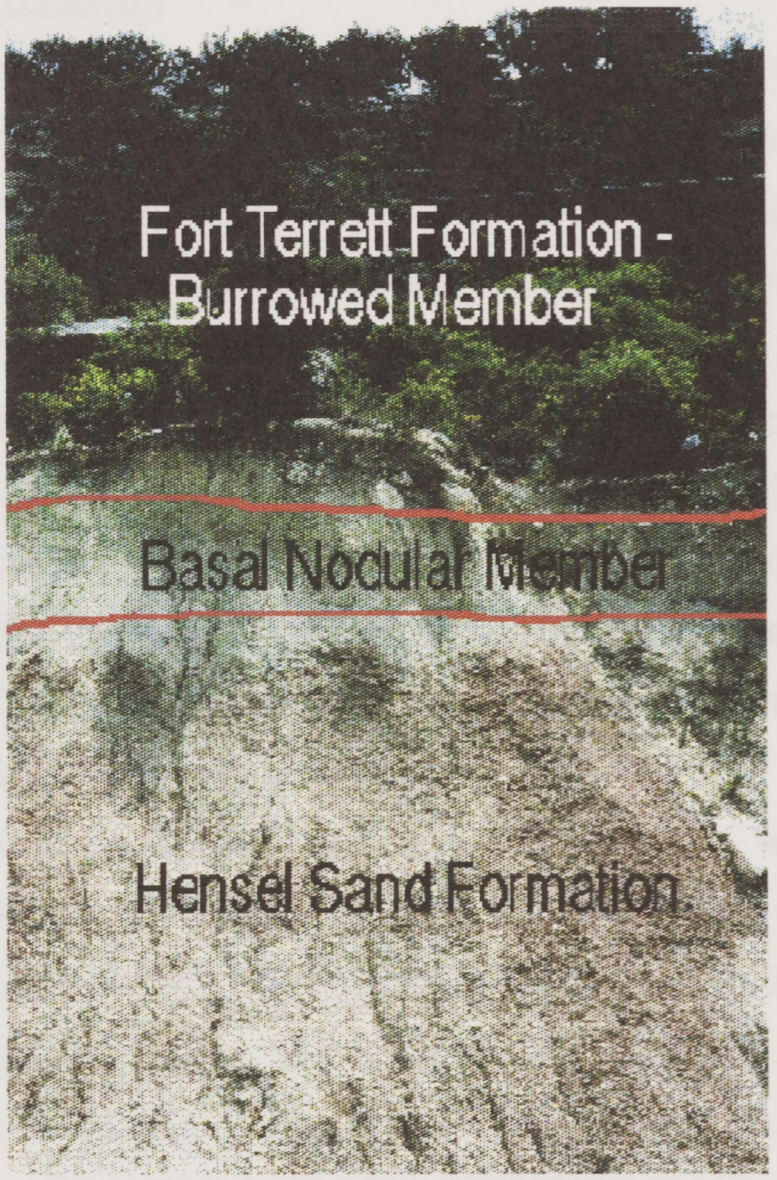

Figure 12. Stratigraphy on the face of the erosional escarpment of the Edwards Plateau. Exposed from bottom to top is the red-orange, friable siltstone at the top of the Hensel Sand Formation, the basal marly limestone member of the Fort Terrett Formation, and the fractured limestones and dolomites of the Fort Terrett.

Formation of the Edwards Group (Edwards). The Fort Terrett Formation and the overlying Segovia Formation of the Edwards Group are together referred to in this report as the Edwards except in cases where it is important to distinguish between the two. The aquifer occuring in both formations will be referred to as the Edwards aquifer.

Hensel Sand Formation

The Hensel, which is Upper Trinity in age, was deposited contemporaneously with the downdip (southeast and east of the study area) Glen Rose Formation. "This depositional couplet is the youngest of three clastic-carbonate couplets, separated by disconformities, that reflect a pattern of cyclic sedimentation superimposed on an overall transgressive regimen" (Stricklin and others, 1971). Each couplet generally onlaps rocks of the previous cycle and documents a major advance of the early Cretaceous sea terminated by an overall drop in sea level. "Episodic rejuvenation in the source area resulted in an increased supply of clastics and a consequent detrital depositional phase, followed by relatively quiescent sedimentation of carbonate deposits, the latter phase in part contemporaneous with and transitional into the clastic phase" (Boone, 1968).

During Jurassic time (60 million year period) most of west-central Texas was emergent and subject to erosion prior to inundation by the Comanchean Sea. Extensive northwest-southeast trending river valleys that had been carved out of the Paleozoic surface, became filled with terrigenous Trinitian age sediments to cause a substantial leveling of the ground surface. Eventually, these sediments formed a wedge which thickens downdip (toward the southeast). The Hensel sediments which fill these valleys were derived from erosion of the Paleozoic surface, and from erosion of Precambrian rocks that were exposed as a paleohigh in the Llano Uplift region. In the study area the average thickness of the Hensel is approximately 60 meters (200 feet).

An interpretation of the Hensel paleoenvironment and a cross-sectional view of the sequence of depositional events occuring during the Lower Cretaceous is depicted in Figure 13 (Payne, 1982). Previous studies (Rapp, 1988; Payne, 1982; Barnes, 1981; Hall, and Turk, 1975; Amsbury, and others, 1974; Inden, 1974; Stricklin, and others, 1971; Boone, 1968; Campbell, 1962; Hughes, 1948; Hill, and Vaughan, 1898) have established the Hensel to be a cemented conglomerate at its base which fines upward to become a friable calcareous siltstone (Figure 12) at its top. The basal conglomerate is attributed to initial high stream gradients, and the fine-grained material at the top is attributed to the low stream energy that developed as the relief became leveled (Stricklin and others, 1971). Sedimentary features observed in the field such as thin beds of carbonate, cross-bedding, ripple marks, crevasse splays, oyster shell orientations, psuedoanticlines, and caliche have lead to the interpretation of an arid to semi-arid fluvial paleoenvironment. The Hensel is described by Hall and Turk (1975) as a dip-oriented multilateral sandstone body characterized by two important facies: (1) a meanderbelt sandstone facies (lenticular coarse-grained framework deposits), and (2) a floodbasin facies (finer-grained matrix deposits).

The complex facies architecture within the Hensel results in an equally complex pattern of ground-water flow. An example of a diagenetic feature that contributes to this complexity is presented in Figure 14. This is a photograph of an exposure with extensive nodular caliche that was deposited between individual grains in the sandstone by circulating ground water. This caliche reduces primary porosity and probably increases the tortuosity of ground-water flow.

Edwards Group Formations

During the Lower Cretaceous Period the study area was situated approximately 25° north of the equator within the belt of prevailing easterlies. Descending air masses at around 30° north resulted in dry adiabatic warming and

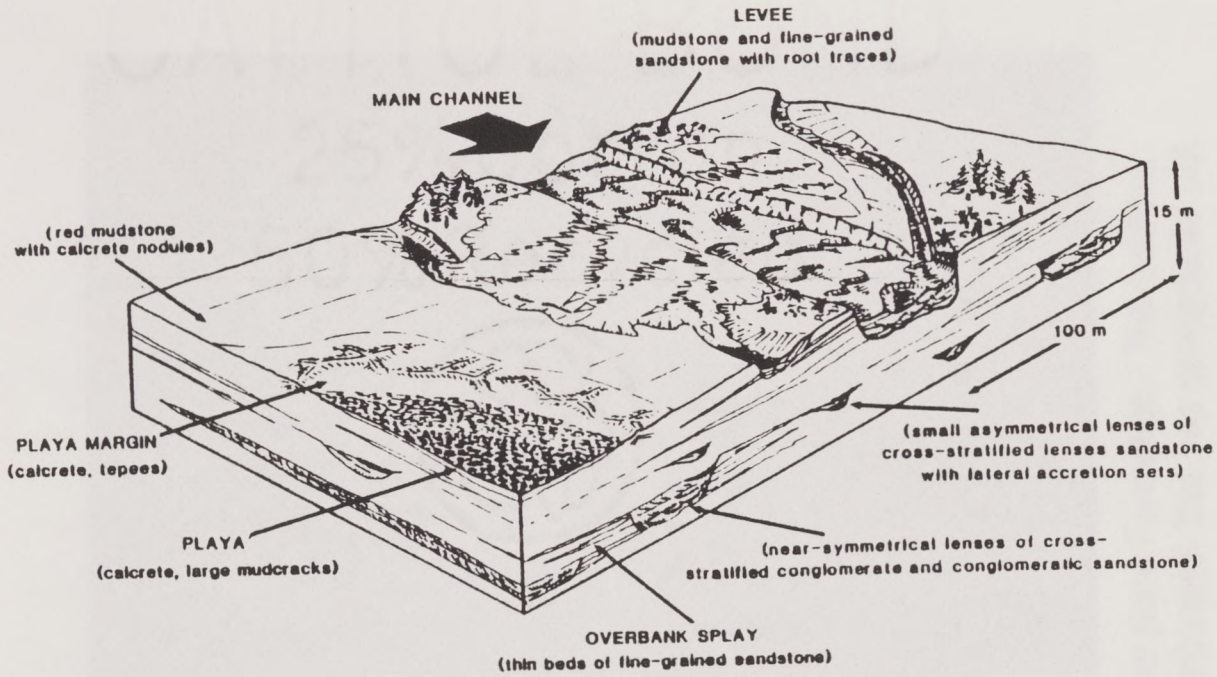

DISTRIBUTION OF MAJOR HENSEL LITHOFACIES

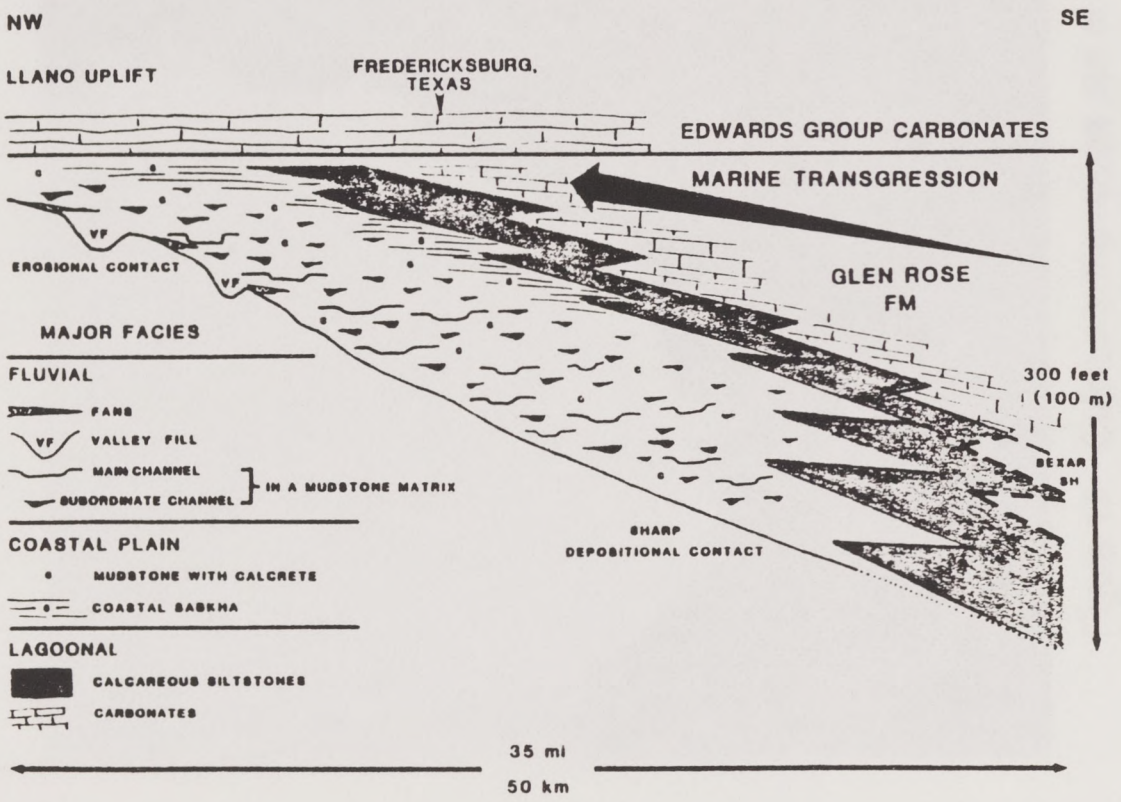

Figure 13. Fluvial paleoenvironment (upper diagram) and model (lower diagram) of Trinity Group deposition (from Payne, 1982).

Figure 14. Outcrop in the middle part of the Hensel Sand Formation. The oxidized silty-sand is impregnated with caliche (calcium carbonate) that has precipitated out of groundwater.

low relative humidity (Rose, 1972). Rainfall, possibly associated with tropical storms was distinctly seasonal. This climate was conducive to the deposition of the carbonates and evaporites that formed the Edwards Group. These sedimentary rocks were deposited in shallow water on the broad Comanche Shelf whose dominant feature (in the study area) was the Central Texas Platform, a wide elongate positive surface that was leveled by deposition of terrigenous Hensel sediments that filled pronounced valleys on the Paleozoic (Wichita Paleoplain) surface (Figure 15). The Edwards is characterized by rudist bioherms, carbonate grainstones and mudstones, and evaporites laid down during three transgressive-regressive sequences under predominantly shallow marine conditions of relatively low wave and current energy (Rose, 1972). These relatively thin, nearly flat-lying strata (Figure 16) dip gently southeastward atop massive Paleozoic and Triassic units that dip westward.

By early Fredricksburg time, an offshore bioherm of rudists, corals and carbonate deposits, named the Stuart City reef trend, had grown to an almost continuous ridge along the seaward edge of the continental shelf in the ancestral Gulf of Mexico basin (Figure 17) (Bebout and Loucks, 1974; Fisher and Rodda, 1969; Rose, 1968). The rapid growth of this reef trend probably resulted from a rapid rise in sea level that may have been triggered by an increase in the rate of seafloor spreading (Bay, 1977). This reef trend sheltered intertidal and restricted marine depositional environments on its leeward side (Comanche Shelf) from deep, open marine conditions in the ancestral Gulf of Mexico basin. During periods of especially low sea level and extreme aridity, the crest of the central Texas Platform became a broad, sahbka-type mudflat where evaporites, dolostone, and thin-bedded dolomitic limestone were deposited (Fisher and Rodda, 1969). Sedimentation was controlled by several factors: climate, influx of terrigenous clastic sediment, distribution of tectonic subsidence and uplift, and energy level of wave and current action (Barker, and

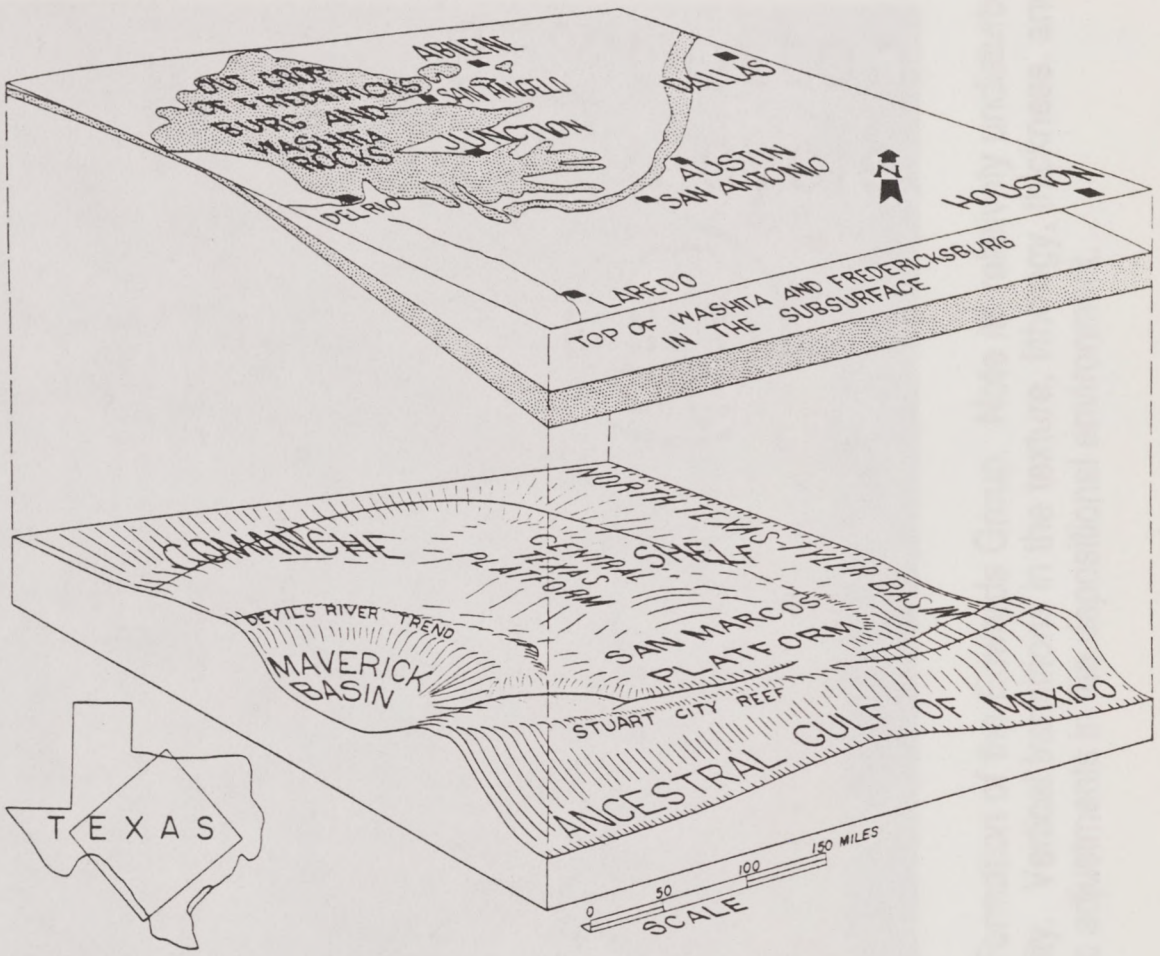

Figure 15. Tectonic framework of central Texas. Cretaceous age carbonate rocks of the Edwards Group were deposited in a broad shallow sea named the Comanche Shelf (from Rose, 1972).

Figure 16. Outcrop of the Segovia Formation of the Edwards Group. Note its relatively undisturbed nature and high degree of horizontality. Vertical transitions in the texture, lithology, thickness, and color of individual beds reflect periodic adjustments in the depositional environment.

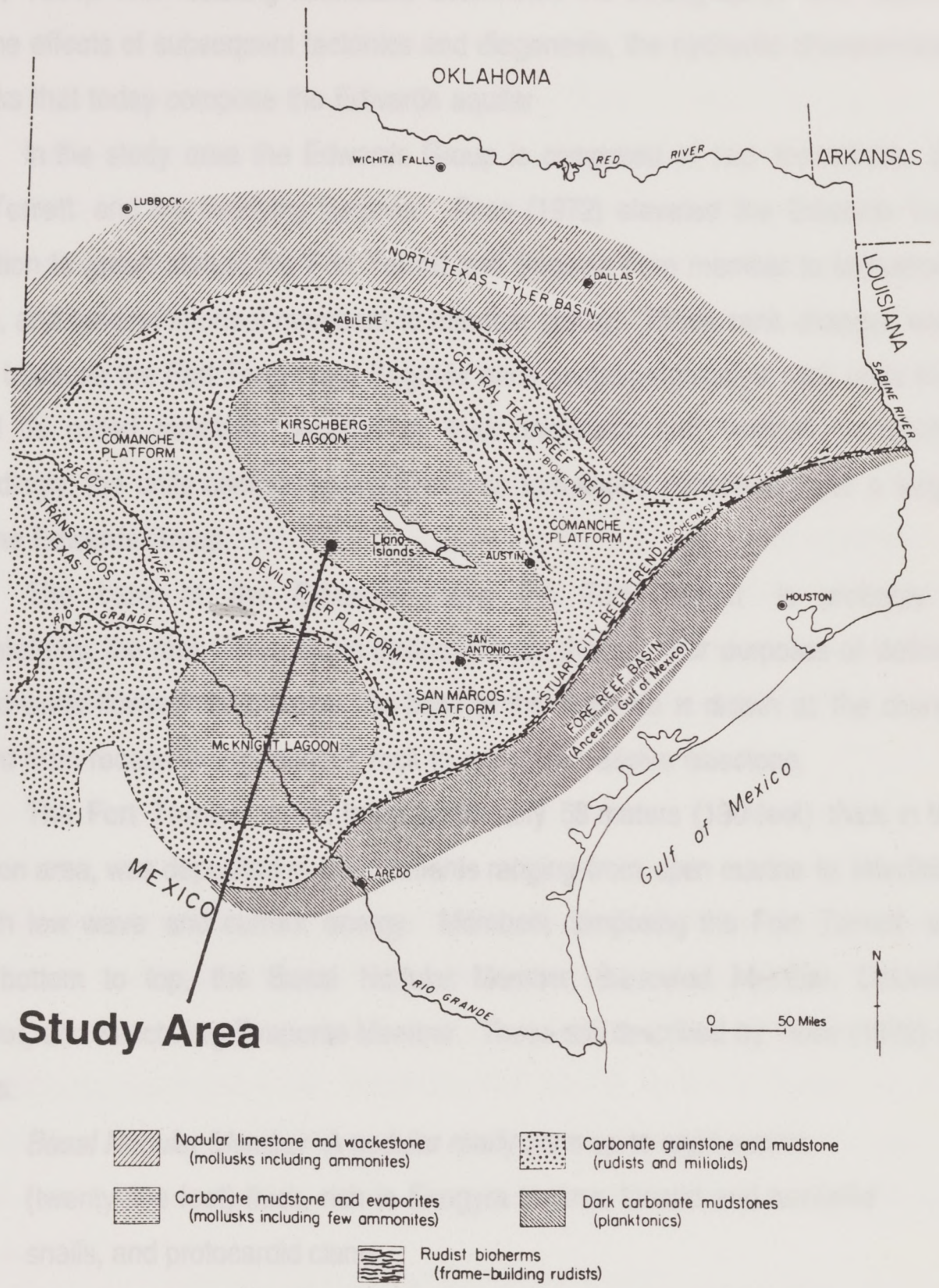

Figure 17. Lower Cretaceous paleoenvironment in central Texas (from Fisher and Rodda, 1969).

others, 1994). The resulting lithofacies determined the stratigraphy, and together with the effects of subsequent tectonics and diagenesis, the hydraulic characteristics of rocks that today compose the Edwards aquifer

In the study area the Edwards Group is composed of two formations, the Fort Terrett and the overlying Segovia. Rose (1972) elevated the Edwards from formation to group status, the Fort Terrett and Segovia from member to formation status, and several informal members to member status. These rank changes were made because the Fort Terrett and Segovia each contain significant rock units that should be called members because of their thickness and vertical variability. Accordingly, the units comprising them rank as formations constituting yet a larger unit, the Edwards Group.

The base of the Edwards below the Fort Terrett is probably a disconformity, the rock above being distinctly more marine. For purposes of defining ground-water flowpath boundaries, the base of the Edwards is drawn at the change upward from recessive argillaceous rock to resistant massive limestone.

The Fort Terrett, which is approximately 58 meters (190 feet) thick in the Junction area, was deposited in environments ranging from open marine to intertidal, all with low wave and current energy. Members composing the Fort Terrett are from bottom to top, the Basal Nodular Member, Burrowed Member, Dolomitic Member, and Kirschberg Evaporite Member. These are described by Rose (1972) as follows:

> *Basal Nodular Member*- A nodular marly zone up to eight meters (twenty-five feet) thick, rich in Exogyra texana, lunatid and turritellid snails, and protocardid clams.
>
> *Burrowed Member*- Massive, resistant layers of porous, burrowed limestone approximately twenty-five meters (eighty feet) thick, thin beds of miliolid and mollusc-fragment biosparite and dolomite, deposited in a

restricted to open shallow marine environment. This member is the chief water-bearing zone of the Edwards, its porosity caused in part by preferential leaching and removal of burrow-fillings to produce widespread honeycomb porosity.

Dolomitic Member- Massive to thin-bedded, fine to medium crystalline, homogeneous dolomite, with abundant chert and beds of miliolids and rudistid biosparite, deposited in an intertidal to restricted shallow marine environment.

Kirschberg Evaporite- Widespread, twelve to twenty meter (forty to eighty foot) thick disturbed and altered zone that marks the former presence of a gypsum horizon. Massive to thin-bedded, cherty, crystalline limestone and travertine containing intervals of limestone, dolomite and chert fragment collapse breccia. Its depositional environment was restricted shallow marine, and in part sahbka-type supratidal and intertidal (Figure 17).

The Segovia, which is approximately 35 meters (115 feet) thick in the Junction area, was deposited in environments ranging from open marine to intertidal. It is composed of the Burt Ranch Member, Allen Ranch Breccia Member, Orr Ranch Bed Member, and Black Bed Member. In the Junction area the Orr Ranch Bed and the Black Bed are eroded atop the Segovia, and the Allen Ranch Breccia does not extend this far north and west. Unlike the Fort Terrett, which is divided into four intergradational members, the Segovia is subdivided into members on the basis of thin, distinctive widespread key beds. The section in the Junction area is described by Rose (1972) as follows:

> *Burt Ranch Member*- Persistent and widespread zone of marly limestone, above the Kirschberg Evaporite Member having a thickness of approximately twenty meters (seventy feet). It includes marl, marly micrite, miliolid

biosparite, and rudist biosparite with a few scattered beds of soft massive dolomite. Clayey or marly fossiliferous zones are particularly common near the base and toward the top and contain Exogyra texana, and turritellid snails. This member reflects distinctly more marine depositional conditions than the underlying Fort Terrett. This claim is supported by its rich and diverse mollusk and ammonite fauna which indicates deposition on a shallow open shelf.

Unnamed Member- Atop the Burt Ranch Member in the Junction area is an unnamed thin-bedded limestone biomicrite and micrite with isolated beds of dolomite about 180 meters (55 feet) thick.

Deposition of carbonates continued during Washita time, but over most of the Plateau, as well as in the study area these sediments are now eroded. Toward the end of the Washita, in response to an upwarping of the Comanchean Shelf, there was a widespread regression of the shallow sea. The Washita Group strata was stripped away and the Edwards became exposed. Since becoming exposed, the Edwards has undergone diagenetic alteration by processes such as fracturing, recrystallization, cementation, dissolution, and collapse of resistent beds. These processes have produced variations in porosity and permeability both laterally and vertically, which have influenced aquifer heterogeneity.

Alluvium and Colluvium

Several types of Quaternary surficial deposits are found in the study area. These are classified as either one of several types of alluvium or as colluvium (Barnes, 1981). Deposition of these sediments occured from the Pleistocene to the Recent, but their exact ages and modes of formation are not known because they have not been studied (Michael Blum; pers. comm., 1995).

Close to the Llano River, near the level of the present floodplain, is a ten meter (33 foot) thick layer of alluvium (Figure 7) that in some places supports shallow, potable aquifers of limited extent. Three types of alluvial deposits were mapped by Barnes (1981) using aerial photos: (1) those that formed in Recent times along the sides of tributaries which are perpendicular to the Llano River, (2) terraces deposited in Recent times which parallel the present course of the Llano River and, (3) remnants of high terraces flanking the edges of the underfit Llano River valley that are older than the low terraces.

The distribution of alluvial deposits is represented in a generallized sense on the map of surface geology (Figure 2). A photograph of a coarse-grained point bar deposit in a tributary that drains the dissected area next to the Edwards Plateau is shown in Figure 18. These rounded gravels which are composed of limestone, dolomite, and chert, were deposited during intense, short duration floods. The source of most of the gravel is probably colluvium that has accumulated at the bottom of steep slopes of the Edwards higher in the tributary reaches. Exposures of terrace gravels throughout the area reveal that they are constructed of a mixture of well-rounded chert and limestone gravel loosely bound by fine-grained travertine. A present day example of fine-grained deposition within the interstices of gravel deposits is shown in Figure 19. This is a photograph of the bed of the Llano River showing how calcium carbonate (travertine) precipitates out of solution when carbon dioxide is lost from the river water. The calcium carbonate settles into the intergranular spaces of the limestone and chert gravel. The result is a tightly-bound alluvial deposit having a bimodal distribution of grains and perhaps a diminished infiltration capacity.

Throughout the area, near the transition between the Edwards and the Hensel, widespread fanplains occur. These surface deposits were referred to as

Figure 18. Coarse-grained point bar deposited by flood waters that ran across the Llano River floodplain within a meandering ephemeral tributary. These point bars build up over time to form terraces as the stream cuts downward.

Figure 19. Bed of the Llano River showing a fine-grained travertine (calcium carbonate) ooze building up between the pebbles and cobbles. Travertine is precipitated from the river water when carbon dioxide is lost to the atmosphere.

"washes" by Hill (1898). Apparently, they are deposited by overland runoff that contains an unsorted mixture of colluvium.

Previous investigations

Previous investigations are grouped into two categories: (1) local hydrogeologic and surface hydrology studies, and (2) hydrogeologic studies outside of the local area yet within the same physiographic province.

Local hydrogeologic and surface hydrology studies

The ground-water study that relates most substantially to the present one is by Alexander and Patman (1969). They "determined the occurrence, availability, dependability,quality, and quantity of the ground-water resources of the County" and provided a qualitative overview of hydrogeology and surface-water hydrology.

A stream gauging study was completed by Holland and Mendieta (1965). From January 17 to January 24, 1962, the flow rates of the Llano River and its principal tributaries were measured at fifty-three points between Junction and Llano, Texas with a portable stream gauge. Holland and Mendieta believed that the flow of the Llano River and its tributaries was being sustained by contact springs. No runoff-producing rains had occured for sixty-six days prior to the investigation. Based on this observation they determined that measured discharge values would quantify low-flow conditions. It was hoped that their results would shed light on surface-water/ground-water interaction to support the present study but, unfortunately, because the rate of discharge measured from one stream gauge to the next did not differ by more than five percent, the data could not be used. Five percent is the margin of error for stream gauging with the portable Price current meter.

Hydrogeologic studies outside of the local area yet within the same physiographic province

A number of hydrogeological studies within the Edwards or Hensel in the Edwards Plateau/Hill Country region were completed outside the study area. These provided insight into the hydrologic regime of the study area, and contained data that were compared with those of this study. These data included transmissivities, hydraulic conductivities, saturated thicknesses, formation thicknesses, spring outlet elevations, well yields, major ion values, and fracture orientations. Previous studies include those of:

(1) Barker and others (1994) who provided an up-to-date overview of the hydrogeology of the Edwards-Trinity aquifer by condensing an array of previous studies.

(2) Kuniansky and Holligan (1993) who presented the results of a digital model of the ground-water flow system in the Edwards-Trinity aquifer. They calculated water budgets for pre-development and post-development conditions, and found that ground water development reduced spring flow and leakage to streams.

(3) The Hill Country Underground Water Conservation District (1994) who produced the "Gillespie County Regional Water Management Plan."

(4) Bush and others (1993) who presented a three-sheet map series on the historical potentiometric surface of the Edwards-Trinity Aquifer System. These maps portray regional water-level patterns over broad areas using the earliest available data at 1,789 well locations.

(5) Ardis and Barker (1993) who created a two-sheet map series illustrating the saturated thickness of the Edwards-Trinity Aquifer System and selected contiguous hydraulically connected units in west-central Texas.

(6) Barker and Ardis (1992) who reported on the configuration of the base of the Edwards-Trinity Aquifer System and hydrogeology of the underlying pre-Cretaceous

rocks, west-central Texas. They reported that the Cretaceous aquifer system is underlain by an extensive complex of rocks ranging from Late Cambrian through Late Triassic in age that are typically ten to one thousand times less permeable than those comprising the aquifer system.

(7) Bluntzer (1992) who evaluated the ground-water resources of the Paleozoic and Cretaceous aquifers in the Hill Country of Central Texas. He claimed that the projected population increase between 1985 and 2010 would double the demand for water from 22,872 acre-feet/year to 47,380 acre-feet/year.

(8) Abbott and Woodruff (1986) who edited a compendium of papers that addressed the geology, hydrology, ecology, and social development in Central Texas near the Balcones Escarpment. Particularly relevant to the present study is the paper by Rose (1986) concerning the potential impact of pipeline oil spills upon the Edwards Plateau Aquifer. He concluded that the aquifer is exceptionally vulnerable to pollution from pipeline oil spills because its fracture permeability would allow oil to sink into the bedrock before cleanup crews could respond.

(9) Ashworth (1983) who assessed the ground-water availability of the Lower Cretaceous formations in eleven counties in the Hill Country. Ashworth described the depositional environments, stratigraphy and structure of the Lower Cretaceous formations and how these factors control the hydrogeology.

(10) Walker (1979) who reported on the occurance, availability, and chemical quality of ground water in the Edwards Plateau region of Texas. He defined five aquifers of different ages located in the twenty-eight county study area.

Methods and Data

Data used in this study came from three sources: existing records, field measurements, and laboratory analyses. Data collection and processing, and the methods used to generate new data are described.

Existing records

Existing records utilized included drillers' reports, specific capacities, Llano River discharge rates, and aerial photos.

Water well inventory

One hundred and twelve water wells were inventoried using data from two State of Texas record archives (Appendices D). Well location maps and drillers' reports for "plotted" wells were obtained from the Texas Natural Resources Conservation Commission (TNRCC). Well location maps and hydrochemical analysis values for "located" wells were obtained from the Texas Water Development Board (TWDB).

Plotted wells

Maps of plotted wells show approximate well locations on U. S. Geological Survey (USGS) 7.5-minute topographic maps. as reported to the TNRCC by individual drillers. These wells assigned approximate locations on Texas Department of Transportation county highway maps. Water well reports may contain information on specific capacity, static water level, lithology, well diameter, and well and screen depths.

Located wells

Located wells are field located by TWDB technicians on USGS 7.5 minute topographic maps. In the study area, many of these wells are easily spotted because they use windmills for pumps. Well reports include information on static

water levels, and field-measured values of specific conductance, and total iron (Alexander and Patman,1969). Reported iron analyses are ferric values. Ferric iron is the undissolved form of iron contributed by rusty well hardware.

Specific capacity tests

Some well reports submitted to the TNRCC included the results of well acceptance tests. These data were used to calculate specific capacity, which in turn was used to estimate transmissivity and hydraulic conductivity (Appendix E). By pumping for a period of time and noting little or no drawdown of the water table, the driller "accepts" the well for its intended use. The well acceptance test is conducted for a much shorter duration (0.5 to 2.0 hours) than the aquifer pump tests performed by hydrogeologists to calculate hydrogeologic parameter values. For this study area, specific capacity calculations were the only source of data to make estimates of transmissivity and hydraulic conductivity.

Fifty-seven specific capacity values from the Hensel aquifer and twenty-six from the Edwards aquifer were used to estimate transmissivity. Hydraulic conductivity was then calculated by dividing transmissivity by the average saturated thickness of each aquifer. The formula used was the modified non-leaky artesian formula (Walton, 1962):

$$Q/s = T/(264\log(Tt/2693r^2S)-65.5) \qquad \text{(eq. 1)}$$

where:

Q/s = specific capacity (L^2/t)

T = transmissivity (L^2/t)

S = storage coefficient [dimensionless]

r = well radius (L)

t = time since pumping started (t)

This equation relates the specific capacity of the well to the transmissivity of the aquifer. It assumes that the well is discharging at a constant rate in a homogeneous, isotropic, nonleaky, artesian aquifer, infinite in areal extent. Estimates of S (.01 to .0001) bracketed the range of probable actual values because the degree of confinement within the portion of the Hensel aquifer occuring below the Edwards was not known.

There are three reasons why specific capacity calculations must be considered approximations. First, pumping periods in some wells may be too short; thus, the water table is not given an adequate amount of time to become depressed as required by the equation. Second, well reports do not indicate how soon after the cessation of pumping that the static water level was measured. A delay between the cessation of pumping and measurement of the water level could cause an erroneously small drawdown which would result in the calculation of an overly large value of specific capacity. Third, the calculated average values of specific capacity probably underestimate T because test results in cases where zero drawdown is observed (i.e. higher transmissivities) cannot be processed by the Walton equation to calculate transmissivity.

Llano River discharge records/precipitation records

Discharge rates recorded at USGS stream gauge # 08150000 (Junction) were used to estimate baseflow in the Llano River. Data from the months of December and January for the years 1939 to 1993 were used (U. S. Geological Survey, 1994, and Appendix F) because they were low-flow months. Surface runoff and evaporation during low-flow months are at a minimum; thus, the water in the river is derived almost entirely from baseflow. These data were coupled with precipitation values (Dunk, 1994, and Appendix B) for the same months and for the same period of record to produce an estimate of annual ground-water recharge in the drainage basin upstream of the river gauge. The estimated recharge in cm/year

was extrapolated to the study area and used as initial input to the numerical flow model.

Low altitude aerial photographs

Black and white aerial photographs of the study area were obtained from the Texas Natural Resources Information Service (TNRIS). Distinct patterns of tree growth observed on the photos correlate strongly with stratigraphic features that control spring discharge from the Edwards aquifer.

New data acquired in the field and laboratory

New data acquired included ground-water level measurements, dissolved ion concentrations, unstable constituent values, and results of an x-ray analysis of sediment.

Ground-water level measurements

Static water levels were measured in 112 wells (Appendix D). Interpolated data points were then used to construct potentiometric surface maps. Measurements were made in wells equipped with windmills and submersible pumps, and in wells with no installed pump. Before measurements were made, the pumps were turned off and the water table was allowed to recover. Depths to water were measured to the nearest .3 meter (one foot) with a chalked steel tape. One foot was considered sufficiently accurate because topographic relief in the study area is about 230 meters (750 feet) and ground elevation control is accurate only to about three meters (ten feet) (one-half of a contour interval) on 7.5-minute USGS topographic maps.

Measurements were taken during an eight month period as access to each property could be secured. Repeat measurements of a half-dozen control wells were made during the study, and water-level values were replicated to within approximately one meter. To calculate the elevation of the potentiometric surface

at each water well, the depth-to-water was subtracted from the ground surface elevation. Ground surface elevations were established from USGS 7.5-minute topographic maps, but where it was not possible to plot a well accurately on the topographic map an engineering transit was used to triangulate from three topographic features to determine location.

Sampling and analysis of ground-water chemistry

Ground-water samples were collected from twenty-one wells. Seven samples were taken from the Edwards aquifer, thirteen from the Hensel aquifer, and one from the thin alluvial aquifer next to the Llano River.

Collection and analysis followed the set of procedures listed in Appendix A and diagrammed in Figure 20. To summarize, wells were pumped until temperature, dissolved oxygen, and pH achieved temporal stability. These indicator values were measured within a flowcell that isolated the aquifer water and the measuring probes from the atmosphere. Alkalinity was measured in the field by titrating with 1.5 N HCL to the 4.5 pH endpoint. Samples were collected in pre-cleaned polyvinyl chloride bottles and preserved for ion analysis in the laboratory.

Anion concentrations were measured with the ion chromatograph (IC), and cation concentrations were measured using the inductively-coupled plasma spectrophotometer (ICP). Anion concentrations were determined using both the conductivity and the absorbance detectors and these calculations were then adjusted by the ratio of the IC measured value of a certified check standard to the manufacturer's measured value.

Ionic charge balance to within 5.2 percent was achieved for each sample that was analyzed for Ca, Mg, Sr, K, Li, Na, and Cl, F, SO_4, HCO_3, Br, NO_3, and NO_2. An ionic charge balance error of less than five percent is believed to rule out analytical error. Several constituents not measured in the lab were measured in the field with a Milton Roy Mini-20 spectrophotometer. These included sulfide, dissolved

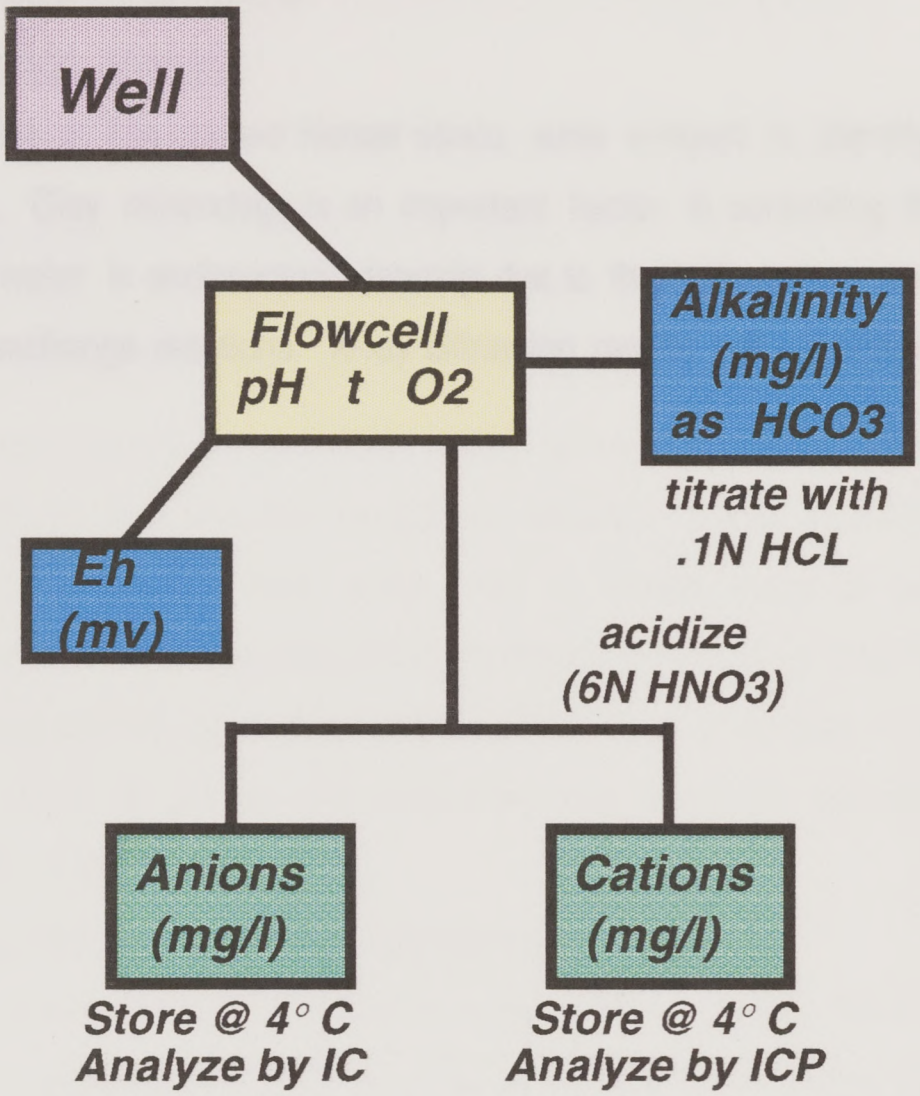

Figure 20. Flowchart of procedures for the measurement of unstable constituents in the field, and collection of groundwater samples for major ion analysis in the laboratory.

oxygen, total Fe, ferrous Fe, phosphate, and ammonia. Results of all water analyses are listed in Appendix G.

X-ray diffraction analysis

Samples of fine-grained Hensel strata were x-rayed to identify classes of clay minerals. Clay mineralogy is an important factor in controlling the major ion chemistry of water in sedimentary deposits due to the high surface area available for chemical exchange reactions. X-ray diffraction results are presented in the next chapter.

Results of Field Observations and Water Chemistry Analyses

Field observations

Observations and measurements made in the field provide a basis for developing a conceptual hydrogeologic model of the study area. Field observations were made of topography, soils, streams, storm runoff, springs, vegetation, and rock outcrops. Measurements included static water levels, saturated thicknesses, major ion concentrations, and unstable constituent values. These measurements, and interpretations of existing data, were used to create maps of potentiometric surfaces, flowlines, recharge distribution, hydraulic conductivity distribution, redox potential, hydrochemical facies distribution, and locations of contact springs. These results were used to set up the finite-difference model of ground-water flow. Summaries of results follow.

Topographic divide on top of the Edwards Plateau

The relatively flat-lying upland surface of the Edwards Plateau (Segovia Formation) is a geomorphically old terrain in comparison to the highly dissected zone near the edge of the Plateau. Pictured in Figure 21 is the topographic (and hydrologic) divide at the higher elevation boundary of the study area. Years of overgrazing on open rangelands stripped grasses, soil erosion, and soil compaction. This created the type of landscape locally referred to as a "goatscape." Surface water runoff is probably higher now than it was in the past, even though focused recharge is hypothesized to be prevalent on the flat surfaces of the plateau. Widespread shallow depression storage is observed to occur on this surface after storms, so it is likely that some of the trapped water percolates downward to recharge the Edwards aquifer. Recharge rates at the plateau are estimated in the mathematical flow model chapter.

Figure 21. Flat-lying surface of the Segovia Formation (Edwards Group). Grazing since the mid-nineteenth century has contributed to extensive soil erosion. This is the recharge area for the upper unconfined aquifer.

Fractures and bedding planes in the Edwards Group Formations

Vertical fractures are observed throughout the Edwards Plateau (Figure 22). The dominant trend directions are approximately N40°E and N40°W. These match the dominant fracture trends inferred from lineaments mapped on aerial photos in the southern part of the Edwards Plateau (Wermund, and others, 1978). The outcrop in Figure 22 is typical for the Edwards Plateau; it shows the interconnectivity that exists between fractures and bedding planes which gives the Edwards an effective porosity of approximately one percent (Robert Mace; pers. comm., 1995). Secondary porosity forms along fractures and bedding planes, and develops in some horizontal beds by dissolution of burrow fillings and by karst breccia (Sharp, 1990; Maclay and Small, 1984; Rose, 1972). Primary porosity exists within grainstones in the form of intergranular pores. Interflow and diffuse ground-water flow, move in an approximate stair-step fashion down fractures, then laterally within permeable beds and along bedding planes. Infiltration of rainwater is favored where fractures intersect the ground surface.

Collapse breccia in the Kirschberg Evaporite Member

A collapse breccia zone occurs at the top of the Fort Terrett Formation (Figure 23). This breccia formed when resistant beds of limestone collapsed in upon a dissolution zone previously occupied by gypsum that had accumulated in the Lower Cretaceous Kirschberg Lagoon (Figure 17). After the gypsum was dissolved by circulating ground water, the less soluble overlying beds collapsed into the space vacated by the evaporites to form a breccia with a higher permeability (Peter Rose; pers. comm., 1995). This breccia allows water to infiltrate the formation at locations where it has become exposed by erosion. Locally, however, porosity and permeability may be reduced where voids have been filled with caliche and soil. Because gypsum is completely dissolved in these zones, the hydrochemistry of the Edwards aquifer does not reflect contact with gypsum.

Figure 22. Hydraulically connected fractures and horizontal bedding planes in the Edwards Group serve as conduits for flow in the unsaturated and saturated zones. A pocket knife at the bottom center of the photograph serves as scale.

Figure 23. Zone of collapse breccia occuring at the top of the Fort Terrett Formation (Edwards Group). Conduits for the infiltration of rainwater exist here due to dissolution of the Kirschberg Evaporite horizon and the consequent collapse of overlying beds.

Contact springs in the Edwards Group Formations

In the foreground of Figure 24 is a concrete structure that serves to capture intermittent spring flow from the Segovia Formation. The concrete structure fills with spring water, and then the water is piped downhill to a stock tank (Figure 25). The source of this water is a contact spring that discharges water from the foot of a colluvial slopewash deposit upslope of the collection structure (Figure 26). This small spring and numerous others occur where bedding planes and/or fractures intersect the sloping ground surface that truncates the ground-water flowpaths. The total discharge from these springs is impossible to measure due to the small size of the springs, their ubiquity, unpredictable discharge schedules, and physical inaccessibiity. Instead, an estimate of spring discharge as a percentage of recharge will be made later by assigning drains to a line of cells within a finite difference flow model.

Discharge from these springs has declined over the last several decades possibly due to the spread of juniper and mesquite trees which use large amounts of soil moisture (Figure 8). The sparse coverage of trees observed in photographs taken earlier in the century, in conjunction with landowner interview reports of higher and more consistent spring discharge in the past, support the contention that spring discharge has declined over time due to these trees. A similar conclusion was reached by Dugas and Hicks (1994) for the Seco Creek Watershed in Texas. They removed trees from an area in the watershed and measured spring discharge before and after the removal. Spring discharge increased after the trees were removed.

Figure 24. The concrete structure in the foreground was designed to capture and pipe spring water to a cattle reservoir. Reduced spring flow to this structure in recent decades, possibly due to the growth of phreatophytes, and the associated increased evapotranspiration, necessitated the drilling of a well.

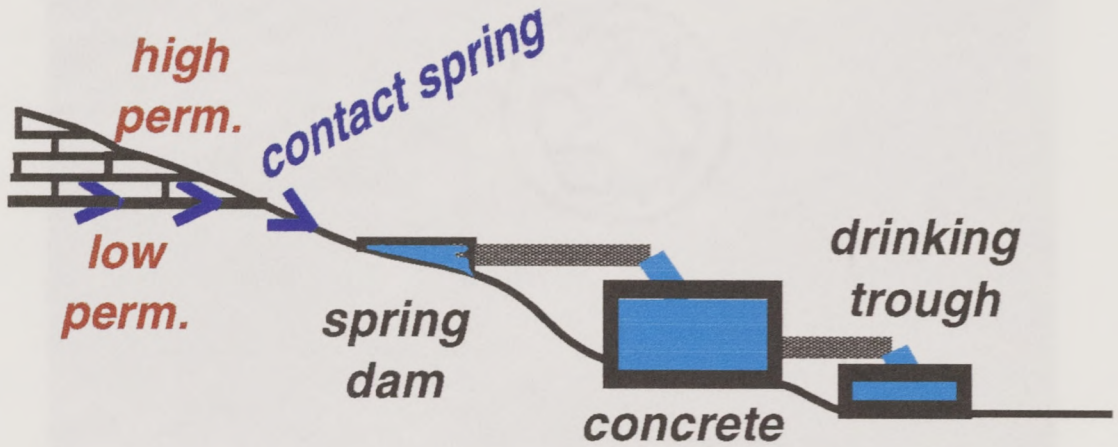

Figure 25. Conceptual diagram showing how the limited volume of water exiting a contact spring in the Segovia Formation (Edwards Group) is captured to fill a livestock reservoir.

Figure 26. Spring water exits the Segovia Formation (Edwards Group) onto a dry streambed from beneath a colluvial slopewash deposit.

Aerial photographs of tree growth patterns on the sides of mesas

Trees growing in distinct patterns are observed in aerial photographs (Figure 27). This pattern is probably related to springs (ground water discharge) and seeps (interflow discharge) along fractures, bedding planes, and higher permeability beds exposed on the mesa slope faces (Figure 28). An example of a discharge point on the face of a tributary canyon is pictured in Figure 6. Note the staining beneath fractures and bedding planes that has been caused by precipitation of minerals from discharging water. The heaviest concentrations of trees occur on the southeastern sides of the mesas because ground water flows along gently dipping bedding planes in that direction. Evaporation from the ground surface, together with evapotranspiration from these trees, constitutes the largest sink in the overall hydrologic cycle here.

Exposure of Lower Cretaceous geological contacts

The outcrop in Figure 12 shows exposures of the fractured Fort Terrett Formation at top, the unfractured Basal Nodular Member of the Fort Terrett in the middle, and the calcareous siltstone of the Hensel Sand Formation at the bottom. The Basal Nodular Member possesses a more consistent density and lithology than the overlying Burrowed Member of the Fort Terrett Formation (Rose, 1972). It is the lowest occuring bed of several low permeability beds in the Edwards Group that causes bedding anisotropy (low K_z/K_x). An even lower value of vertical anisotropy would exist if vertical fractures were not present to provide conduits for downward percolation.

Llano River

The Llano River is a tributary of the Little Colorado River (Figure 29). It receives water from two main tributaries, the North Llano River and the South Llano River, which together drain an area of 4,789-square km. (1,849-square miles). The Llano is a perennial, predominantly effluent river, fed by spring discharge from the

Figure 27. Low altitude aerial photograph of a portion of the study area. Note the pattern of tree growth. It is believed that this pattern is related to the discharge of ground water via contact springs in the flat-lying rocks.

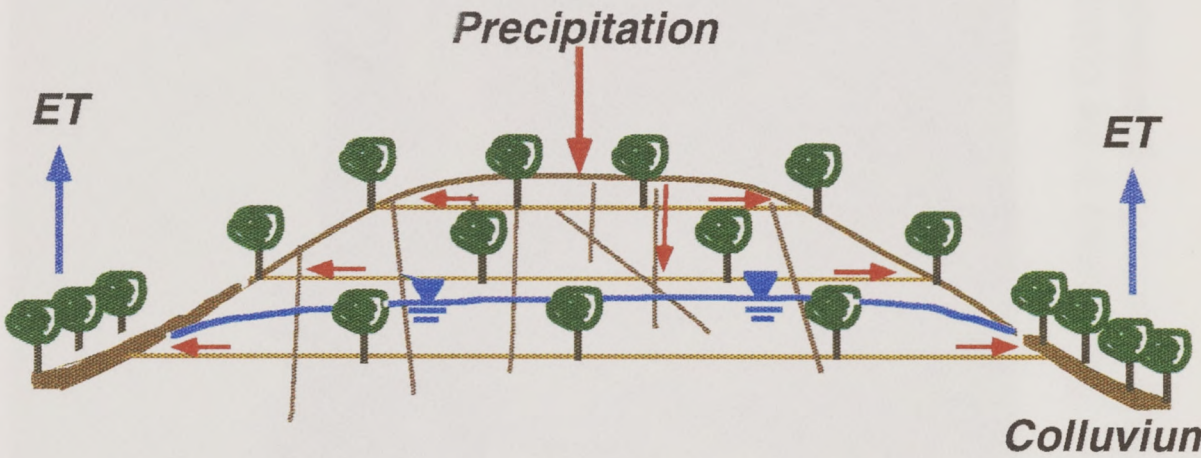

Figure 28. Conceptual diagram showing how phreatophytes grow in distinct rings around mesas of the Edwards Plateau to exploit contact springs that discharge from horizontal bedding planes.

Figure 29. The Llano River. This tributary to the Colorado River serves as the primary discharge area for the groundwater system.

Edwards aquifer, and baseflow seepage from the Hensel aquifer. It maintains an average daily flow during the low-flow months of December and January of approximately 233,800 cubic meters (8,256,072 cubic feet) at the Junction, TX stream gauge, located a short distance upstream of the study area (Appendix F). The amount of baseflow seepage added to the Llano River as it flows past the study area is estimated in the mathematical model chapter.

Potentiometric surfaces

Static water levels were measured in over one hundred water wells completed in both the Hensel and the Edwards aquifers (Figures 30 and 31, and Appendix D). Water table elevations were contoured and two separate potentiometric surfaces were defined (Figure 32). Several water wells, completed within both aquifers, were excluded from the dataset because their water levels represented a composite of the potential from each aquifer. Study objectives required development of maps and datasets for distinct aquifers.

Separate water tables were mapped in the area; one for the Edwards aquifer (under the Plateau), and one for the Hensel aquifer (beneath the Llano River floodplain). It was not possible to measure the potential in the part of the Hensel aquifer that occurs beneath the Edwards because there are no wells that penetrate the entire thickness of the Edwards, and draw from the Hensel aquifer only. Hydraulic heads in this part of the Hensel aquifer had to be predicted with the numerical flow model.

Measured water table elevations in the Edwards aquifer ranged from 584 to 628 meters (1,918 to 2,060 feet). Water table elevations in the Hensel aquifer ranged from 463 to 529 meters (1,520 to 1,737 feet). Farther back under the Plateau, toward the point occuring directly below the topographic divide, it is possible that the potential of the Hensel aquifer increases to an elevation equal to or exceeding that of the confining bed at the base of the Edwards, but not as high as heads in the

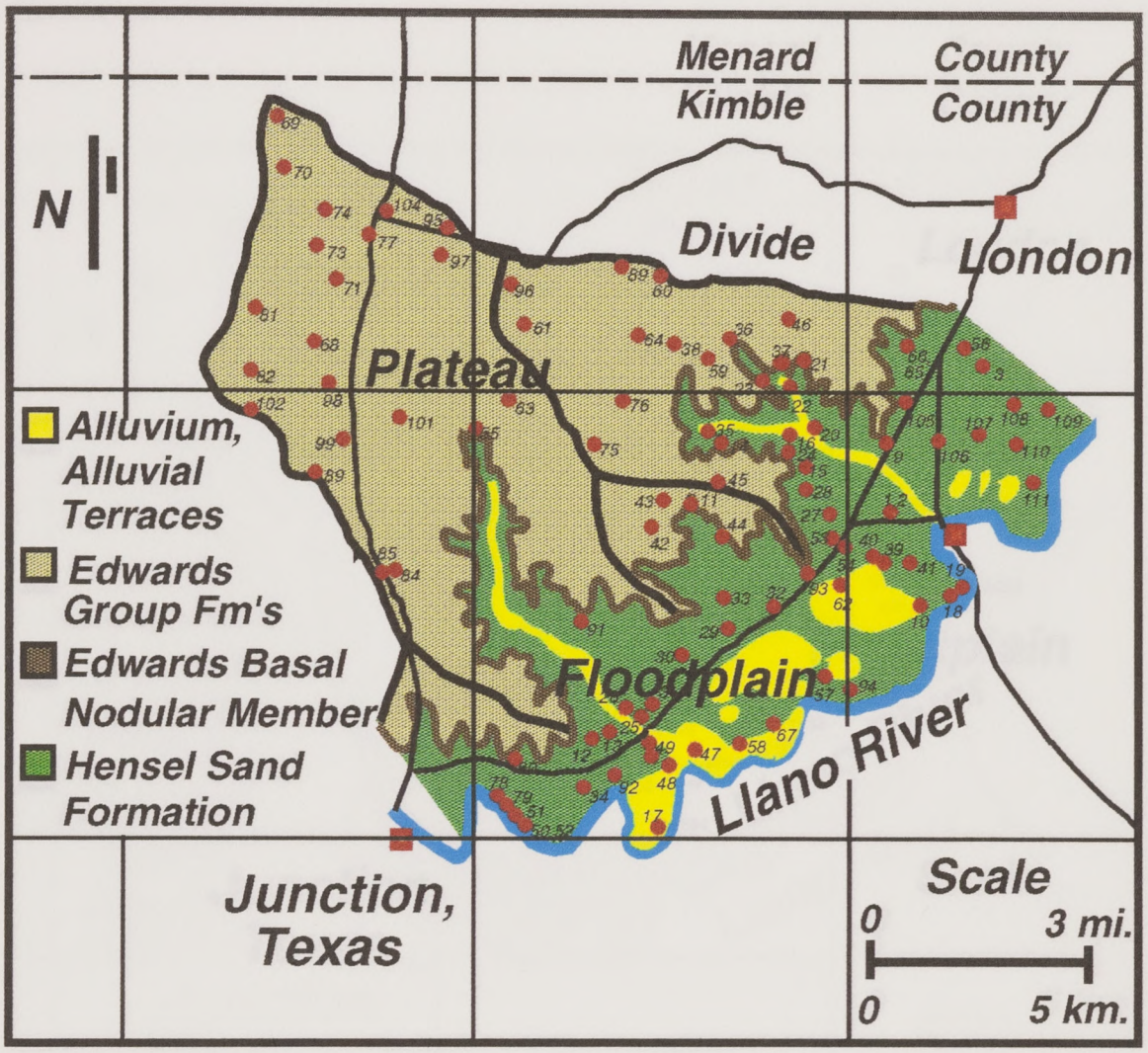

Figure 30. Locations and project numbers of water wells used to measure the depths to water for water table elevation calculations. Well specifics are listed in Appendix D.

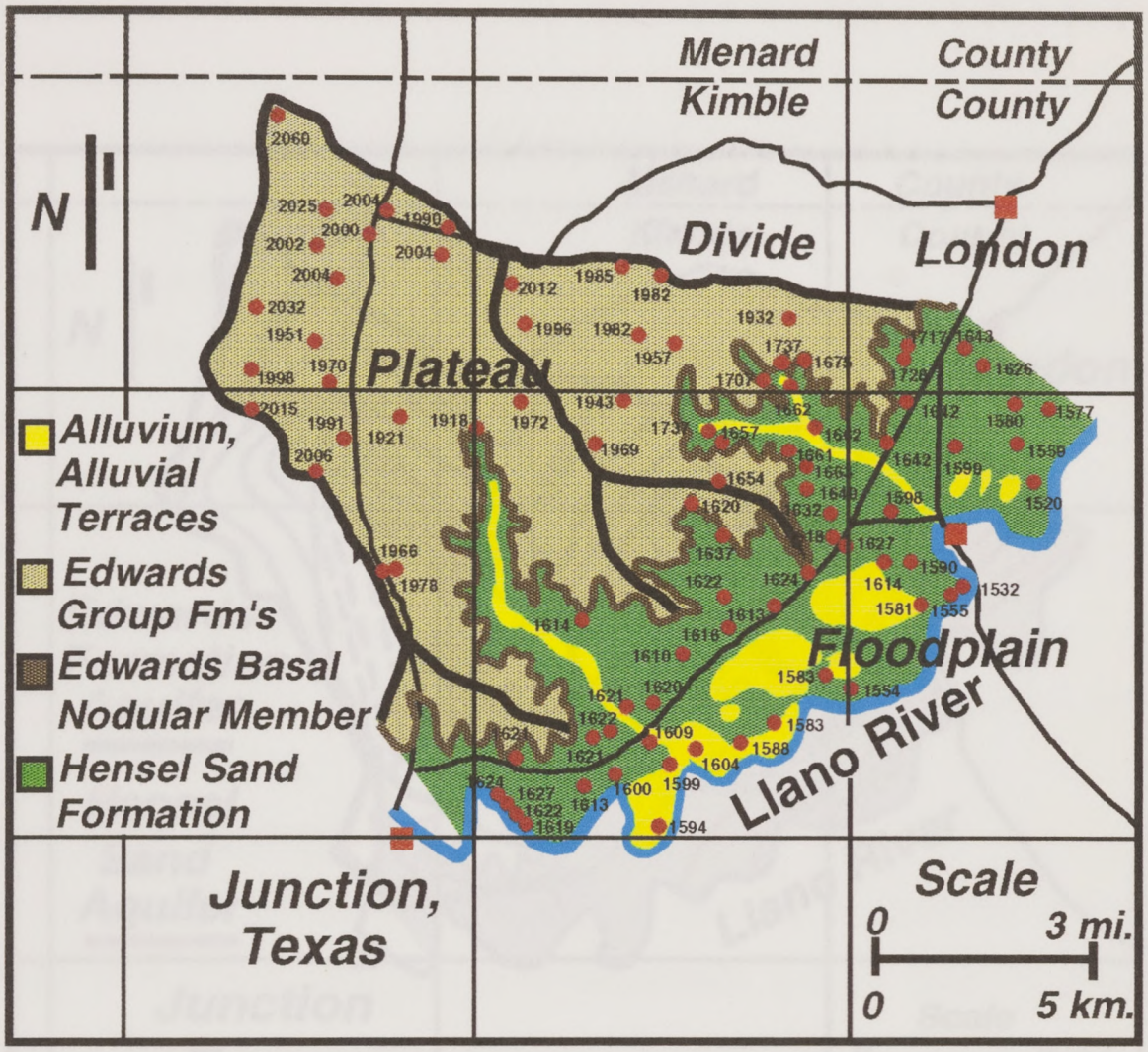

Figure 31. Water table elevations calculated using steel tape measurements of depth-to-water in wells. These elevations were used to draw potentiometric surfaces.

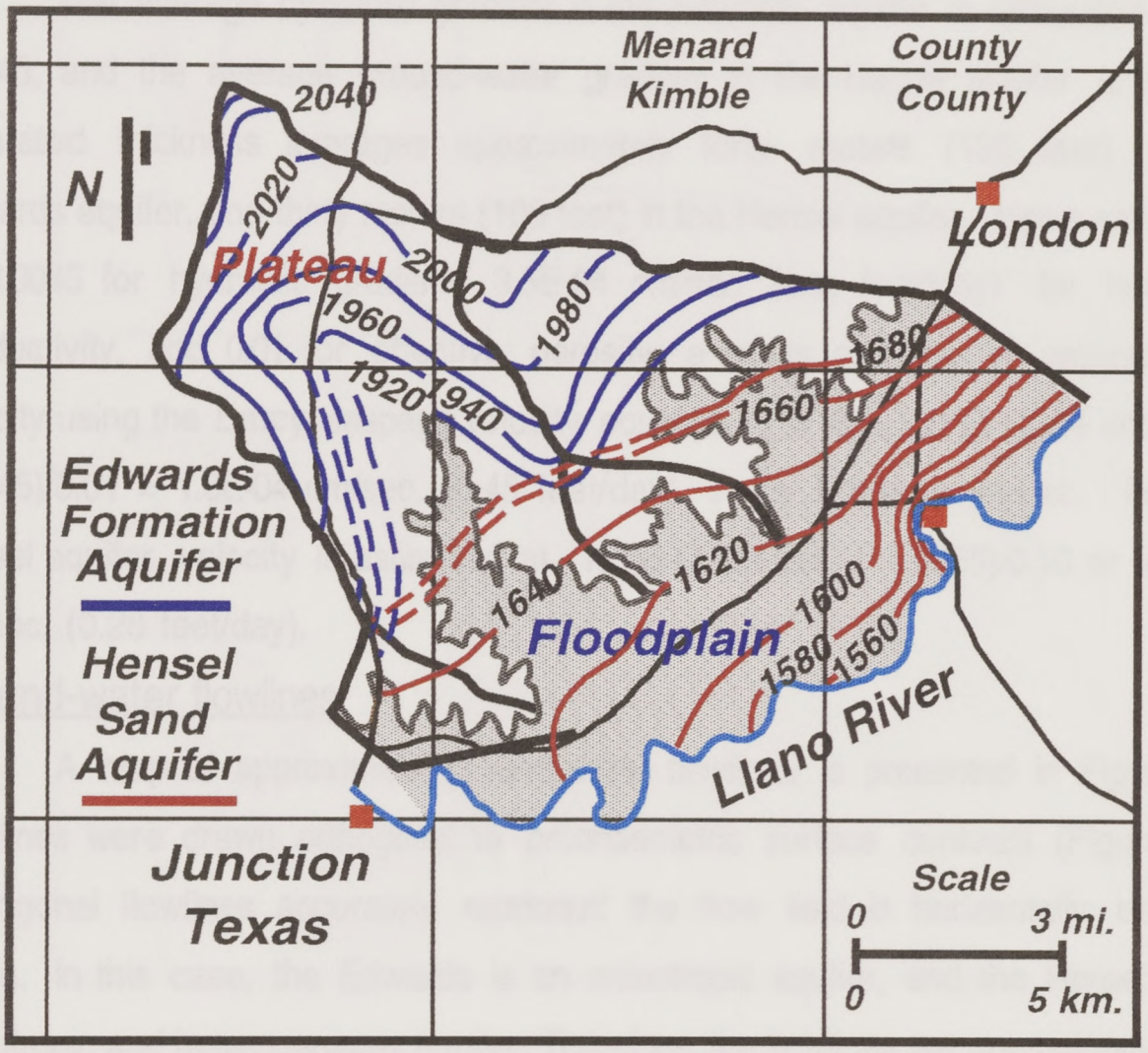

Figure 32. Potentiometric contours for the unconfined Edwards Group aquifer and the unconfined portion of the Hensel Sand Formation aquifer. Contours are dashed where inadequate well control exists.

overlying Edwards aquifer. It is hypothesized, therefore, that there is leakage downward from the higher potential Edwards aquifer to the lower potential Hensel aquifer through this confining bed. This hypothesis is tested in the mathematical model chapter.

The average hydraulic gradient in the Edwards aquifer is calculated to be 0.0045, and the average ground-water gradient in the Hensel aquifer is 0.0055. Saturated thickness averages approximately forty meters (130 feet) in the Edwards aquifer, and thirty meters (100 feet) in the Hensel aquifer. Using estimates of 0.0045 for hydraulic gradient, 3.5E-04 cm/sec (one foot/day) for hydraulic conductivity, and 0.01 for effective porosity, a gross estimate of ground-water velocity using the Darcy seepage velocity equation ($v = ki/n_e$) is (3.5E-04 cm/sec * 0.0045)/0.01 = 1.6E-04 cm/sec. (0.45 feet/day) in the Edwards aquifer. For the Hensel aquifer, velocity is estimated at (1.75E-03 cm/sec * 0.0055)/0.10 or 9.7E-05 cm/sec. (0.28 feet/day).

Ground-water flowlines

A map of approximate ground-water flowlines is presented in Figure 33. Flowlines were drawn orthogonal to potentiometric surface contours (Figure 32). Orthogonal flowlines accurately represent the flow field in horizontally isotropic media. In this case, the Edwards is an anisotropic aquifer, and the Hensel is an anisotropic and heterogeneous aquifer. Therefore, the flowlines are approximations.

Flowlines in the Edwards aquifer converge at the steep tributary valleys incised in the Edwards. Flowlines in the Hensel converge at the Llano River. Plotted on the map are the approximate locations for several strong springs that discharge from the Edwards aquifer. Note that these occur where there is a dense convergence of flowlines.

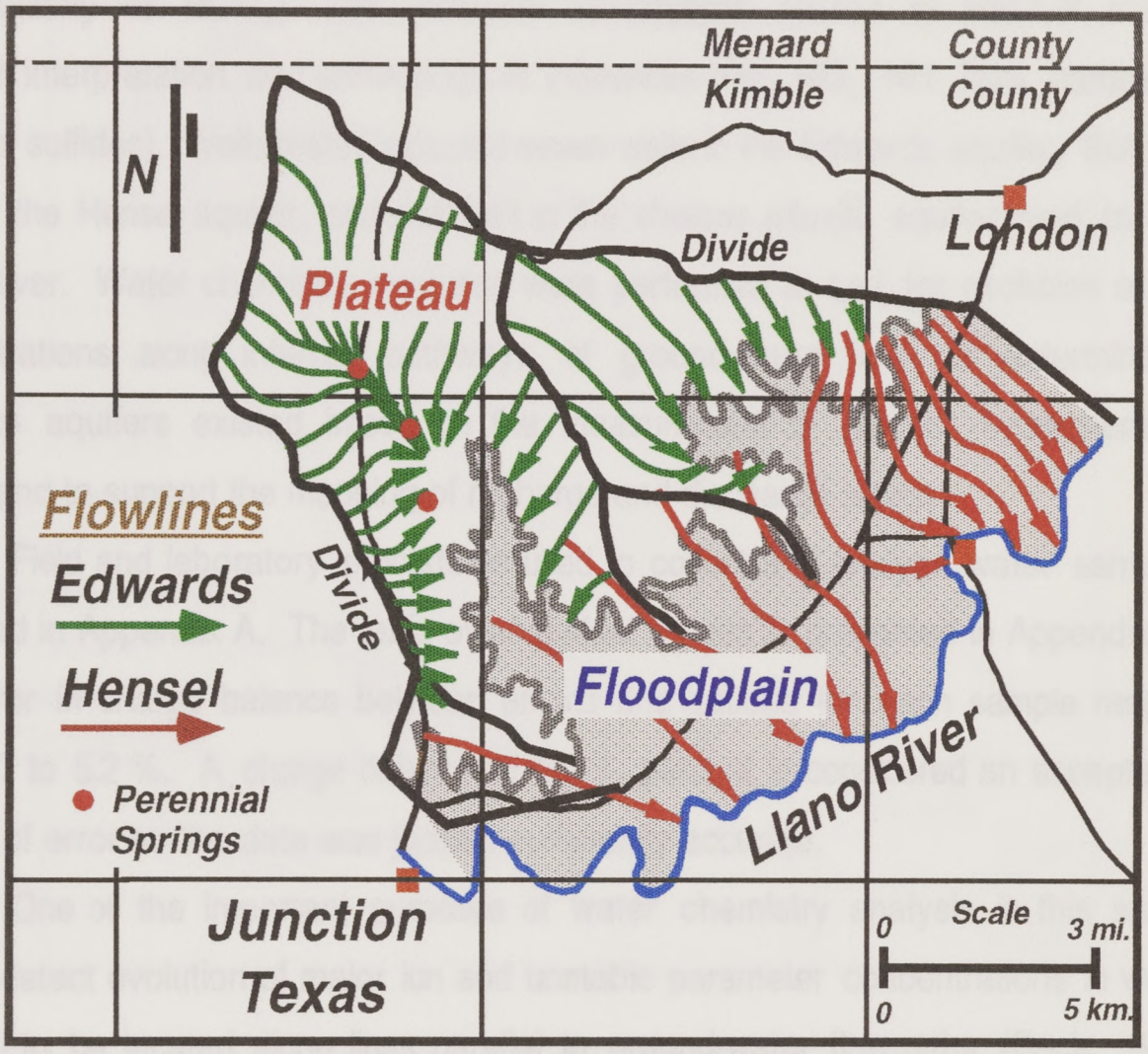

Figure 33. Generalized ground-water flowlines within the Edwards Group aquifer and the Hensel Sand Formation aquifer. Flowlines diverge from recharge areas and converge toward discharge areas such as the three mapped springs.

Water chemistry analyses

Twenty-two wells were selected (Figure 34) for analyses of major ions (Ca, Mg, Na, K, Cl, and SO_4), unstable parameters (pH, Eh, dissolved O_2, temperature, and alkalinity as HCO_3), and additional constituents related to REDOX state, flowpath interpretation, and anthropogenic influences (Fe_2, NO_3, NH, TDS, hardness, and total sulfides). Wells tested included seven wells in the Edwards aquifer, thirteen wells in the Hensel aquifer, and one well in the shallow alluvial aquifer next to the Llano River. Water chemistry analyses were performed to test for evolution of ion concentrations along inferred pathways of ground-water flow, to determine if separate aquifers existed based on the measurement of distinct hydrochemical facies, and to support the mapping of recharge and discharge areas.

Field and laboratory procedures used to collect and analyze water samples are listed in Appendix A. The table of analytical values is presented in Appendix G. The error in charge balance between anions and cations for each sample ranged from 0.7 to 5.2 %. A charge balance of 5.0 % percent is considered an acceptable margin of error so the data was judged sufficiently accurate.

One of the important purposes of water chemistry analysis in this study was to detect evolution of major ion and unstable parameter concentrations in wells believed to be located along lines parallel to ground-water flowpaths (Back, 1966; Chebotarev, 1955). Chebotarev explained that ground water tends to evolve chemically toward the composition of seawater. He observed that this evolution was normally accompanied by the following regional change in dominant anion species:

travel along flowpath (increasing age) $\longrightarrow$

$$HCO_3^- \longrightarrow HCO_3^- + SO_4^{2-} \longrightarrow SO_4^{2-} + HCO_3^- \longrightarrow SO_4^{2-} + Cl^- \longrightarrow Cl^- + SO_4^{2-} \longrightarrow Cl^-$$

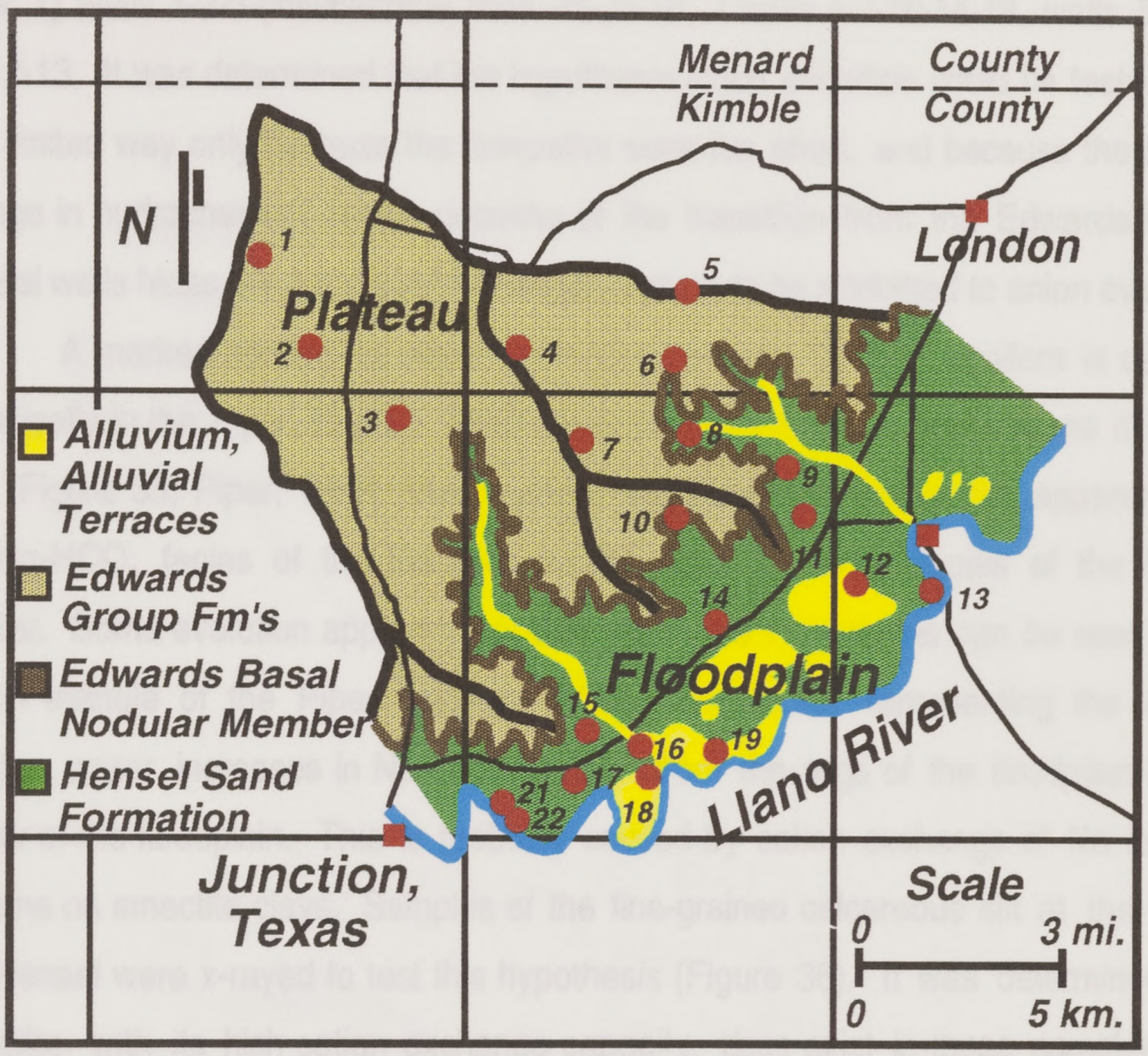

Figure 34. Locations of wells used to sample ground water for major ions, selected minor ions, and unstable constituents.

Wells located along three transects extending from the upland area to the center of the floodplain were included in the analysis (Figure 34). These transects were: 1) wells 1-2-3-(inaccessible zone)-15-16-18, 2 wells 4-7-10-14-19, wells 5-6-8-9-11-12-13. It was determined that the hypothesis of ion evolution could be tested here in a limited way only because the flowpaths were too short, and because the abrupt change in hydrochemical facies occuring at the transition from the Edwards to the Hensel wells hides the more subtle changes that could be attributed to anion evolution.

A marked contrast in water chemistry between the two aquifers is depicted graphically in the Piper diagram which displays the relative concentrations of major ions (Figure 35, Piper, 1953). Two distinct hydrochemical facies are apparent; the Ca-Mg-HCO_3 facies of the Edwards aquifer, and the mixed facies of the Hensel aquifer. Some evolution apparently occurs within the Hensel; this can be seen in the cation triangle of the Piper diagram. Along the vector representing the Hensel aquifer, water increases in Na concentration from the edge of the floodplain to the center of the floodplain. This is probably caused by cation exchange of Na ions for Ca ions on smectite clays. Samples of the fine-grained calcareous silt at the top of the Hensel were x-rayed to test this hypothesis (Figure 36). It was determined that smectite, with its high cation exchange capacity, does exist in these samples (Leo Lynch; pers. comm., 1995), thus, evolution probably occurs as a result of this phenomenon. Referring to Figure 37 it is observed that not only is there a high Na concentration in the Hensel aquifer relative to the Edwards, but also a high Cl concentration. High Cl is most likely caused by the dissolution of halite. Likewise, the high measured Na concentrations are probably due in part to halite dissolution. The Hensel was deposited in a semi-arid to arid, near-shore environment where sahbka conditions existed periodically (Stricklin, and others, 1971). It is probable that Na, Mg, Cl, and SO_4 in the Hensel aquifer (Figures 37 and 38) are derived from the

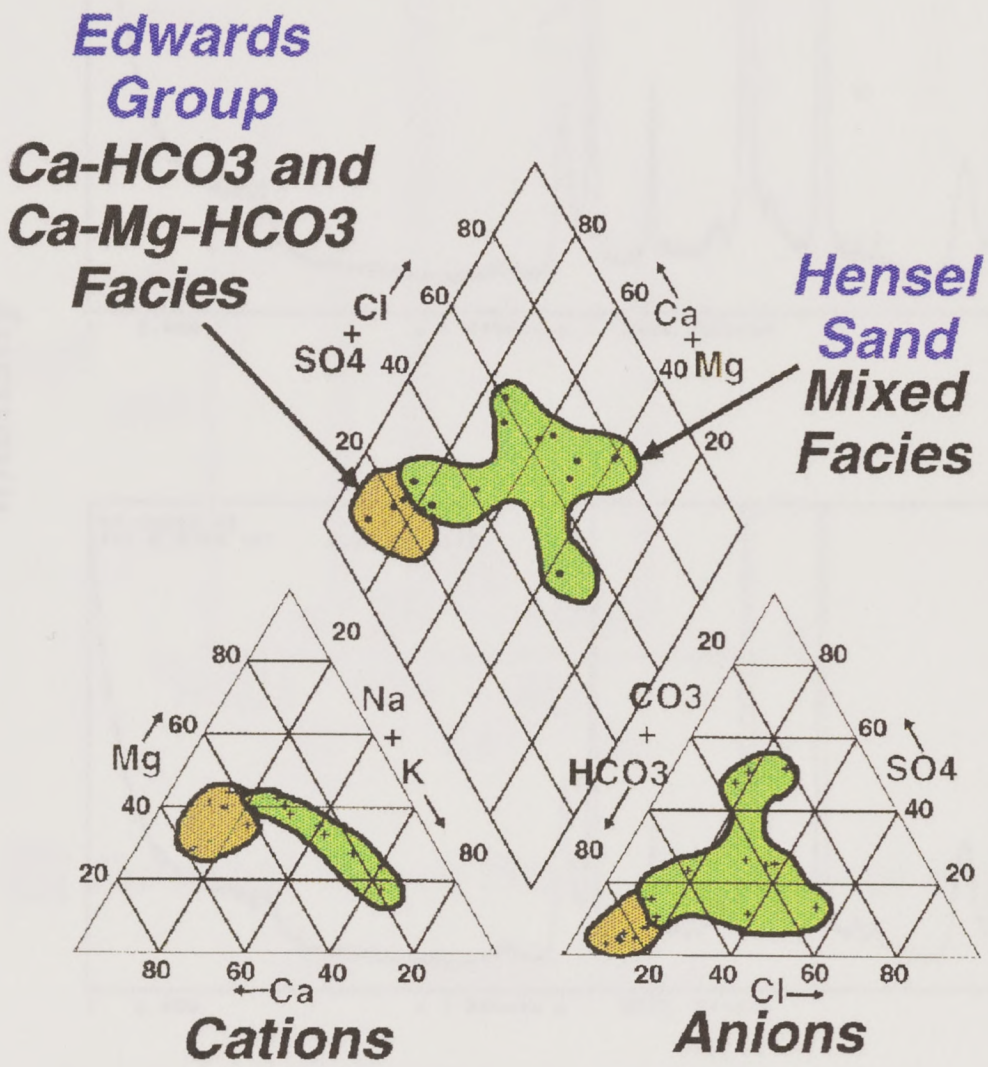

Figure 35. Piper diagram illustrating the relative concentrations of major ions measured in ground water from twenty-one wells in the Edwards aquifer and the Hensel aquifer.

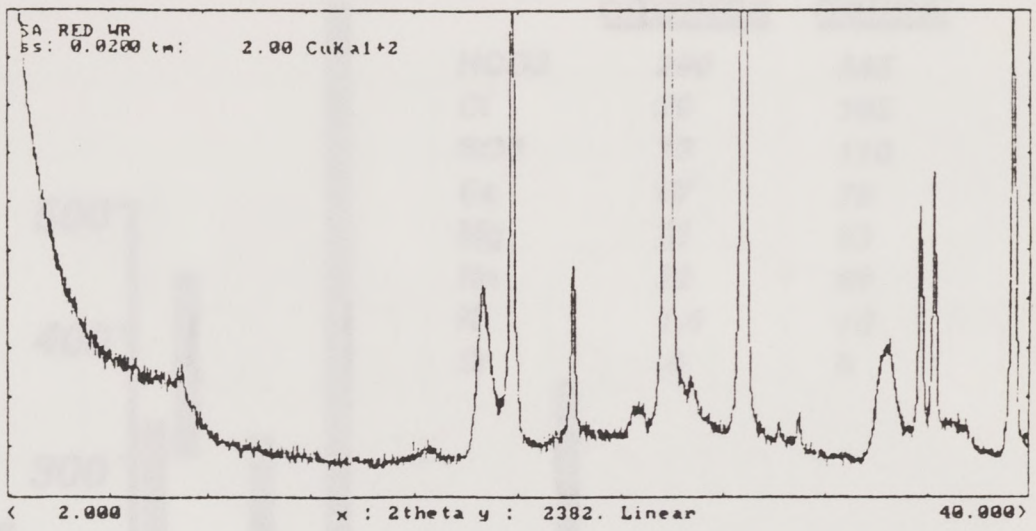

Figure 36. X-ray diffraction patterns for samples of red siltstone (top) and green siltstone (bottom) from an outcrop at the top of the Hensel Sand Formation.

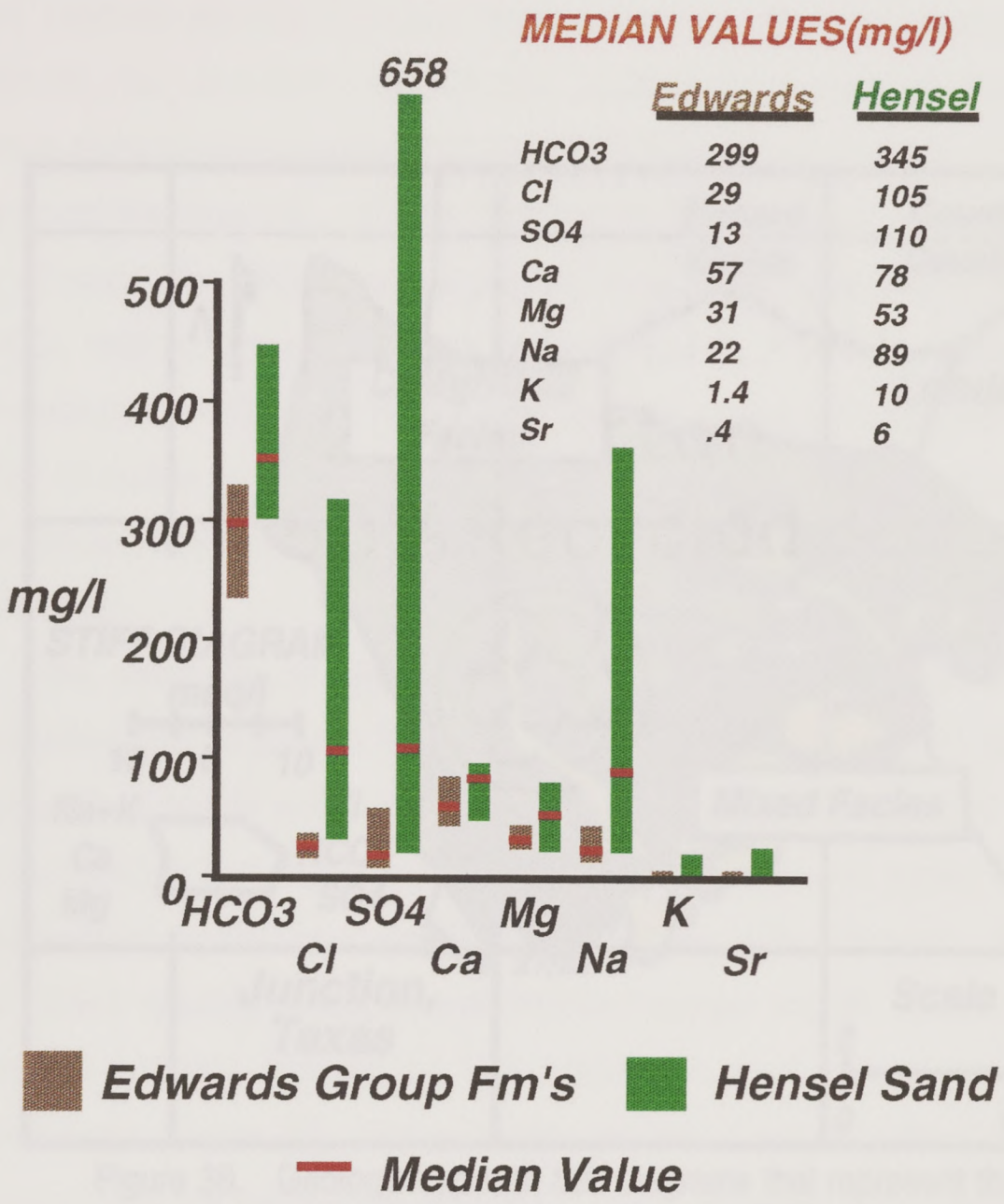

Figure 37. Concentration ranges and median values of major ions in the Edwards and Hensel aquifers. Hensel water samples have higher TDS.

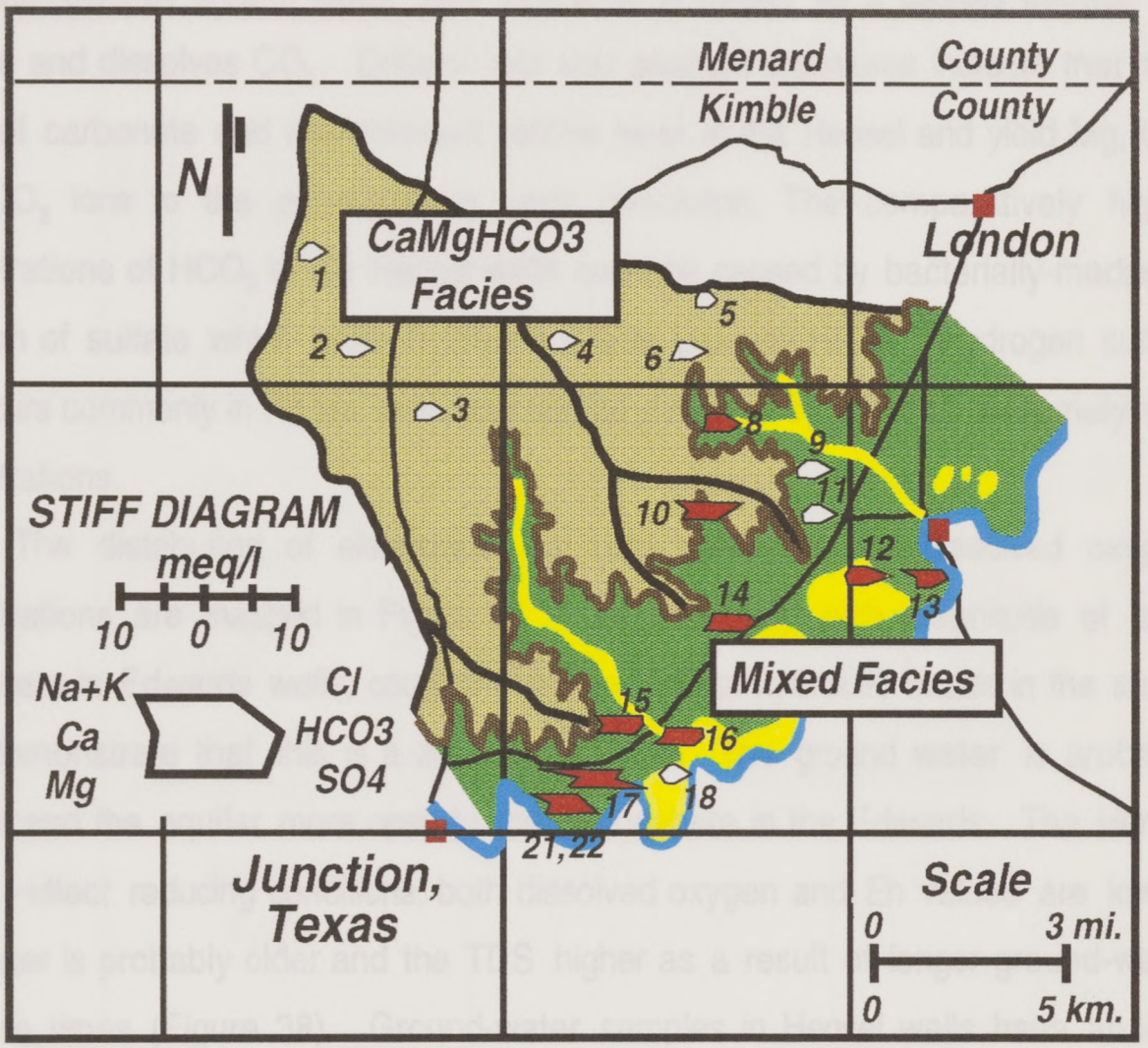

Figure 38. Geology map with Stiff diagrams that represent the spatial distribution of absolute ion values and TDS. The higher the TDS, the larger the size of the diagram.

dissolution of disseminated veins of evaporitic minerals within low permeability, fine-grained, overbank deposits that have withstood flushing. Elevated concentrations of the ions Mg, Ca, and HCO_3 exist in both aquifers as a result of dissolution of carbonate rocks by ground water that increases in acidity as it passes through the soil zone and dissolves CO_2. Drillers' logs and geologic exposures indicate that thin layers of carbonate and disseminated caliche exist in the Hensel and yield Mg, Ca, and HCO_3 ions to the ground water upon dissolution. The comparatively higher concentrations of HCO_3 in the Hensel wells could be caused by bacterially-mediated reduction of sulfate which yields hydrogen sulfide gas and HCO_3. Hydrogen sulfide gas occurs commonly in Hensel wells and can be detected by smell at extremely low concentrations.

The distribution of electrochemical (Eh) potentials and dissolved oxygen concentrations are mapped in Figure 39. The relatively high magnitude of both parameters in Edwards wells, coupled with the highest hydraulic heads in the study area, demonstrate that this is a zone of recharge. The ground water is probably younger and the aquifer more open to the atmosphere in the Edwards. The Hensel waters reflect reducing conditions; both dissolved oxygen and Eh values are lower. This water is probably older and the TDS higher as a result of longer ground-water residence times (Figure 38). Ground-water samples in Hensel wells have an iron taste and a hydrogen sulfide smell as a result of the reduction of iron hydroxide and sulfate by bacteria in the presence of organic matter.

An exception to this overall pattern is observed at the northeastern end of the floodplain (Figures 38 and 39). Here, the dissolved oxygen is intermediate and the Eh potential is high. Closely-spaced potentiometric contours exist here, but without the higher TDS that might be expected in water that is moving through less permeable media. As it turns out, the Hensel thins in this area as it gets closer to

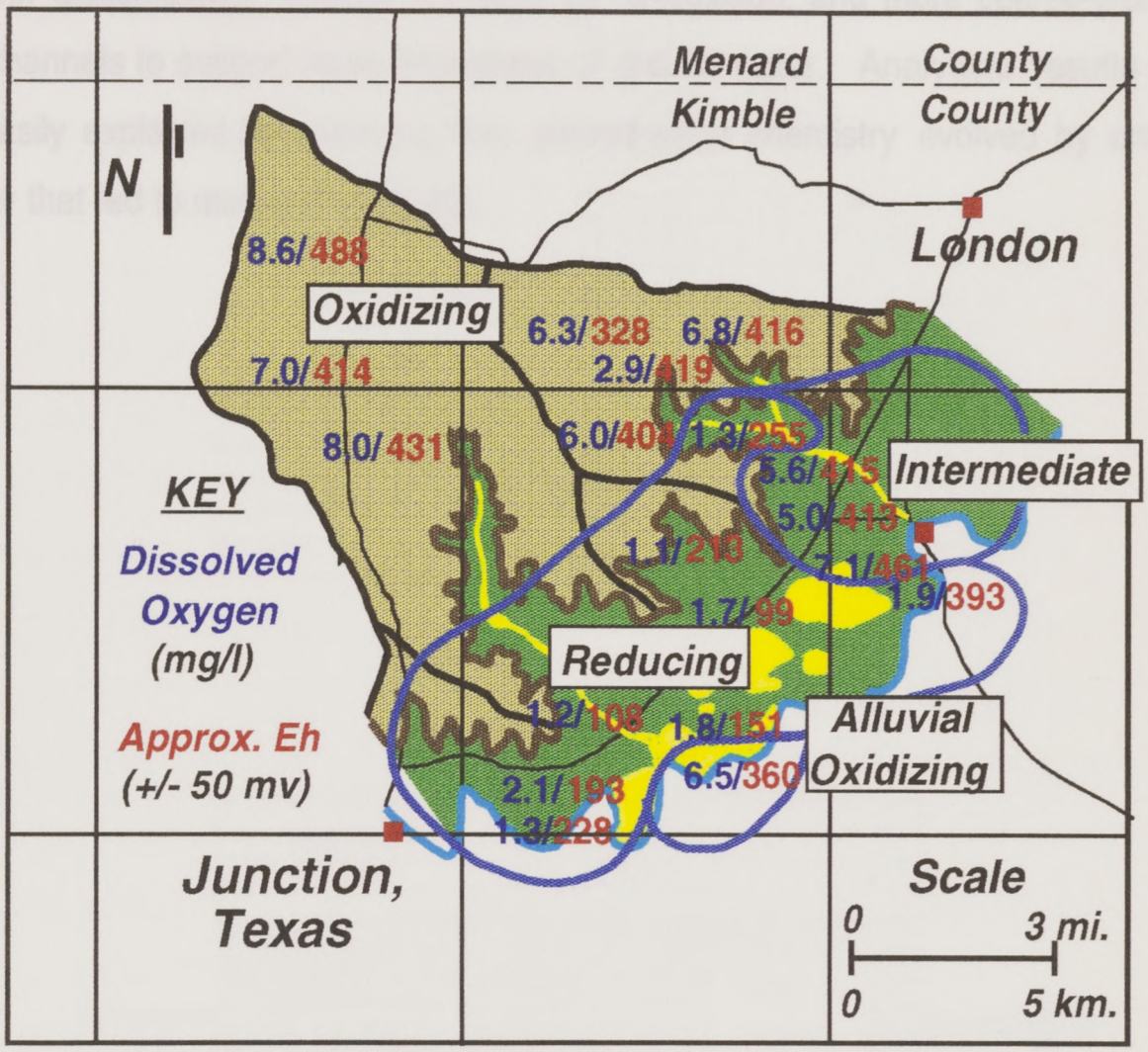

Figure 39. Spatial distribution of dissolved oxygen and Eh. High values of both parameters indicate an oxidizing environment; low values, a reducing environment.

the Llano Uplift, and there are beds of carbonate rock (recorded in drillers' logs) that may serve to slow ground-water flow. At the southwestern end of the floodplain the Hensel is thicker, there is more fine-grained sedimentary rock (recorded in drillers' logs) with disseminated minerals available for dissolution, and more coarse-grained fluvial channels to support rapid throughput of ground water. Analytical results are most easily explained by assuming that ground-water chemistry evolved by cross-bed flow that led to mixing (Figure 40).

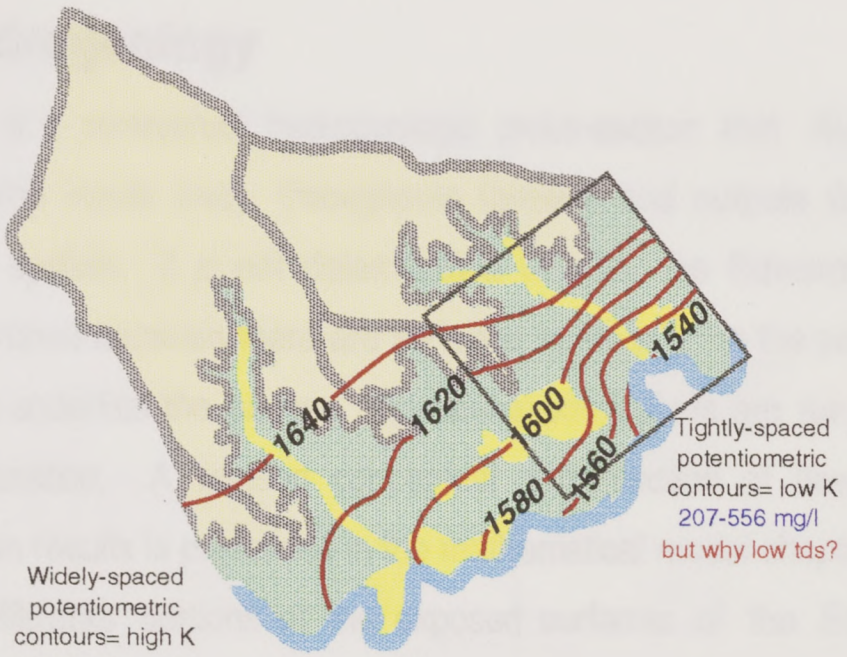

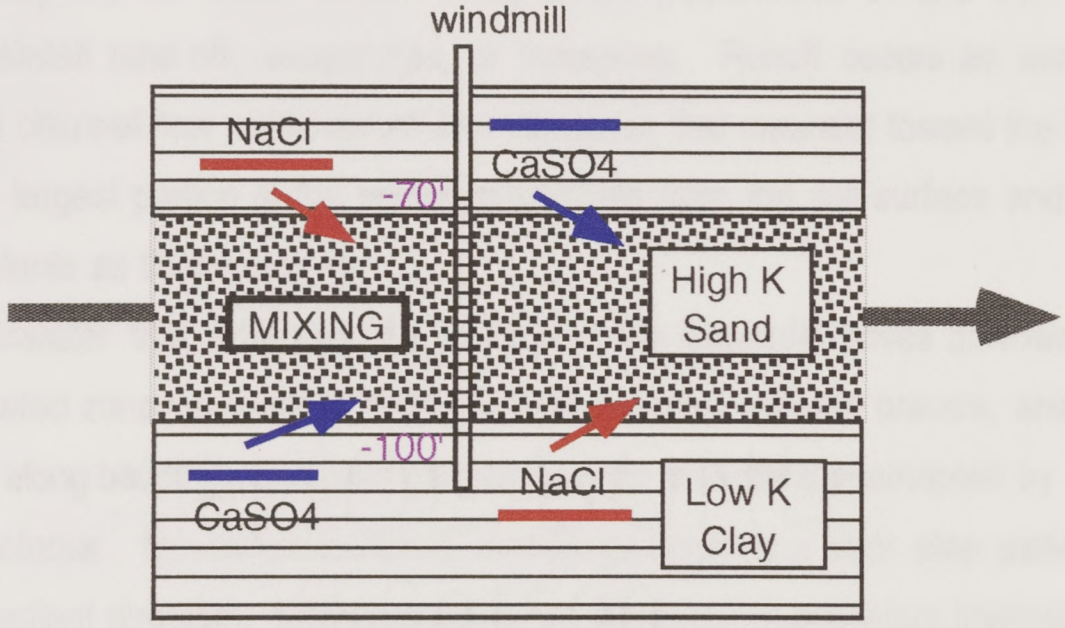

Figure 40. A contrast in potentiometric surface contour densities, and anomalous TDS concentrations, occur in the ground waters from one end of the Llano River floodplain to the other due to a change in lithologic facies. Pictured is the mechanism believed responsible for the co-occurence of high K and high TDS at the southwest end of the floodplain.

Conceptual Model of Ground-Water Flow

Physical hydrogeology

Figure 41 is a conceptual hydrogeologic cross-section that illustrates the architecture, and the inputs (red), throughputs (green), and outputs (blue) of the ground-water flow system. It is not determinable whether the Edwards aquifer is partially or fully perched because there are no water level data for the portion of the Hensel aquifer that underlies the plateau. Numerical simulations are run to attempt to answer this question. A revised conceptual cross-section of flow based on numerical simulation results is presented in the mathematical model chapter.

Rainfall infiltrates portions of the exposed surfaces of the Edwards and Hensel to recharge the aquifers within these formations. The amount of rainfall recharging the aquifers is calculated at approximately 5.06 percent or 3.10 cm/year (1.22 inches/year) of mean annual precipitation (Appendices B and F). The remaining rainfall runs off, evaporates, or transpires. Runoff occurs as overland flow and as channel flow within ephemeral tributaries that meander toward the Llano River. The largest portion of the rainfall evaporates from the soil surface and from trees and plants as they transpire.

Rainwater that infiltrates the surface of the Edwards moves downward in the unsaturated zone via vertical fractures and zones of collapse breccia, and then horizontally along bedding planes and permeable beds, until being intercepted by other vertical fractures. Movement therefore, occurs generally in a stair step pattern in the downgradient direction. Where structural or stratigraphic pathways intersect the escarpment surface in tributary valleys, water exits there in the form of seeps. If rainwater infiltrates the flat top of the plateau surface close to the edge of a mesa (thus having a short flowpath) it may be short-circuited (as interflow) to one of these seepage points. The infiltrating rainwater that does not seep out of the

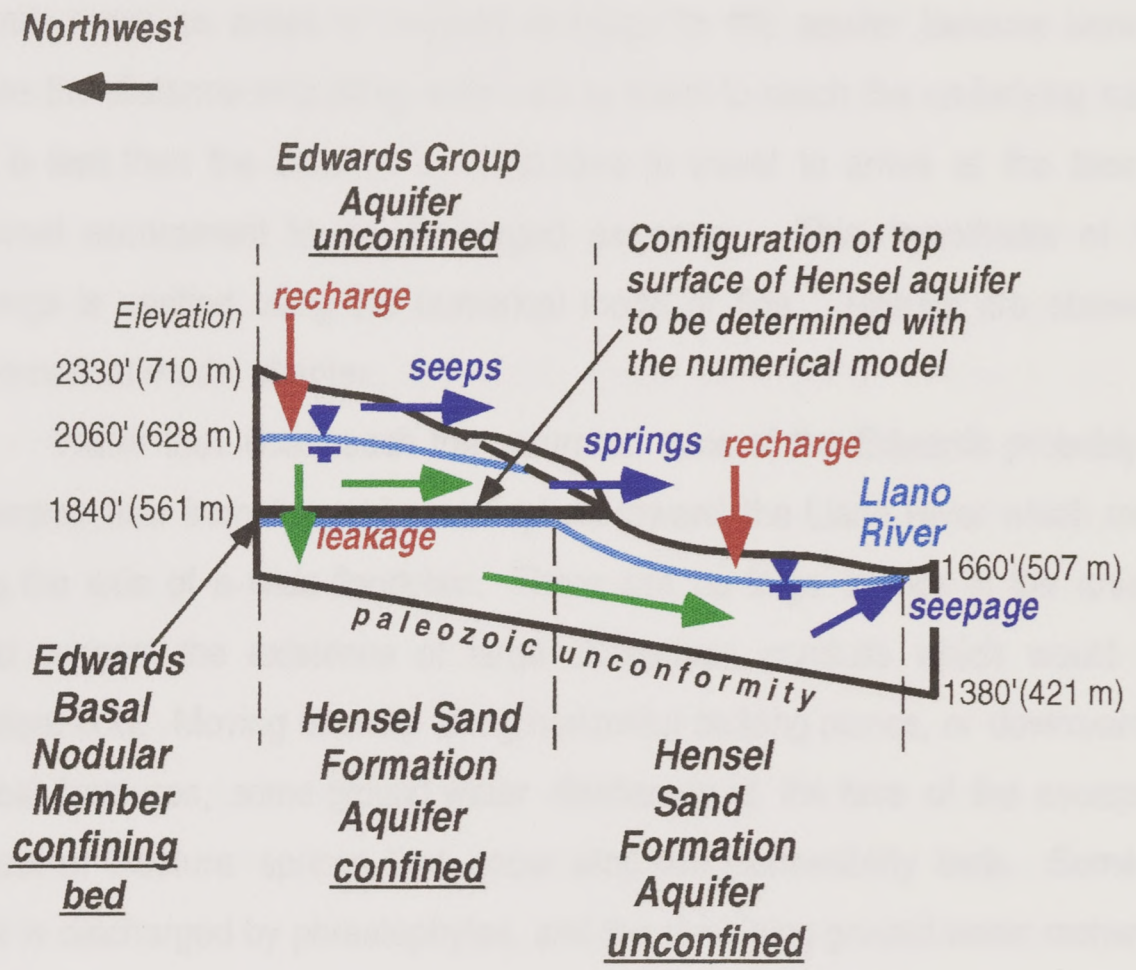

Figure 41. Conceptual cross-section of the study area illustrating the architecture, and inputs (red), throughputs (green), and outputs (blue) of the ground-water flow system.

system at these points continues to move downward until it recharges the unconfined aquifer. Rainwater that infiltrates the surface at the topographic divides between subwatersheds probably reaches the aquifer as recharge. It is likely that these summits serve as areas of focused recharge to the aquifer because beneath the divides the distance infiltrating water has to travel to reach the underlying saturated zone is less than the distance it would have to travel to arrive at the face of the erosional escarpment to be discharged as seeps. This hypothesis of focused recharge is verified using the numerical model of flow. Results are shown in the mathematical model chapter.

Water that does reach the saturated zone of the Edwards probably moves as laminar flow from the carbonate upland toward the Llano River which meanders along the axis of a wide floodplain. There are no large springs in the area which would suggest the existence of large subsurface conduits which would support turbulent flow. Moving laterally along horizontal bedding planes, or downward within vertical fractures, some ground water discharges at the face of the escarpment in contact or fracture springs that occur atop low permeability beds. Some ground water is discharged by phreatophytes, and the remaining ground water recharges the underlying Hensel aquifer by cross-formational flow. Spring discharge and cross-formational flow are quantified in the numerical model.

Downward leakage of ground water to the Hensel aquifer occurs through a fifteen foot thick marly limestone bed (Basal Nodular Member) which is present throughout the region forming the base of the Edwards. The Hensel Sand Formation forms a sediment wedge that is approximately 20 meters (66 feet) thick below the main west-east topographic divide in the study area, and increases to more than 300 meters (1000 feet) in thickness southeast of the Plateau region (Cartwright, 1932). As a result, the saturated thickness of the Hensel aquifer decreases toward the northwest until the formation pinches out beyond the study area.

It was not possible to estimate precisely the saturated thickness of the Edwards aquifer because wells do not fully penetrate the saturated zone, and because the thickness of the host formations is variable. A range of 20 to 64 meters (66 to 210 feet) was calculated by subtracting the average elevation of the flat-lying Edwards-Hensel contact from water-table elevations measured in the Edwards aquifer wells.

Ground-water flow in the Hensel aquifer at the western end of the floodplain occurs by preferential movement along relatively high permeability sand and gravel fluvial channel deposits encased within lower permeability overbank and sahbka deposits (John Ashworth, pers. comm., 1994). Ground water exits the Hensel aquifer by seeping into the Llano River which operates as the regional base level across which no ground water can flow. A small part of its flow is captured by low capacity livestock and domestic wells which occur at a density of less than one/square mile.

It is not likely that a great volume of the Hensel ground water moves downward into the Paleozoic rocks because the Paleozoics are less permeable than the Cretaceous rocks; and they host aquifers which are highly compartmentalized (Barker and Ardis, 1992). Gamma-neutron logs from oil tests fifty miles to the southwest provide independent evidence for this claim. The cross-section of these logs demonstrated that below the Cretaceous (i.e., below the Wichita Paleoplain Unconformity), the log response over most of the upper 150 meters (500 feet) of Paleozoic rocks surpasses the magnitude established as the "shale line." Therefore, the permeability of the Paleozoic formations is probably low. Contrasting this, the magnitude of the gamma-neutron response within the overlying Cretaceous rocks is uniformly lower than the "shale line" value (Erica Boghici, pers. comm., 1995).

The saturated thickness of the unconfined portion of the Hensel aquifer could not be determined exactly. A range of 15 to 70 meters (50 to 225 feet) was

calculated by subtracting elevations of the Hensel/Paleozoic contact from elevations of the water table.

Chemical hydrogeology

Figure 42 is a conceptual cross-section of the study area which shows the dominant hydrochemical species found in each aquifer and the hydrochemical mechanisms believed responsible for their occurance.

In the Edwards, water infiltrating the surface dissolves carbon dioxide in the soil zone to reduce the pH of the water that recharges the aquifer. This ground water then slowly dissolves the limestones and dolomites of the Edwards to yield low concentrations of dissolved Ca, Mg, HCO_3, and total dissolved solids (TDS, 279 to 418 mg/l). High dissolved oxygen (DO) (6.0 to 8.6%) and high electrochemical potential (Eh) (328 to 488 mV), in conjunction with the highest hydraulic heads in the study area, demonstrate that this is a recharge zone (see Figures 32 and 39).

In the Hensel aquifer, low concentrations of dissolved Ca, Mg, and HCO_3 are attributed to the dissolution of the carbonate beds and caliche that can be seen in outcrops, and by cross-formational transfer of Edwards waters. Elevated concentrations of Cl are derived from dissolution of halite that accumulated in nearshore Cretaceous sahbkas (Stricklin and others, 1971). Elevated concentrations of Na are caused by dissolution of halite, and also by ion exchange. Smectite clays are found throughout the Hensel (see diffractogram, Figure 36). These clays possess a high cation exchange capacity, and are probably exchanging bound Na for Ca and Mg in solution. Dissolution of plagioclase feldspar is a possible source of smaller amounts of Na. High concentrations of SO_4 are caused by dissolution of gypsum; the absence of associated high concentrations of Ca is probably due to loss by adsorption.

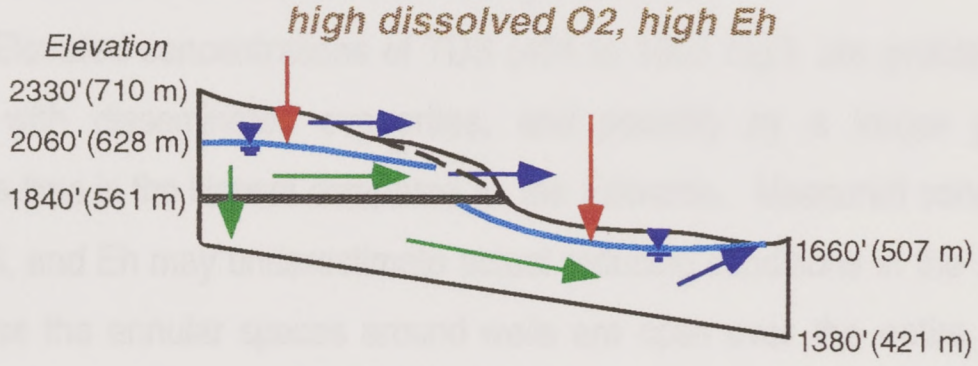

42. Schematic diagram of the gross mechanisms believed to control the occurances and relative concentrations of major ions in the Edwards and Hensel aquifers.

The Hensel aquifer is more isolated from the oxidizing influence of the atmosphere than the Edwards aquifer. The iron taste and hydrogen sulfide smell observed in many of the wells, coupled with the low measured concentrations of DO (1.1 to 2.1%) and Eh (99 to 228 mV), support the interpretation of a reducing environment. Apparently, sulfate and iron hydroxide are being reduced during the bacterially mediated oxidation of organic matter. These reactions yield hydrogen sulfide, ferric iron, and bicarbonate to the ground water.

Elevated concentrations of TDS (404 to 1603 mg/l) are probably caused by contact with disseminated evaporites, and possibly by a longer ground water residence time in the Hensel compared to the Edwards. Measured concentrations of DO, TDS, and Eh may underestimate actual reducing conditions in the aquifer. This is because the annular spaces around wells are open over the entire length of the wells. As a result ground water in reduced zones will mix with and become diluted by water in zones that are more oxidized.

In the Hensel aquifer the distribution of hydrochemical facies is related to the architecture and mineralogy of the rocks through which the ground water flows (Figure 38). The higher average value of TDS measured in ground water from wells at the west end of the floodplain is probably due to ground water contact with overbank clays as it flows preferentially through sinuous sand and gravel deposits that are juxtaposed against these clays (Figure 40). This interpretation is supported by lithologic log data which indicates the existence of these deposits. It is supported also by potentiometric contours which are widely spaced. This wide spacing indicates that flow is occuring through the more highly permeable fluvial sands and gravels recorded in drillers' logs. The portion of the aquifer at the east end of the floodplain, where wells yield water with a lower TDS, would be expected to have lower density potentiometric contours indicative of high hydraulic conductivity. However, unexpectedly, the contours are tightly spaced (Figure 40). Drillers' logs

show that there is a lithologic facies change to sand and silt with interbedded carbonates, thus there is a west to east transition to a more marine paleoenvironment. During calibration of the numerical model, the process of estimating the spatial distribution of K in the Hensel to produce a potentiometric contour match is very important.

Mathematical Model of Ground-Water Flow

Introduction

For this study a deterministic numerical model was used to simulate ground-water flow in the Edwards and Hensel aquifers. The model simulates flow in a regional system utilizing a set of fundamental approximations. First, the porous medium is assumed to be a continuum that replaces the real complex system of solids and voids. Second, ground-water flow is assumed horizontal because the ratio of aquifer thickness to horizontal length is small. Third, Darcy's Law is assumed. This equation is:

$$\partial/\partial x\left(-K_{xx}\partial h/\partial x\right)+\partial/\partial y\left(-K_{yy}\partial h/\partial y\right)+\partial/\partial z\left(-K_{zz}\partial h/\partial z\right)-w=0 \qquad \text{(eq. 2)}$$

where:

x, y, and z are cartesian coordinates axes of the flow system,

with hydraulic conductivity tensors K_{xx}, K_{yy}, K_{zz} (L/t)

h is hydraulic head (L)

w is the volumetric flux per unit volume representing sources and sinks (L^3/t)

Finite-difference ground-water flow simulation

U. S. Geological Survey modular flow model (MODFLOW)

The computer code used for the analysis was the U. S. Geological Survey Modular Flow Model (MODFLOW) (McDonald and Harbaugh, 1988). MODFLOW simulates ground-water flow through porous media using a finite-difference

approximation to solve the steady-state or transient ground-water flow equation at discrete and regularly arranged points (nodes) by an iterative algorithm. The region being modeled is divided into a grid of cells with a node at the center of each cell, and each cell is defined to be either no-flow, variable-head, or constant-head. The model calculates a value for hydraulic head at the nodes of all variable-head cells, whereas head at constant-head cells is specified by the user. Cells are designated as no-flow cells if they contain impermeable material or are unsaturated. MODFLOW can simulate flow in two or three dimensions, under confined or unconfined conditions, in formations that are heterogeneous and uniformly anisotropic, and in those that have irregular boundaries.

Special notation is used to describe the position of nodes in finite-difference grids so they can be addressed when the finite-difference equation is solved iteratively (Figure 43). The method of solution is to make an initial guess of the value of head for each of the nodes in the mesh. Based on these head values, the finite-difference equation is solved for each node by using the values at the surrounding four nodes:

$$(h_{i-1,j} - 2h_{i,j} + h_{i+1,j})/(\Delta x)^2 + (h_{i,j-1} - 2h_{i,j} + h_{i,j+1})/(\Delta y)^2 = -R/T \qquad \text{(eq. 3)}$$

where:

h is hydraulic head (L)

R is used to simulate both distributed and point sources/sinks (L/t)

T is transmissivity (L^2/t)

This equation is solved for each node in the finite difference mesh using an initial estimated value at the node. Once the heads at each node have been recomputed,

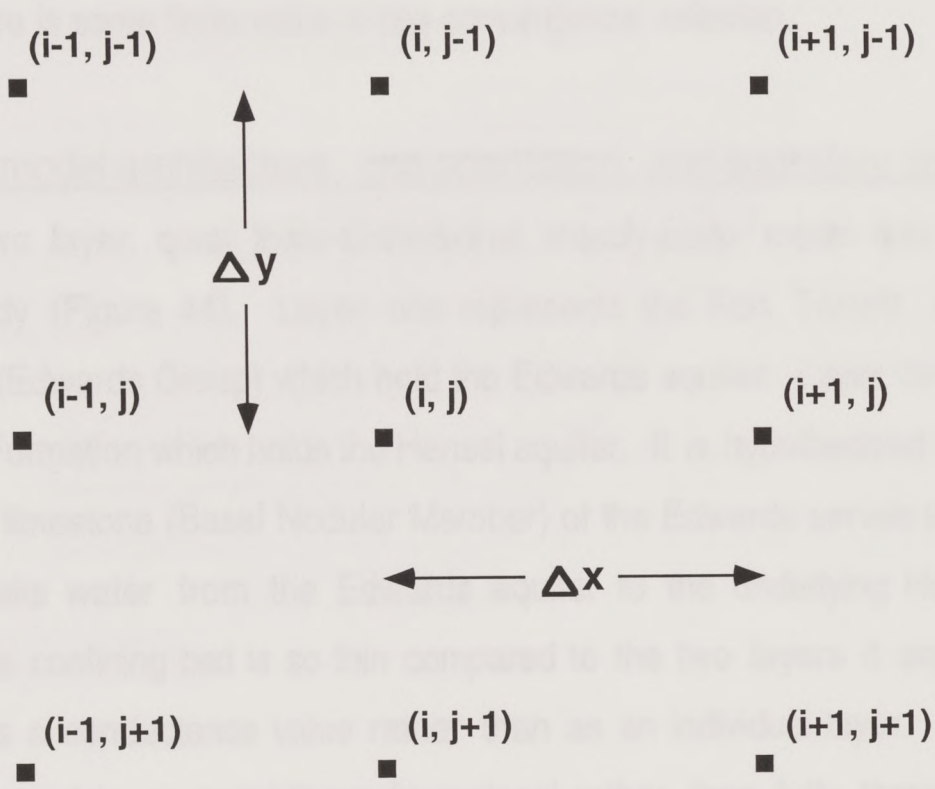

Figure 43. Notation for the finite-difference grid. Spacing between nodes is 506 meters.

the difference between the initial value and the recomputed value is calculated. This process is repeated until the maximum difference in head values from one iteration to the next is less than a preset convergence criterion. When the solution has converged, the equation has been solved. The solution is necessarily approximate because there is some finite value to the convergence criterion.

Numerical model architecture, grid orientation, and boundary conditions

A two layer, quasi three-dimensional, steady-state model was constructed for this study (Figure 44). Layer one represents the Fort Terrett and Segovia Formations (Edwards Group) which hold the Edwards aquifer. Layer two represents the Hensel Formation which holds the Hensel aquifer. It is hypothesized that the thin basal marly limestone (Basal Nodular Member) of the Edwards serves as a confining bed that leaks water from the Edwards aquifer to the underlying Hensel aquifer. Because this confining bed is so thin compared to the two layers it separates, it is simulated as a conductance value rather than as an individual layer. This type of model is referred to as quasi three-dimensional rather than fully three dimensional. This layer functions as a head dependent flux boundary because the flux across the bed is a function, in part, of the difference in head between the two aquifers (Anderson and Woessner, 1992). Confining layers are not explicitly represented in quasi three-dimensional models, nor are heads in confining beds calculated. Quasi three-dimensional models are preferred over fully three-dimensional models when the difference in hydraulic conductivity between the confining bed and the aquifer host rocks is at least two orders of magnitude (Anderson and Woessner, 1992).

Finite difference grids for layer one (Figure 45) and layer two (Figure 46) consist of 56 rows and 55 columns to produce a total of 3,080 model blocks (cells), 1,456 of which are active. Model blocks are square with 506 meter (1,660-foot) sides. Because MODFLOW is a block-centered model, the values of hydrogeologic

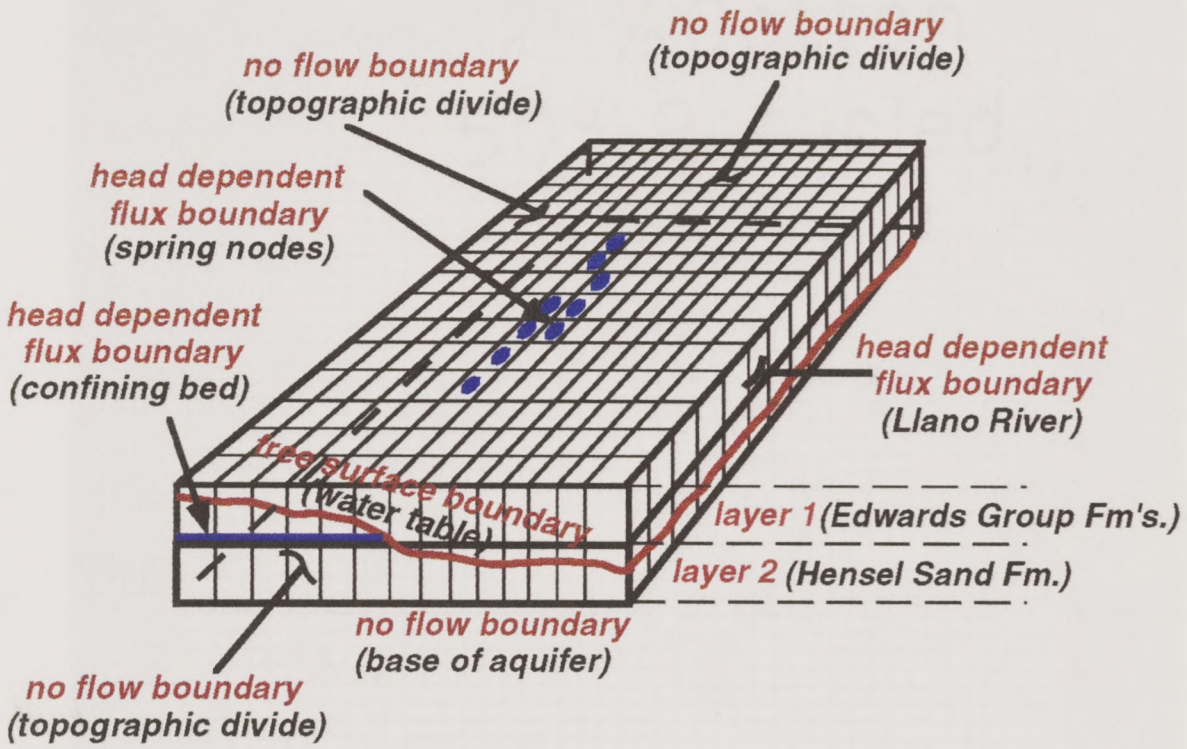

total cells	*3080*
active cells	*1456*
cell size	*506 m x 506 m*
# layers	*2*
type	*steady-state, saturated, quasi 3-d*

Figure 44. Idealized block diagram of the finite difference grid and associated boundary conditions for the numerical model of ground-water flow.

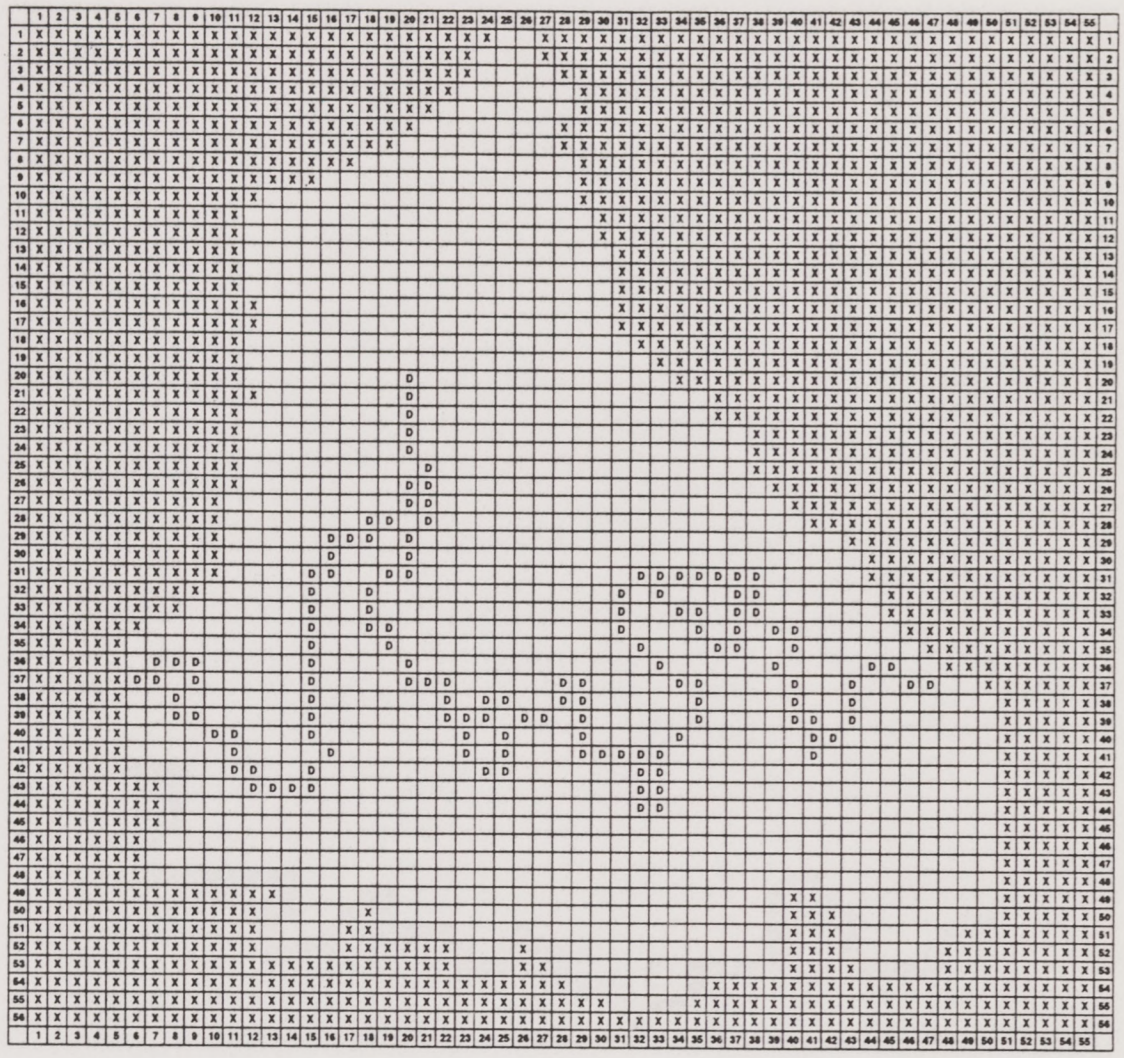

Figure 45. Finite-difference grid for layer one - Segovia and Fort Terrett Formations (Edwards Group), showing no-flow boundaries and drain cells.

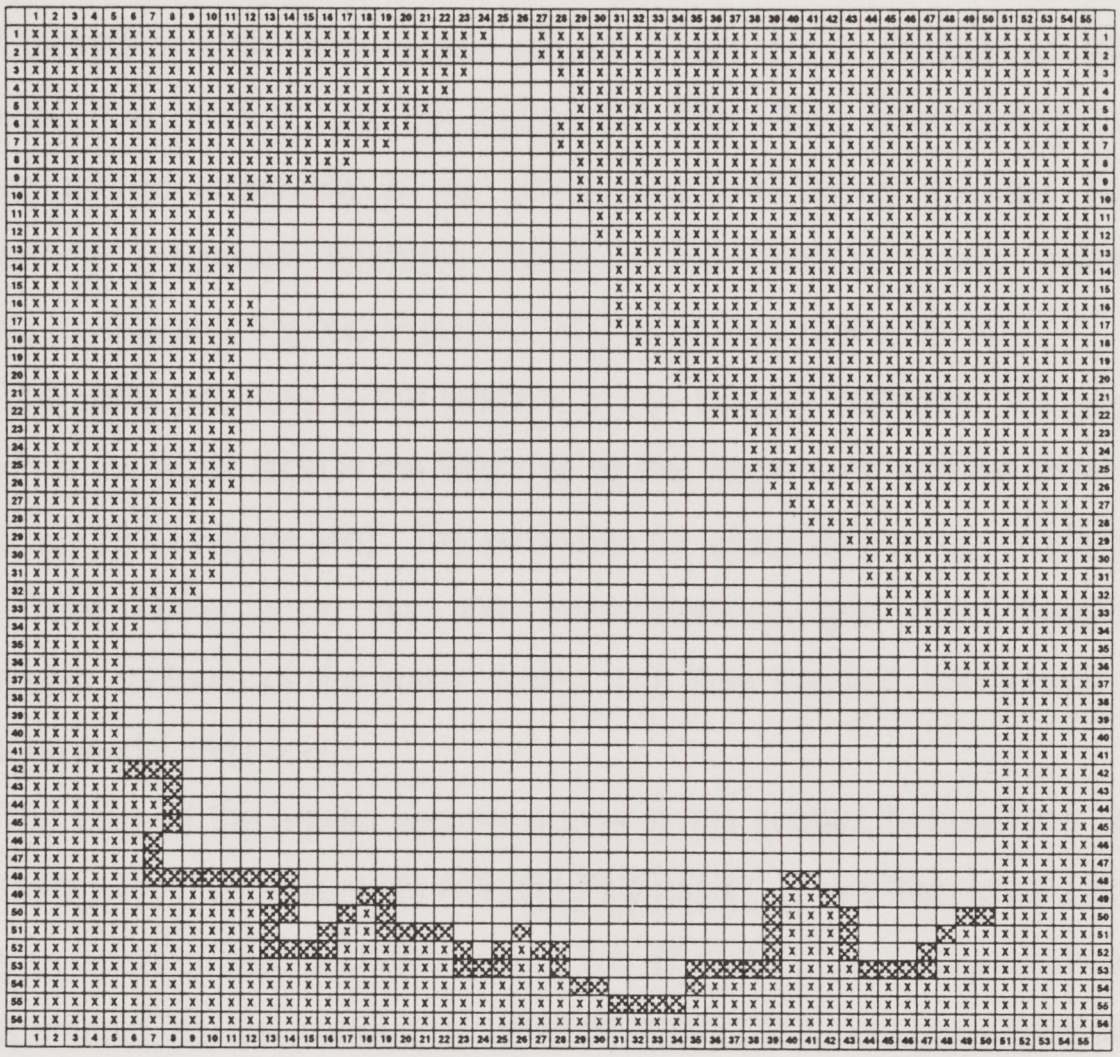

Figure 46. Finite-difference grid for layer two - Hensel Sand Formation showing river cells.

parameters and calculated state variables, are assigned to the center points (nodes) of each block.

Columns of cells were aligned parallel to the major direction of inferred ground-water flow which is down the topographic slope. Also, columns and rows of cells were aligned subparallel to air photo lineaments which are the surface expressions of orthogonal fractures found in the Edwards Group formations throughout the Edwards Plateau (Figure 47, Wermund, and others, 1978).

The upper boundary of the model is a free surface boundary. Its physical expression is the water table in the Edwards aquifer (layer one), and the water table in the Hensel aquifer (layer two). The procedure for assigning starting heads to the variable head nodes is to lay the finite-difference grid atop hand-drawn potentiometric contours of the water tables, and then transfer interpolated head values to the model grid nodes.

The base of the aquifer system occurs at the contact between the Hensel and the underlying Paleozoic strata (Wichita Paleoplain). It was treated as a no-flow boundary (a specified flux boundary with a flux of zero). The configuration of the base was entered into the model by transferring interpolated elevation values from a structure map of this surface (Barker and Ardis, 1992) to the model grid nodes.

A single value of elevation was used for the Edwards/Hensel contact because the contact is relatively horizontal throughout the Edwards Plateau (Rose, 1972). This value was calculated by averaging the elevation of ten contacts observed on the face of escarpments circumscribing the study area. The elevations were read from USGS 7.5-minute topographic maps and found to vary from 1,820 to 1,860 feet so an average elevation of 1,840 feet was assigned to all grid nodes to represent this contact.

Areas of greatest ground surface elevation coincide with both surface-water divides and ground-water divides. Ground-water divides on the Edwards Plateau

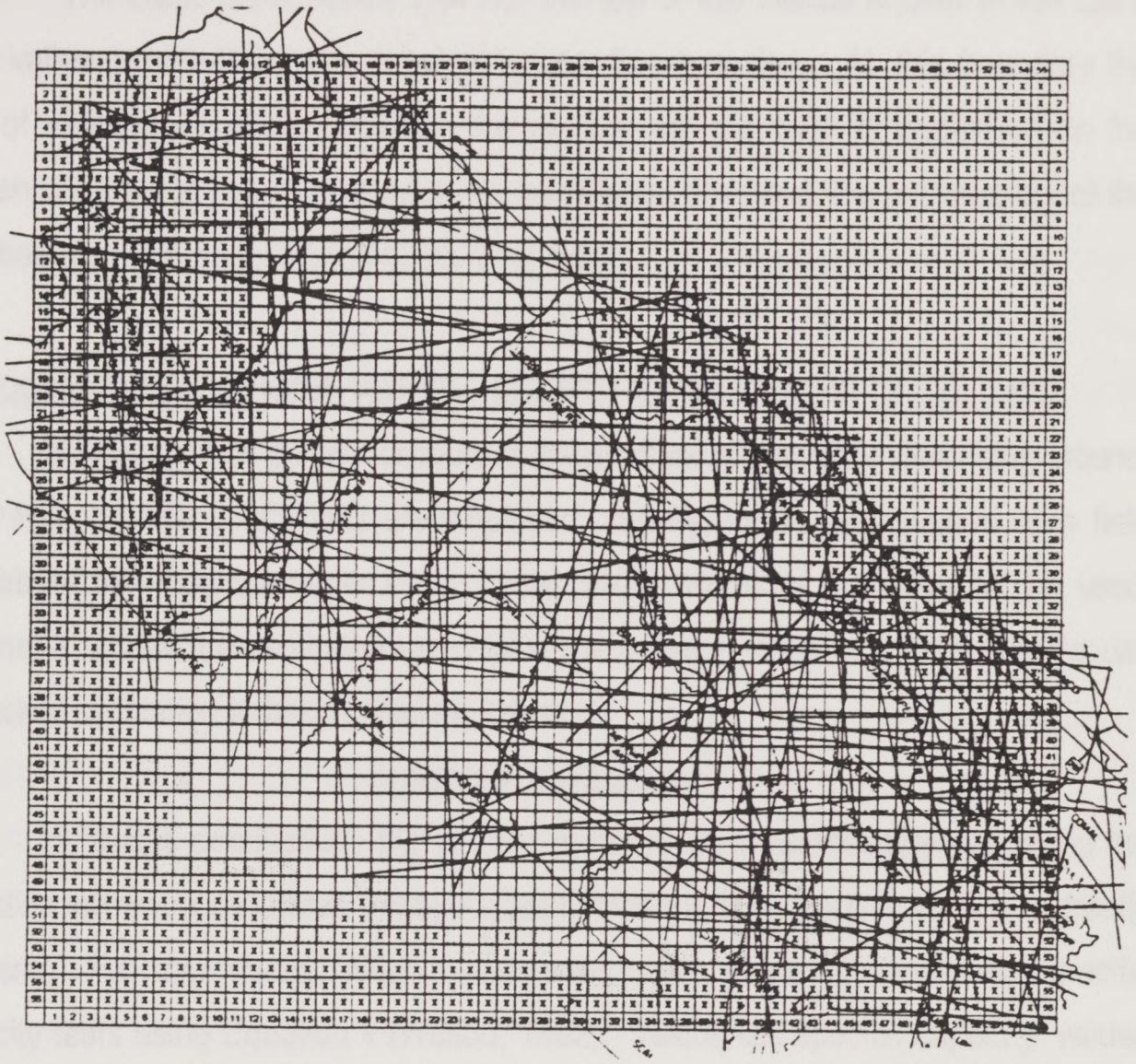

Figure 47. Orientation of the finite-difference grid. Columns are aligned parallel to the topographic slope. Columns and rows are aligned sub-parallel to lineaments mapped in the southern portion of the Edwards Plateau (Wermund, and others, 1978).

function as no-flow boundaries along the northwestern end of the study area.

The Llano River, which cuts into the top of the Hensel aquifer in the Llano River valley, is simulated as a head-dependent flux boundary. At this boundary the rate of seepage of water between the aquifer and the river is dependent on the difference in hydraulic head between the aquifer and the river, the permeability of the river bed, and the surface area of the river bed.

Hydrogeologic parameter values - starting estimates for model input

In moving from the microscopic to the macroscopic level of describing ground-water flow, several coefficients are employed. Ideally, these are obtained from field and laboratory measurements; but in cases where these methods cannot be used, parameter values are estimated using literature values. Another approach is to use numerical simulation to back-calculate values.

Hydraulic conductivity

Hydraulic conductivity (K) is the coefficient of proportionality describing the rate at which water can move through a permeable medium along a sloping hydraulic gradient. For this study, initial K estimates were made by analyzing specific capacity tests using Equation 1 (Walton, 1962). Twenty-six specific capacity values from Edwards aquifer wells, and fifty-seven from Hensel aquifer wells, were used in the equation to calculate transmissivity (T) (see discussion in Methods chapter, and calculations in Appendix F). Estimated K values of 3.53E-05 cm/sec (.1 foot/day) for the Edwards and 3.53E-04 cm/sec (one foot/day) for the Hensel were then calculated by dividing the arithmetic averages of T by the estimated saturated thicknesses. These values compared reasonably well with those calculated in other studies in the Edwards Plateau/Hill Country region (Table 1).

The condition under which the hydraulic conductivity of an aquifer varies with direction is termed anisotropy. Horizontal anisotropy occurs when the value of

K_y/K_x is more or less than one. Simulations were run initially using an horizontal anisotropy of one (no anisotropy) because at the regional scale the system can be visualized as an equivalent isotropic porous medium.

Confining bed vertical conductance (leakance)

Vertical leakance is equal to the ratio of the estimated vertical hydraulic conductivity of the confining bed to the thickness of the confining bed. For model input, an initial leakance estimate of 7.0-E-10 cm/sec (2.0E-06 feet/day) was assigned to the grid nodes. This was calculated by dividing an estimated hydraulic conductivity (Table 1) of 7.0E-09 cm/sec (2.0E-05 feet/day) by an estimated confining bed thickness of 3.1 meters (10 feet).

Drain conductance

Drains were assigned to the nodes of 138 cells that are crossed by the 565 meter (1855-foot) topographic contour on the face of the erosional escarpment (Figure 45). These drain cells were used to simulate the discharge of Edwards ground water from numerous small contact springs whose exact elevations could not be established due to property access limitations, or because their discharges were too meager or too sporadic. Drain cells simulate the removal of ground water at a rate proportional to the difference in elevation between the water table elevation and a fixed drain elevation. The 1855-foot elevation was used for model input because it is the approximate elevation of the top of the ten-foot thick low permeability marly limestone layer that forces overlying ground water toward spring outlets. The starting drain conductance (hydraulic conductivity of the drain material multiplied by the length of the drain) used in the simulation was .0139 m^2/ day (.150 $feet^2$/day).

River conductance

Seventy-two cells across which the Llano River flows were assigned an initial hydraulic conductance value of 93 m^2/day (1000 $feet^2$/day) in the river package input file. River cells simulate baseflow seepage across the aquifer-stream

Source	Hydraulic conductivity cm/sec (ft/day)			Notes	Data quality
	Edwards Group	Hensel Sand	Confining Bed		
From specific capacity/ transmissivity calculations in Appendix E)	2.06E-05 to 4.41E-05 (.059-.126)	3.26E-04 to 5.67E-04 (.93-1.62)		T is determined using the Walton equation (Walton, 1962). K is calculated by dividing T by an average saturated thickness. A range of values is determined by using a plausible range of storativity of between .02 to .00002 in the equation.	Questionable. (1) An average saturated thickness is estimated because wells are not fully penetrating (2) Bias towards overly high K is introduced because dry holes are not sc-tested (3) Bias towards overly low k estimates is introduced because wells that do not draw down during the specific capacity test cannot be included in the Walton equation (Walton, 1962) (4) An advantage is that the measurements are site-specific (5) The reported K value is an average rather than a median value. It is not known how this affects the model results (6) Storativity is estimated (7) There are no aquifer test data to compare sc data to (8) Standard procedures for sc calculation were not followed by all drillers
Bluntzer (1992)		2.40E-04 to 4.30E-04 (.685-1.233)			Questionable Based on one aquifer test
Hill Country Underground Conservation District (1994)	1.90E-04 to 4.10E-02 (.53-117.5)	2.3E-04 to 4.2E-04 (.67-1.2)			Questionable Hensel value is based on one aquifer test The source of the Edwards values are not referenced
Fetter (1988)		9.8E-06 to 9.8E-04 (.028-2.8) (silty sand)	9.8E-07 to 9.8E-08 (.00028-.0028) (high end of clay to low end of silt)		A plausible range of values determined from other studies Suffers from lack of site specificity

Table 1. Ranges of hydraulic conductivity used to produce estimates for initial input to the numerical model of ground-water flow.

interface. The rate of seepage is proportional to the difference in elevation between the Hensel aquifer water table and the stage of the river. Elevations in both the aquifer and the river decrease from the west end of the study area to the east.

Sources and sinks

Estimates for initial model input were made for sources and sinks including precipitation recharge, discharge to the Llano River, well pumpage, and spring discharge.

Precipitation recharge and discharge to the Llano River

Initially, the same recharge value was applied to the highest active cell in each vertical column of the model grid. This value was estimated by calculating the percentage of rainfall that recharges the aquifer in the adjacent drainage basin which drains the North and the South Llano Rivers in a large area upstream of the point where they converge to form the Llano River. In making this calculation it was assumed that the mechanics of recharge are similar in both this drainage basin and the study area because of similar topography, stratigraphy, and structure. This is a valid assumption because the calculated value was only used as an initial estimate.

A flow gauge on the Llano River positioned just below the confluence of these two rivers records all ground and surface water exiting the large drainage system. During the winter months when precipitation (Figure 2) and evapotranspiration are low, the water in these rivers is derived almost entirely from baseflow seepage. Under steady-state conditions this ground-water discharge is equal to aquifer recharge. The average rainfall in the area for the low-flow months of December and January for the period 1939 to 1988 was 138,685,128 cubic meters/month (112,419 acre-feet/month). This value was divided into the average monthly river gauge discharge of 7,014,505 cubic meters (5,686 acre-feet) to yield a discharge of 5.06 % of rainfall. The value of recharge assigned to model cells in the

study area was therefore, .0506 x 61.34 cm/year (24.15 inches/year) rainfall = 3.10 cm/year (1.22 inches/year).

Well pumpage

Total pumpage from approximately 150 domestic and livestock wells in the 389-square km (150-square mile) area was ignored in the model because with a density of one well/square mile, well pumpage was calculated to be insignificant relative to the annual throughput of water. The Texas Natural Resource Conservation Commission suggests a value of 5.67E-01 cubic meters/day (150 gallons/day) as an estimate of domestic water use by a family of four. Total domestic use in the study area would be 5.67E-01 X 150 X 365 = 31,043 cubic meters/year. The volume of recharge to the area is estimated to be 3.10E-02 meters/year X 389 square km X 1000 meters X 1000 meters = 12,059,000 cubic meters/year. As a percentage of discharge, well pumpage would be 31,043/12,059,000 or .26 %.

There are no irrigation wells that draw from the Edwards or Hensel aquifers; the source of water used to irrigate the few hay and pecan crops that exist is either the Llano River or the saturated alluvium immediately adjacent to the Llano River.

Discharge by evapotranspiration (ET)

ET refers to the combined effect of plant transpiration and direct evaporation from the ground surface. A quantitative estimate of ET was not required for this study because recharge was not estimated by subtracting ET and runoff from precipitation. Instead, the magnitude and distribution of recharge assigned to the calibrated model was determined by trial and error simulations.

Steady-state simulation and model calibration

This ground-water system is assumed to operate under steady-state flow conditions because magnitudes and directions of the flow velocity are constant with

time. Under steady-state conditions there is no change in storage in the aquifer. This is a reasonable assumption because of the lack of aquifer development in the area.

Calibration of the model was achieved by comparing simulation output with available data or state conditions that the model simulates. After each of numerous trial and error simulations, adjustments were made to the magnitude and spatial distribution of model input values until calibration goals were met. Calibration goals required that (1) simulated potentiometric surface contours closely matched hand-drawn interpretive contours, and (2) model-calibrated parameter values matched field-measured parameter values reasonably well.

Potentiometric contours were first matched as closely as possible, then a key parameter value (vertical conductance through the confining bed) was adjusted above and below the value used for the simulation run which exhibited the good contour match. By using this method an estimate could be made of the range of volumes entering and leaving layer one of the model. This approach is diagrammed in a series of simulated contour comparisons (Figures 48A-48E). The simulation with the best fit (48C) calculated the percentage of Edwards recharge that discharged from springs to be 13.7%. The percentage of Edwards recharge that discharged to the underlying Hensel aquifer by way of cross-formational leakage was calculated to be 86.3% (Figure 49).

To estimate throughput in the Hensel aquifer, the simulated leakage per year to the Hensel aquifer was added to the estimated recharge per year applied to the Hensel aquifer in the floodplain. This sum equaled the model-calculated seepage into the Llano River minus the model-calculated seepage out of the Llano River (Figure 49).

The process of matching simulated contours to hand-drawn interpretive contours to calibrate the model required approximately one hundred simulations. The

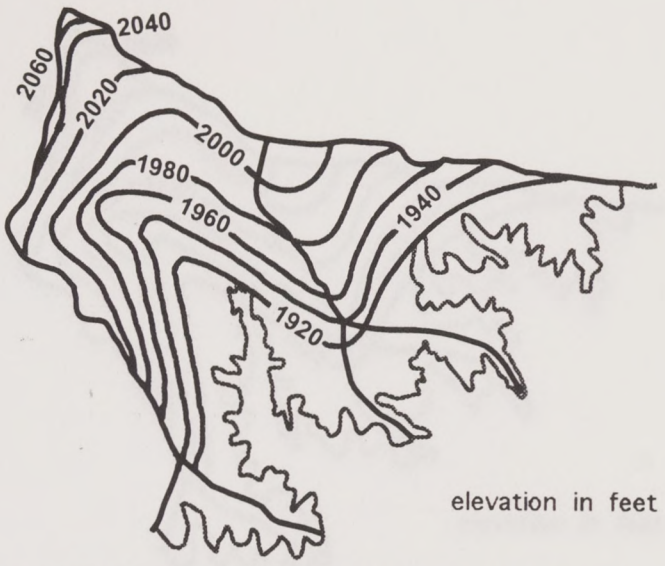

HAND-CONTOURED POTENTIOMETRIC SURFACE OF THE EDWARDS AQUIFER

SIMULATED POTENTIOMETRIC SURFACE OF THE EDWARDS AQUIFER

Groundwater Budget m^3/year ($feet^3$/year)

Using leakance of	8.5435E-10 to 9.503E-10 cm/sec (2.410E-06 to 2.715E-06 feet/day)	
IN		
total recharge:	2,308,264 (81,506,508)	
OUT		
discharge to drains (springs):	11,360 (401,130)	0.5 %
cross - formational flow: (Edwards aquifer to Hensel aquifer)	2,296,904 (81,105,378)	99.5 %

Figure 48A (Simulation A) The potentiometric surface of the Edwards aquifer is simulated in a series of five model runs as the vertical conductance (leakance) of the confining bed is decreased. The assigned leakance is too high in Simulation A; too much of the precipitation recharge leaks to the underlying Hensel aquifer.

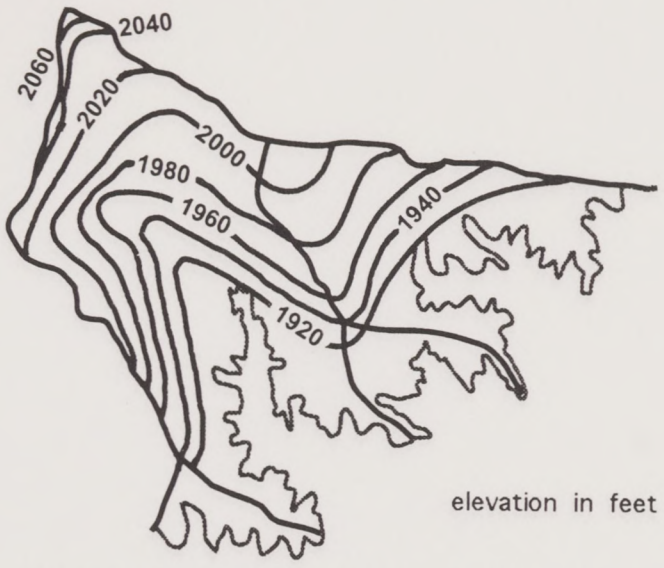

HAND-CONTOURED POTENTIOMETRIC SURFACE OF THE EDWARDS AQUIFER

SIMULATED POTENTIOMETRIC SURFACE OF THE EDWARDS AQUIFER

Groundwater Budget m^3/year ($feet^3$/year)

Using leakance of	5.985E-10 to 8.785E-10 cm/sec (1.710E-06 to 2.510E-06 feet/day)	
IN		
total recharge:	2,596,825 (91,695,805)	
OUT		
discharge to drains (springs):	130,988 (4,625,300)	5.0 %
cross - formational flow: (Edwards aquifer to Hensel aquifer)	2,465,837 (87,070,505)	95.0 %

Figure 48B (Simulation B) The potentiometric surface of the Edwards aquifer is simulated in a series of five model runs as the vertical conductance (leakance) of the confining bed is decreased. The assigned leakance is still too high. This causes a leakage of too much precipitation recharge to the Hensel aquifer but not as much as in Simulation A.

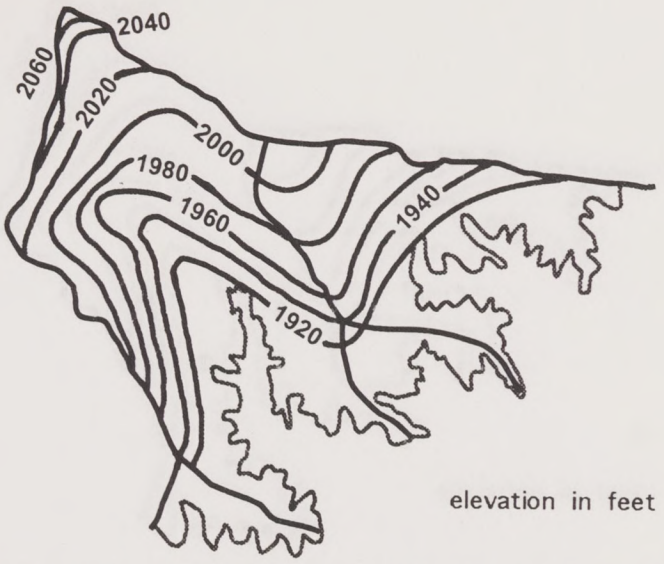

HAND-CONTOURED POTENTIOMETRIC SURFACE OF THE EDWARDS AQUIFER

SIMULATED POTENTIOMETRIC SURFACE OF THE EDWARDS AQUIFER

Groundwater Budget m^3/year ($feet^3$/year)

Using leakance of (3.535E-10 to 7.735E-10 cm/sec)
1.010E-06 to 2.210E-06 feet/day

IN		
total recharge:	2,759,727 (97,447,971)	
OUT		
discharge to drains (springs):	378,582 (13,368,000)	13.7 %
cross - formational flow: (Edwards aquifer to Hensel aquifer)	2,381,145 (84,079,971)	86.3 %

Figure 48C (Simulation C) The potentiometric surface of the Edwards aquifer is simulated in a series of five model runs as the value of vertical conductance (leakance) of the confining bed is decreased. Simulation C produces the best match between simulated and hand-drawn contours. It is believed to be the most accurate simulation of the groundwater system.

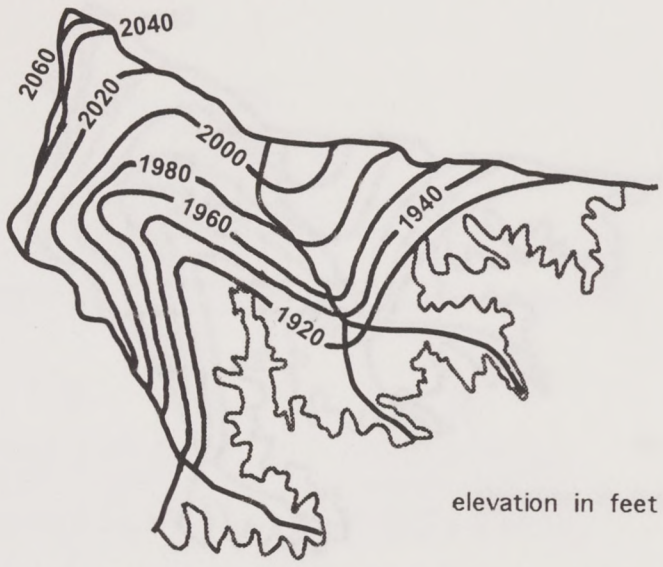

HAND-CONTOURED POTENTIOMETRIC SURFACE OF THE EDWARDS AQUIFER

SIMULATED POTENTIOMETRIC SURFACE OF THE EDWARDS AQUIFER

Groundwater Budget m^3/year ($feet^3$/year)

Using leakance of	2.644E-10 to 2.858E-10 cm/sec (7.555E-07 to 8.166E-07 feet/day)	
IN		
total recharge:	2,759,727 (97,447,971)	
OUT		
discharge to drains (springs):	556,007 (19,633,000)	20.1 %
cross - formational flow: (Edwards aquifer to Hensel aquifer)	2,203,719 (77,814,971)	79.9 %

Figure 48D (Simulation D) The potentiometric surface of the Edwards aquifer is simulated in a series of five model runs as the vertical conductance (leakance) of the confining bed is decreased. The assigned leakance is too low in Simulation D. As a result, the confining bed does not leak enough water to the underlying Hensel aquifer. This causes the simulated water table of the Edwards aquifer to be too shallow.

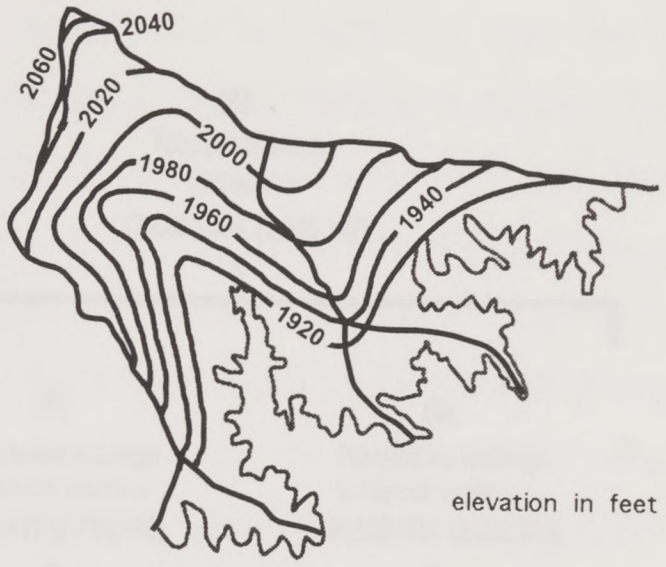

HAND-CONTOURED POTENTIOMETRIC SURFACE OF THE EDWARDS AQUIFER

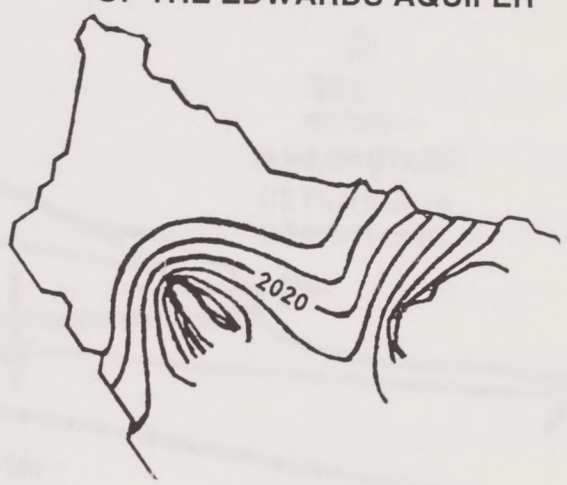

SIMULATED POTENTIOMETRIC SURFACE OF THE EDWARDS AQUIFER

Groundwater Budget	m^3/year ($feet^3$/year)	
Using leakance of	1.7654E-10 to 2.524E-10 cm/sec (5.010E-07 to 7.210E-07 feet/day)	
IN		
total recharge:	2,759,727 (97,447,971)	
OUT		
discharge to drains (springs):	964,664 (34,063,000)	35.0 %
cross - formational flow: (Edwards aquifer to Hensel aquifer)	1,795,062 (63,384,971)	65.0 %

Figure 48E (Simulation E) The potentiometric surface of the Edwards aquifer is simulated in a series of five model runs as the vertical conductance (leakance) of the confining bed is decreased. Simulation E uses a value of leakance lower than the one used in Simulation D. Simulation results are unacceptable because not enough water is leaked to the underlying Hensel aquifer.

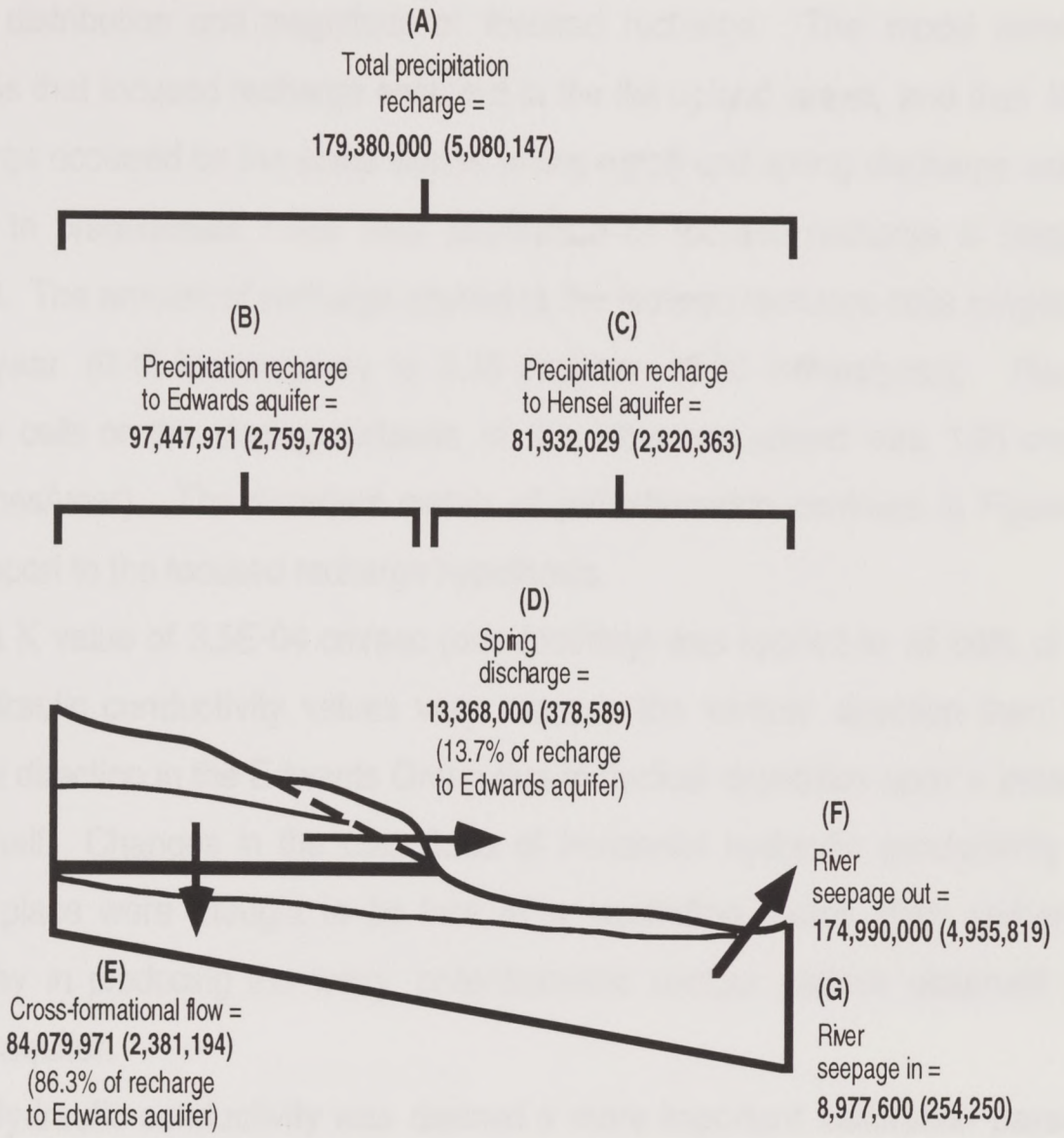

Figure 49. Water budget for the ground-water system (feet^3/year(m^3/year)).

parameter deemed most important for calibrating layer one (Edwards Formation) was the distribution and magnitude of focused recharge. The model tested the hypothesis that focused recharge occurred in the flat upland areas, and that little or no recharge occurred on the steep slopes where runoff and spring discharge would be expected to predominate. The final distribution of focused recharge is mapped in Figure 50. The amount of recharge applied to the focused recharge cells ranged from 1.00 cm/year (0.40 inches/year) to 8.13 cm/year (3.20 inches/year). Recharge applied to cells on the sloping surfaces of the limestone upland was 1.25 cm/year (0.50 inches/year). The excellent match of potentiometric contours in Figure 48C lends support to the focused recharge hypothesis.

A K value of 3.5E-04 cm/sec (one foot/day) was applied to all cells of layer one. Hydraulic conductivity values vary more in the vertical direction than in the horizontal direction in the Edwards Group due to cyclical deposition upon a broad flat marine shelf. Changes in the magnitude of horizontal hydraulic conductivity from place to place were thought to be less of a controlling factor than recharge or topography in producing the wavy potentiometric contour pattern observed in the Edwards aquifer.

Hydraulic conductivity was deemed a more important calibration parameter than others for layer two. Lithologic descriptions in drillers' reports indicate that the Hensel Sand Formation is heterogeneous. In addition, there is a transition in lithologic facies from a more coarse-grained fluvial nearshore paleoenvironment at the west end of the area to a shallow marine paleoenvironment at the east end. Consequently, K was adjusted across the domain in layer two as simulations were performed. Hydraulic conductivity values ranged from 1.06E-04 cm/sec (.3 feet/day) at the east end to 1.73E-02 cm/sec (49 feet/day) in the west (Figure 51).

Simulated contours for the Hensel aquifer beneath the floodplain match hand-drawn contours very closely (Figure 52). Simulated contours for the Hensel aquifer

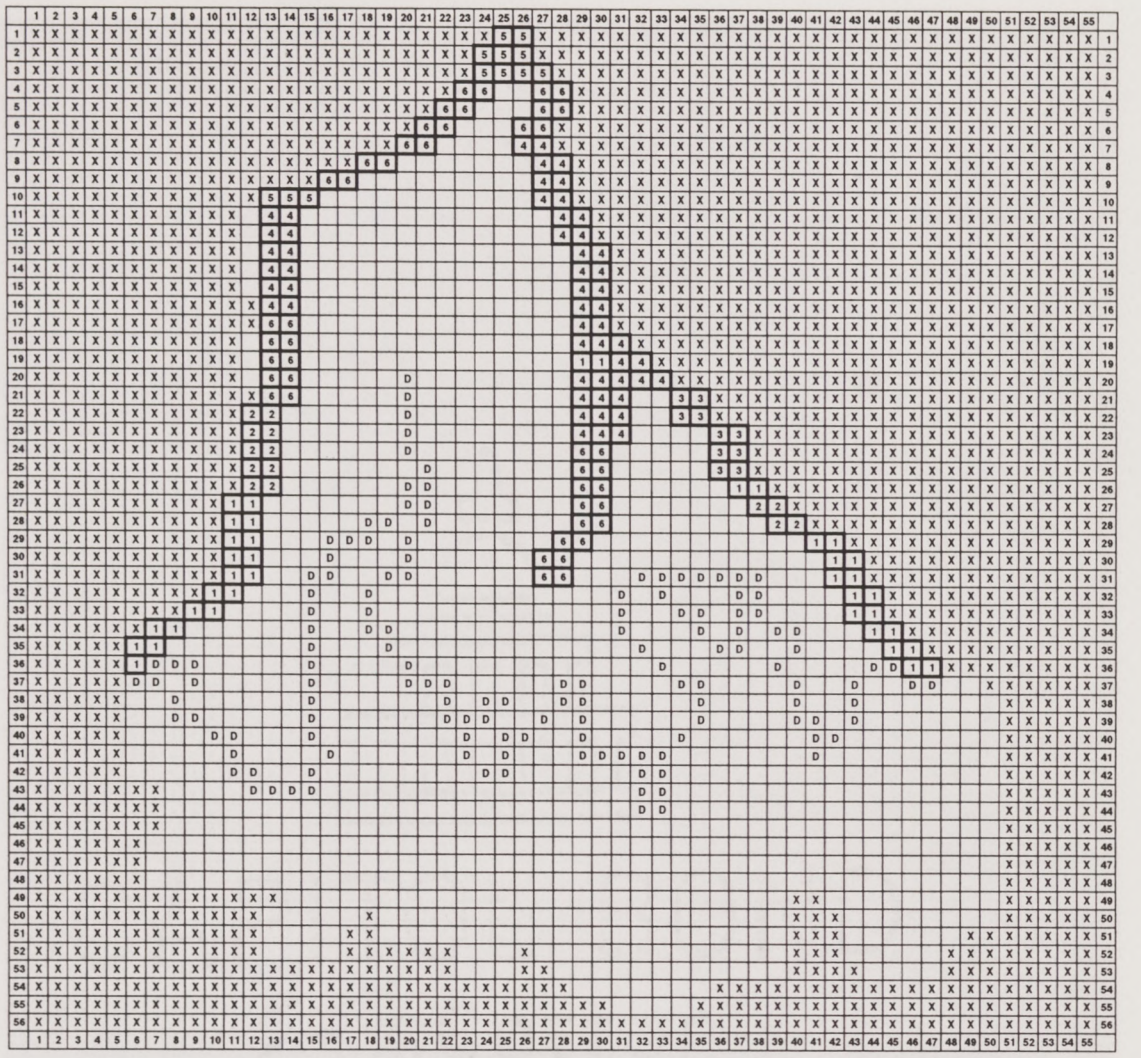

X *Inactive Cell*

Active Cell

D *Drain Cell*

2 *Focused Recharge Cell*

Cell size equals 506 m x 506 m

Assignment of focused recharge values

1.	0.23 - 0.50 inches/year	(0.58 - 1.27 cm/year)
2.	1.09 - 1.50 inches/year	(2.77 - 3.81 cm/year)
3.	1.60 - 1.71 inches/year	(4.06 - 4.34 cm/year)
4.	2.03 - 2.40 inches/year	(5.16 - 6.10 cm/year)
5.	2.62 - 3.00 inches/year	(6.65 - 7.62 cm/year)
6.	3.01 - 3.50 inches/year	(7.65 - 8.89 cm/year)

Figure 50. Distribution and magnitude of focused recharge to active cells of layer one on the flat upland areas which divide drainage basins.

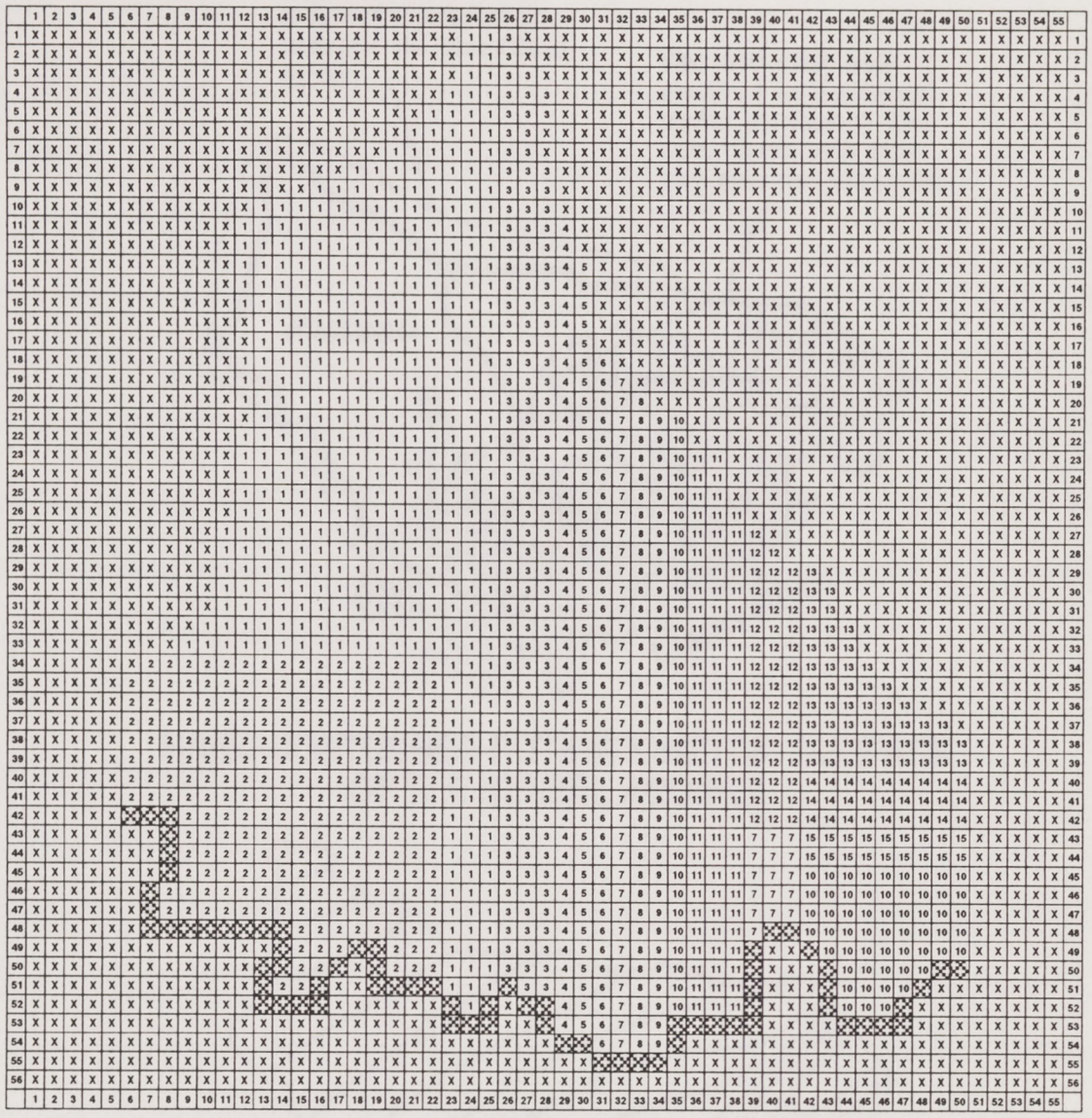

X **Inactive Cell**

Active Cell

River Cell

Cell size equals 506 m x 506 m

Assignment of hydraulic conductivity values (cm/sec (feet/day))

1	.0077 (22)	7	.0019 (5.5)	13	.00032 (.9)
2	.017 (49)	8	.0018 (5)	14	.00018 (.5)
3	.0046 (13)	9	.0016 (4.5)	15	.00011 (.3)
4	.0033 (9.5)	10	.0014 (4)		
5	.0025 (7)	11	.00053 (1.5)		
6	.0023 (6.5)	12	.00035 (1)		

Figure 51. Hydraulic conductivity values used in the calibrated run of the finite-difference grid representing layer two - Hensel Sand aquifer.

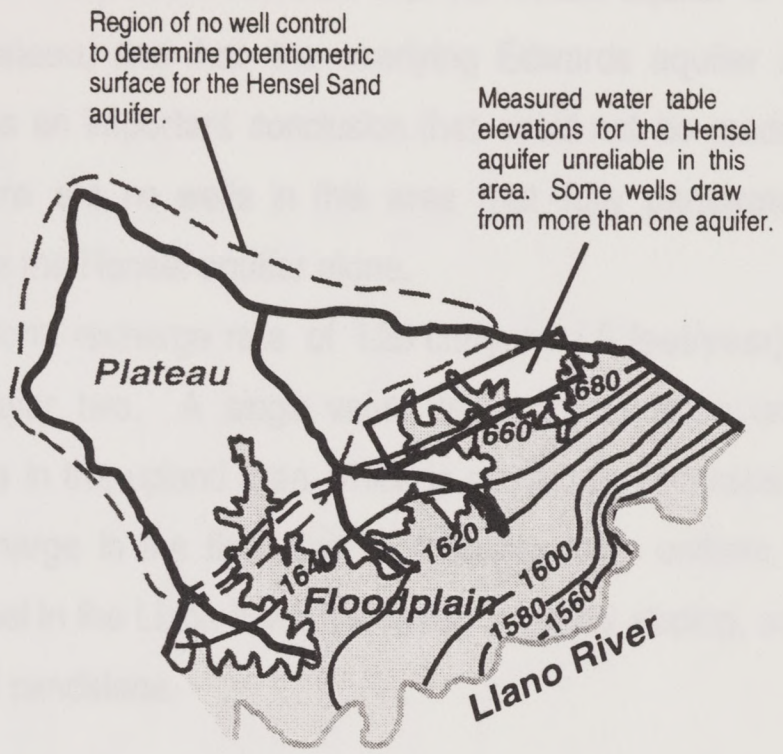

HAND-CONTOURED POTENTIOMETRIC SURFACE OF THE HENSEL AQUIFER

SIMULATED POTENTIOMETRIC SURFACE OF THE HENSEL AQUIFER

Figure 52. Comparison of the simulated potentiometric surface of the Hensel aquifer to the potentiometric surface drawn using available water levels in wells. This good match constitutes attainment of one of the calibration criteria set for accurate simulation of the Hensel simulation.

in the region beneath the plateau establish that the Hensel aquifer is unconfined near the edge of the plateau, and that the overlying Edwards aquifer is fully perched (Figure 53). This is an important conclusion that could not be made by measuring water levels. There are no wells in this area that fully penetrate the Edwards Group, to draw from the Hensel aquifer alone.

A final uniform recharge rate of 1.25 cm/year (.5 feet/year) was assigned to model cells in layer two. A single value was used because unlike the varied pattern of recharge in the upland area which is caused by contrasts in topography and structure, recharge in the floodplain is probably more uniform. The exposed surface of the Hensel in the Llano River floodplain is gently sloping, and composed of friable siltstone and sandstone.

Calibration sensitivity analysis

The integrity of the solution can be judged by the accuracy of the input parameters that the solution is most sensitive to. Using the calibrated model, input parameter values are varied within a realistic range, and simulations are run to observe the effect of these changes upon the potentiometric surface. If a large effect is seen it means that the parameter being adjusted is a dominant one. If its value is inaccurate, uncertainty in model results is increased.

In this study, the model parameters judged to have the greatest potential for contributing to uncertainty are horizontal anisotropy and vertical leakance (Table 2). When the values of these parameters were adjusted during trial and error simulation, a pronounced effect was observed in the simulated potentiometric surface, and the model-calculated water balance. There are no straightforward ways of determining the anisotropy ratio, so it was maintained at 1:1. The estimate of leakance might be improved by running laboratory permeameter tests on undisturbed oriented samples of the confining bed material, but the methodology is complicated, and the

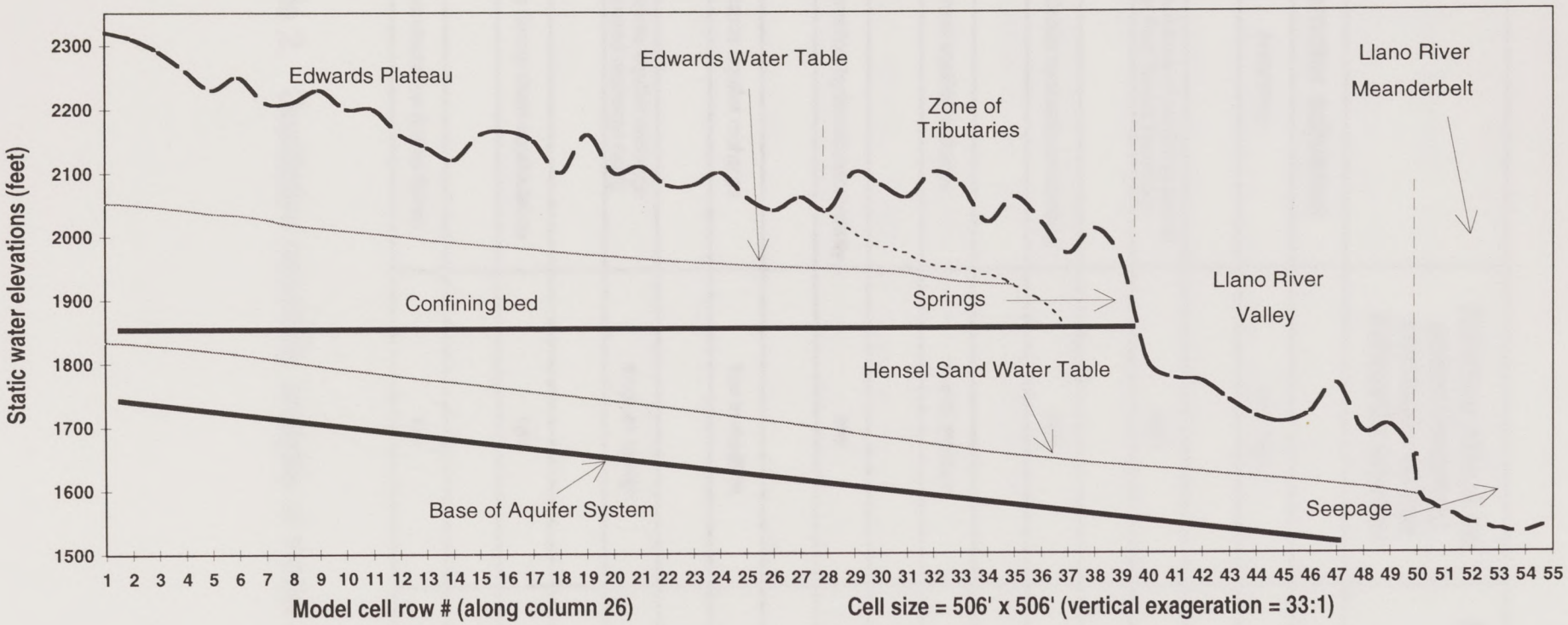

Figure 53. Cross-section of simulated water tables in the Edwards and the Hensel aquifers. The regional confining bed at the base of the Fort Terrett Formation causes the Edwards aquifer to operate as a fully perched aquifer.

	Relative effect on potentiometric contours of the Edwards aquifer	Relative effect on potentiometric contours of the Hensel aquifer
Parameter adjusted		
Anisotropy	very high	very high
Vertical leakance of confining bed at base of Fort Terrett Formation	high	medium to high
Edwards Group hydraulic conductivity	high	low to medium
Hensel aquifer recharge	low to medium	high
Hensel Formation hydraulic conductivity	low	medium
Edwards aquifer recharge	low to medium	low
Edwards aquifer recharge (focused recharge cells)	medium to high	low
Edwards Group drain conductance	low	low
River conductance (Llano River)	low	low

Table 2. Qualitative sensitivity analysis of model input parameters.

results uncertain, because these are not in-situ measurements.

Simulation results were very sensitive to two other parameters whose assigned values are believed to be more accurate than the two discussed above. These are the Edwards Group hydraulic conductivity and the Hensel aquifer recharge. Actual data (specific capacity) exists to estimate the Edwards Group hydraulic conductivity so the model's sensitivity to it is not of major concern. The estimated value of recharge applied to the Hensel aquifer is believed to be accurate because the distributed value of recharge calculated for the adjacent drainage basin, and then applied to this one, compares favorably with values calculated at another site in the Texas Hill Country (Ashworth, 1983).

Adjustments to the Hensel Formation hydraulic conductivity, Edwards aquifer recharge, and Edwards aquifer focused recharge, had a medium effect upon the simulation results. These are parameters that had been estimated using independent sources of data, thus they are thought to be fairly accurate.

The sensitivity of model results to adjustments in the values of drain conductance and river conductance was low. This means that uncertainty in their values is more tolerable than uncertainty in the values of the parameters discussed earlier.

Conclusions

1. Two separate unconfined aquifers are defined based on potentiometric surfaces constructed from static water levels in wells. These are the Edwards aquifer which occurs beneath the Edwards Plateau, and the Hensel Sand aquifer which occurs below the Edwards Plateau and the Llano River valley.
2. Based on numerical simulation results, the water table of the Hensel Sand aquifer extends below the Edwards Plateau where it is overlain by an unsaturated zone that thins toward the interior of the Plateau as the Hensel Sand Formation thins. The Edwards aquifer overlies this unsaturated zone where it is fully perched atop a thin, marly limestone (Basal Nodular Member) which is the lowermost member of the Fort Terrett Formation.
3. Ground-water movement in the Edwards aquifer occurs principally within fractures and solution-enhanced bedding planes of the Fort Terrett and Segovia Formations. The Edwards aquifer is a diffuse-flow aquifer. Evidence for diffuse flow includes the relative steepness of the hydraulic gradient, the absence of observable karst features, low average specific capacity, and spatially uniform hydrochemistry.
4. Ground-water movement in the Hensel aquifer occurs principally within coarse-grained fluvial paleochannel deposits encased within finer-grained overbank matrix deposits.
5. The low permeability, marly limestone member at the base of the Fort Terrett Formation slowly leaks water from the perched Edwards aquifer to the underlying Hensel aquifer.
6. Total precipitation recharge applied to the active cells of the numerical model grid was 5,080,147 meters^3/year (179,380,000 feet^3/year). Of this total, 2,759,783 meters^3/year (97,447,971 feet^3/year) was applied to the Edwards aquifer, of

which 378,589 meters^3/year (13,368,000 feet^3/year) (13.7 %) was calculated by the model to be discharged as springflow, and 2,381,194 meters^3/year (84,079,971 feet^3/year) (86.3 %) was calculated to be discharged as cross-formational flow. Precipitation recharge applied to the Llano River valley portion of the Hensel Sand aquifer was 2,320,363 meters^3/year (81,932,029 feet^3/year). The discharge from the Hensel Sand aquifer via seepage to the Llano River was calculated to be 4,955,819 meters^3/year (174,990,000 feet^3/year). This rate of seepage to the Llano is equal to the sum of three components of recharge: (1) cross-formational flow to the Hensel aquifer, (2) precipitation recharge to the Llano River valley portion of the Hensel aquifer, and (3) seepage of Llano River water into the Hensel aquifer.

7. Based on the results of numerical simulation, focused recharge to the Edwards aquifer occurs where rainwater infiltrates the flat ground surface near the topographic divides above and between two watersheds.
8. Recharge to the portion of the Hensel aquifer that lies beneath the Llano River valley occurs by infiltration of rainfall through the silty sand surface of the Hensel Sand Formation. Focused recharge may occur by infiltration of flood waters through the streambeds of ephemeral tributaries, but this hypothesis is not tested. Additional recharge occurs by cross-formational flow to that part of the Hensel aquifer which underlies the Edwards Group Formations.
9. Mesas at the margin of the Edwards Plateau are substantially dewatered because ground-water flowlines converge to form springs upgradient of mesa locations at the heads of ephemeral streams that have cut steep-walled canyons into the edge of the plateau.
10. Spring discharge from the Edwards aquifer appears to have declined over time. This may be caused by the proliferation of mesquite and juniper trees that

extract potential recharge water from the soil zone. Additional field research is needed to test this hypothesis.

11. The Edwards aquifer is a Ca-Mg-HCO_3 facies water, and the Hensel is a mixed facies water. Even though there is cross-formational flow between these aquifers, the existence of two distinct hydrochemical facies suggests that these aquifers operate semi-independently.
12. Based on field measurements of high dissolved oxygen (6.0 to 8.6 mg/l), high Eh (404 to 488 mv), and the highest water table elevations in the study area, ground water in the Edwards aquifer is determined to occur in a recharge zone which is open to the atmosphere.
13. Based on field measurements of low dissolved oxygen (1.1 to 2.1 mg/l), comparatively low Eh (99 to 255 mv), iron taste, sulfide odor, and the lowest water table elevations in the study area, ground water in the Hensel aquifer is determined to be more isolated from the oxidizing influence of the atmosphere, and is located either in an intermediate zone of regional flow or a discharge zone. Higher values of dissolved oxygen (5.0 to 7.1 mg/l) and Eh (393 to 461 mv) at the eastern end of the floodplain are believed related to a facies change to more calcareous sediments, and to a thinning of the Hensel Sand Formation in the direction of the Llano Uplift area. This thinning results in a shallowing of the aquifer as well.
14. The Llano River is a gaining river on average. This is demonstrated by a baseflow potentiometric surface pattern of "V's" that open in the downstream direction. The flow of this perennial river is sustained by surface waters that begin as Edwards aquifer springs, and by baseflow seepage from the adjacent Hensel aquifer.

15. Calculated using Darcy's Law, the average linear ground-water velocities are approximately 1.6E-04 cm/sec (0.45 feet/day) in the Edwards aquifer, and 9.7E-05 cm/sec (0.28 feet/day) in the Hensel Sand aquifer.

Appendices

Appendix A
Water chemistry sampling and analysis procedures

Water chemistry sample collection and analysis procedures

(Field, laboratory, and computer processing)

Field

1. Immerse Eh Zobell solution bottle, pH buffer bottles, and HCL alkalinity titrant bottle in bucket of sample water to bring them to temperature equilibrium.

2. Turn on windmill or submersible pump and let water run strongly for 20 minutes. Note any smells and tastes in water especially hydrogen sulfide smell and/or iron taste which might indicate reducing conditions.

3. Check batteries in pH-Eh-temp meter, dissolved oxygen meter and spectrophotometer.

4. Check filling solutions in Eh probe and pH probe.

5. Calibrate pH meter with 4 pH and 10 pH buffers.

6. Attach flowcell to water supply after water has run for 20 minutes. Reduce flow to minimum volume necessary to keep flowcell 100% full (completely removing contact with the atmosphere).

7. Insert pH, temp, and dissolved oxygen probes into flowcell.

8. Monitor temp, pH, and dissolved oxygen until stability occurs. Record readings.

9. Using a .45 um filter fill one 60 ml plastic bottle with well water for cation analysis after adding 2 drops 6N reagent-grade nitric acid (reduces pH to 3 to prevent precipitation of metal ions).

10. Using a .45 um filter fill two 60 ml pvc bottles with well water. One is for anion analysis, the other is a duplicate.

11. Put sample bottles in cooler keeping them at 4° C using “blue ice”.

12. Turn on spectrophotometer and warm for 10 minutes.

13. Using a pipet transfer 100 ml of filtered (.45 um) sample to a volumetric flask for alkalinity (as HCO_3) titration with 1.5 N HCL. Using a burette titrate to the 4.5 pH endpoint using magnetic stirrer, stirring bar, and pH meter. Record ml of titrant required and calculate alkalinity as HCO_3 using the formula: Alkalinity as mg/l HCO_3= (normality of titration acid) * (volume of titration acid in ml near pH=4.5) * (61000/volume of sample in ml).

14. Measure dissolvedO_2 with CHEMetrics chemet kit # K-7512 (0-12 ppm) and/or # K-7501 (0-1ppm) by snapping a vacuum ampule inside a flow cell opening (to eliminate atmospheric interaction). Record reading.

15. Measure manganese with CHEMetrics chemet kit # K-6502 (0-2 ppm). Record reading.

16. After spectrophotometer has warmed, set instrument to correct wavelength to measure transmittance for each of the following constituents. Prepare each sample using the specialized CHEMetrics vacu-vile kits. Use calibration charts provided by CHEMetrics (specific to the Mini Spec-20 spectrophotometer) to convert transmittance to concentration in mg/l.

16a. Measure phosphate (ortho) with # K-8503 (0-40 ppm). Record reading.

16b. Measure sulfide with # K-9503 (0-1.6 ppm). Record reading.

16c. Measure silica(SiO_2) with # K-9010 (0-10 ppm) after diluting 5:1 with ultra-pure distilled water. Record reading.

16d. Measure total iron with # K-6003 (0-5 ppm). Record reading.

16e. Measure ferrous iron with # K-6003 (0-5 ppm). Record reading.

16f. Measure ammonia with # K-1503 (0-7 ppm). Record reading.

Laboratory

17. Measure anions SO_4, Cl, F, NO_2, NO_3, Br, and PO_4 using the ion chromatograph(IC). Prepare fresh supply of recommended eluent, use new(cleaned) sample vials for placement of sample within the automated wisp system sample tray, and set instrument for proper eluent pump flow rate. Pick an appropriate analysis method from existing methods that have worked successfully in the past. Integrate peaks using data acquisition software. Adjust computer-generated values by comparing them to a certified check standard. Record readings.

18. Measure cations Mg, Ca, Li, Na, K, Ba, and Sr using the inductively-coupled plasma spectrophotometer (ICP). Record readings.

Computer processing

19. Calculate ion charge balance. Milliequivalents of cations must equal milliequivalents of anions within 5% to rule out analytical errors. If the balance exceeds 5% investigate the cause and reanalyze if necessary.

20. Enter data into Microsoft Excel spreadsheet to make additional calculations like TDS, hardness, and ion ratios.

Appendix B
Rainfall record
(1939-1993)

Rainfall records (in inches) collected by the Dunk family, Junction, Texas for the National Weather Service(1939-1993)

Year	Jan	Feb	Mar	Apr	May	Jun	Jul	Aug	Sep	Oct	Nov	Dec	Year
1939	2.51	1.31	0.70	1.12	1.36	4.25	1.11	1.31	0.00	3.09	1.25	2.29	**20.30**
1940	0.58	2.14	2.07	2.83	2.83	11.71	0.00	3.55	0.61	3.56	2.07	2.27	**34.22**
1941	0.45	2.20	3.60	2.23	1.22	1.44	2.35	3.28	4.89	8.95	0.00	0.78	**31.39**
1942	0.00	0.38	0.10	4.84	0.00	1.08	1.90	6.52	2.57	3.72	1.92	0.85	**23.88**
1943	0.32	0.00	1.88	1.23	2.15	4.33	1.81	0.00	7.58	1.95	1.98	1.90	**25.13**
1944	4.10	2.15	1.71	0.35	6.60	1.21	0.29	4.28	2.42	0.28	2.56	1.55	**27.50**
1945	1.78	1.55	2.72	2.24	0.77	3.01	2.61	1.48	1.90	1.77	0.21	0.36	**20.40**
1946	1.91	1.02	0.56	3.25	3.07	1.13	1.34	0.64	4.15	2.90	2.23	0.41	**22.61**
1947	4.18	0.38	1.74	1.16	3.34	6.84	0.90	1.17	0.52	1.09	2.60	1.60	**25.52**
1948	0.98	0.75	1.03	3.60	1.93	6.79	2.93	0.10	2.70	0.27	0.11	0.07	**21.26**
1949	3.46	4.51	0.60	4.60	3.12	5.19	1.47	4.60	4.45	5.87	0.00	2.23	**40.10**
1950	0.62	1.09	0.00	1.66	3.11	2.90	3.37	2.61	3.16	0.00	0.00	0.00	**18.52**
1951	0.00	0.57	1.75	0.99	2.49	2.26	0.00	3.31	0.35	0.55	0.00	0.33	**12.60**
1952	0.09	0.80	1.46	2.67	2.71	0.56	0.35	0.77	2.14	0.00	1.65	3.02	**16.22**
1953	0.00	1.04	2.03	0.72	4.13	0.00	1.97	0.82	1.09	1.19	0.30	0.30	**13.59**
1954	0.46	0.39	0.00	2.19	3.82	2.61	0.00	0.31	0.37	2.46	0.23	0.00	**12.84**
1955	1.43	0.45	0.76	0.07	5.22	2.09	2.97	2.96	6.12	0.08	0.87	0.41	**23.43**
1956	0.31	1.17	0.00	1.03	1.28	1.26	1.38	0.00	0.20	0.70	0.30	0.80	**8.43**
1957	0.65	2.21	2.55	9.47	7.78	1.27	0.45	2.07	3.13	9.38	4.29	0.47	**43.72**
1958	2.96	2.81	3.18	2.00	3.89	4.78	0.21	3.06	6.46	3.90	0.55	0.69	**34.49**
1959	1.43	0.00	3.75	2.40	0.00	6.76	1.11	0.97	0.00	3.49	1.44	2.34	**23.69**
1960	1.29	2.03	1.15	0.25	0.90	0.24	3.99	5.55	0.77	3.77	0.74	4.03	**24.71**
1961	2.44	1.77	0.62	0.00	2.06	8.37	1.93	2.01	1.46	0.82	1.51	0.55	**23.54**
1962	0.18	0.36	0.46	2.90	1.26	1.70	1.06	1.44	2.72	2.99	0.79	0.63	**16.49**
1963	0.00	1.11	0.17	0.85	4.79	2.05	0.00	6.71	0.98	1.20	2.81	0.43	**21.10**
1964	1.30	1.32	1.83	3.04	1.65	1.03	0.73	5.99	6.19	1.72	1.27	0.55	**26.62**
1965	2.29	3.73	0.00	1.65	7.25	1.96	0.89	0.28	2.58	0.99	0.48	1.28	**23.38**
1966	0.87	1.18	1.03	4.34	3.87	0.56	0.36	5.22	6.03	0.31	0.00	0.00	**23.77**
1967	0.25	0.93	0.40	1.01	2.31	0.67	3.40	0.80	2.08	2.41	3.25	1.68	**19.19**
1968	6.05	2.03	2.53	4.12	1.61	2.97	0.78	0.60	3.54	0.44	3.91	0.00	**28.58**
1969	0.25	1.00	1.40	3.58	1.59	3.38	2.03	1.76	1.62	6.93	1.39	1.81	**26.74**
1970	0.39	3.07	1.96	0.60	4.59	2.03	0.80	2.40	3.17	1.25	0.00	0.00	**20.26**
1971	0.00	1.02	0.00	1.70	1.82	1.69	2.12	8.24	0.98	4.55	0.63	1.12	**23.87**
1972	0.77	0.24	0.39	1.17	4.51	1.69	0.72	5.45	1.92	1.41	0.65	0.00	**18.92**
1973	2.27	2.64	2.08	1.22	1.08	3.21	5.69	0.43	1.79	8.94	0.31	0.00	**29.66**
1974	0.60	0.20	0.54	0.93	2.87	0.98	2.10	8.56	2.42	0.00	2.80	1.55	**23.55**
1975	0.00	2.40	0.53	2.06	6.30	3.13	2.13	0.55	0.71	1.68	0.67	0.41	**20.57**
1976	0.46	0.00	1.64	5.13	1.96	4.55	6.35	1.17	3.67	4.75	0.67	1.59	**31.94**
1977	1.17	0.55	1.97	4.89	3.75	0.23	0.00	0.00	1.78	2.47	2.05	0.00	**18.86**
1978	0.47	1.25	0.60	0.75	4.61	1.99	1.71	1.91	3.49	1.59	3.37	1.06	**22.80**
1979	0.71	1.70	1.58	5.27	1.93	2.49	2.86	5.07	0.00	0.00	0.50	1.76	**23.87**
1980	1.64	0.65	1.14	0.43	4.12	1.43	0.00	0.85	13.20	2.45	2.56	1.23	**29.70**
1981	0.93	0.69	3.51	5.59	3.18	9.37	0.00	1.97	0.58	5.97	0.42	0.00	**32.21**
1982	0.00	1.69	0.00	1.34	5.14	4.34	1.66	4.40	0.65	0.99	3.81	1.47	**25.49**
1983	0.82	2.62	2.94	0.00	3.08	2.25	5.11	2.13	1.36	0.00	1.07	2.02	**23.40**
1984	1.18	0.00	0.00	0.30	1.80	1.37	1.91	0.15	1.51	3.44	2.02	7.48	**21.16**
1985	1.02	0.78	1.52	1.22	2.32	1.75	1.92	0.00	5.19	3.10	0.59	0.00	**19.41**
1986	0.60	2.24	0.13	0.31	5.03	2.71	1.32	3.70	5.10	7.38	1.94	3.24	**33.70**
1987	0.00	2.65	0.94	1.26	4.37	6.43	0.65	1.59	2.59	0.15	1.12	0.89	**22.64**
1988	0.14	0.00	0.77	0.60	3.26	2.75	7.06	0.43	4.18	1.63	0.09	0.54	**21.45**
1989	2.97	3.02	1.43	3.16	3.12	3.17	0.35	3.00	0.92	1.57	1.10	0.00	**23.81**
1990	0.51	5.22	2.50	2.52	3.75	0.00	5.85	2.27	2.42	2.25	2.30	0.33	**29.92**
1991	1.60	0.94	0.40	1.21	1.36	3.50	1.87	2.62	4.24	2.21	0.65	5.50	**26.10**
1992	2.66	4.79	4.71	3.06	4.32	4.88	0.80	0.99	0.63	0.00	2.82	1.96	**31.62**
1993	1.28	1.29	1.56	2.17	3.21	2.95	0.00	0.70	3.47	1.45	0.17	1.15	**19.40**
Average	**1.19**	**1.49**	**1.36**	**2.17**	**3.08**	**2.97**	**1.76**	**2.41**	**2.70**	**2.47**	**1.33**	**1.22**	**24.15**

Appendix C
Descriptions of soil types

Descriptions of soil types

Tarrant soils

Found on limestone hills and ridgetops. These are very shallow to shallow clayey soils with limestone cobbles on gently sloping to steep slopes. These soils form in residuum weathered from the underlying fractured limestone bedrock. They are well drained, surface runoff is rapid, infiltration is moderately slow, and available water capacity is very low. They are well suited for vacation homes, wildlife habitat and rangeland but not to recreation and urban uses. They belong to hydrologic unit group D which has a very slow infiltration rate and high runoff potential. Clays with a high shrink-swell potential are common.

Tarrant-Real-Brackett soils

Very shallow to shallow soils on upland ridges and foothills. They are found along the base of limestone hills that slope toward the Llano River and are found along the larger creeks. They form in material weathered from interbedded limestone and calcareous clay loam. Slopes range from 1-50%. They are well drained, runoff is rapid, and available water capacity is very low. These soils are not suited to cultivation; they are used as rangeland and wildlife habitat. Belonging to hydrologic group C-D, they have a slow to very slow infiltration rate and high runoff rate.

Menard-Hext-Latom soils

Moderately deep to deep, form on upland plains from either loamy calcareous sediment of ancient alluvium or weakly consolidated sandstone. They are found on low ridges and knolls with slopes of from 1-12%. They are well drained and moderately permeable. These soil zones are used mainly as rangeland but are well suited to grains, fruit, and vegetables because of high natural fertility. They are well suited to recreational uses, rangeland, and wildlife habitat, and moderately suited to urban uses. They belong to hydrologic group B-D which has a moderate to very slow infiltration rate.

Nuvalde-Dev-Frio soils

Deep, gravelly and loamy, nearly level to gently sloping, and well drained. They are found on upland outwash plains formed from ancient alluvium, or on bottomlands formed from recent calcareous, loamy, and gravelly alluvial sediment of recent origin. Surface runoff is slow, permeability is moderate, and available water capacity is low to high. These are well suited to grains, pecans, wheat, corn, and alfalfa, and are used for wildlife habitat as well as urban and recreation purposes. Assigned to hydrologic group A-B they have a high infiltration rate and low runoff potential when thoroughly wet.

Appendix D
Table of water levels in wells

Table of water levels in wells

Project well #	Date measured (1994)	Windmill (w) Submersible pump (s)	Ground elevation (feet asl)	Depth to water (state data) (feet)	Depth to water (measured) (feet)	Water table elevation (feet asl)	Total depth (state data) (feet)	Total depth (measured) (feet)	Bottom of hole elevation (calculated) (feet asl)
1	13-Feb	s	1620	_	21	1599	104	104	1516
2	13-Feb	s	1620	_	24	1596	40	_	1580
3	13-Feb	s	1665	_	41	1624	_	_	_
4	13-Feb	s	1690	_	48	1642	80	_	1610
5	13-Feb	w	1750	_	24	1726	100	_	1650
6	13-Feb	s	1700	_	58	1643	90	_	1610
7	13-Feb	w	1640	_	50	1590	90	_	1550
8	13-Feb	w	1620	_	21	1599	100	_	1520
9	13-Feb	s	1690	58	48	1642	76	_	1566
10	27-Feb	s	1645	_	64	1581	_	_	_
11	27-Feb	w	1860	_	240	1620	_	_	_
12	5-Mar	s	1750	_	129	1621	183	_	1567
13	5-Mar	s	1705	_	83	1622	115	_	1590
14	5-Mar	w&s	1780	_	123	1654	155	182	1598
15	5-Mar	w	1730	_	68	1662	90	_	1620
16	5-Mar	s	1725	_	73	1652	102	_	1627
17	6-Mar	s	1625	_	31	1594	50	_	1575
18	6-Mar	s	1590	_	35	1555	55	_	1535
19	6-Mar	s	1580	_	49	1531	120	_	1460
20	6-Mar	w	1749	_	87	1662	115	158	1591
21	6-Mar	w	1862	_	187	1675	220	220	1642
22	6-Mar	w	1783	_	121	1662	150	135	1648
23	6-Mar	w	1833	_	124	1707	180	245	1588
24	15-Mar	w	1760	_	95	1661	159	180	1580
25	16-Mar	w	1647	_	39	1609	_	>285	<1347
26	16-Mar	w	1665	_	45	1621	75	_	1590
27	16-Mar	w	1675	45	43	1632	100	_	1620
28	16-Mar	w	1735	94	86	1649	100	_	1635

Table of water levels in wells

Project well #	Date measured (1994)	Windmill (w) Submersible pump (s)	Ground elevation (feet asl)	Depth to water (state data) (feet)	Depth to water (measured) (feet)	Water table elevation (feet asl)	Total depth (state data) (feet)	Total depth (measured) (feet)	Bottom of hole elevation (calculated) (feet asl)
29	16-Mar	w	1740	_	124	1616	_	140	1600
30	16-Mar	w	1700	_	90	1610	170	_	1600
31	16-Mar	w	1688	72	68	1620	80	_	1598
32	16-Mar	w	1716	105	104	1612	115	_	1601
33	16-Mar	s	1770	146	148	1622	200	155	1615
34	17-Mar	s	1655	_	42	1613	120	_	1535
35	17-Mar	s	1840	_	103	1737	150	113	1727
36	17-Mar	w	1913	_	222	1691	450	280	1633
37	17-Mar	w	1840	110	104	1736	127	130	1710
38	17-Mar	w	2056	_	100	1957	180	_	1876
39	17-Mar	s	1645	_	31	1614	80	_	1565
40	17-Mar	s	1666	_	39	1627	90	_	1576
41	18-Mar	s	1650	_	60	1590	110	_	1540
42	19-Mar	w	2018	_	68	1950	120	_	1898
43	19-Mar	w	1910	_	15	1895	60	_	1850
44	19-Mar	s	1845	_	208	1637	250	_	1595
45	19-Mar	w	2020	370	_	1650	>400	_	1620
46	20-Mar	w	2052	_	120	1932	168	165	1887
47	5-Apr	s	1704	_	100	1604	_	_	_
48	5-Apr	s	1640	_	41	1599	_	_	_
49	5-Apr	s	1660	_	54	1606	_	_	_
50	6-Apr	s	1680	68	58	1622	101	_	1579
51	6-Apr	s	1695	_	73	1622	_	_	_
52	6-Apr	s	1680	_	61	1619	_	_	_
53	7-Apr	s	1680	_	62	1618	_	_	_
54	7-Apr	s	1700	_	83	1617	_	_	_
55	7-Apr	s	2010	_	92	1918	_	_	_
56	8-Apr	s	1670	_	27	1643	100	_	1570

Table of water levels in wells

Project well #	Date measured (1994)	Windmill (w) Submersible pump (s)	Ground elevation (feet asl)	Depth to water (state data) (feet)	Depth to water (measured) (feet)	Water table elevation (feet asl)	Total depth (state data) (feet)	Total depth (measured) (feet)	Bottom of hole elevation (calculated) (feet asl)
57	8-Apr	w	1640	_	57	1583	90	_	1550
58	8-Apr	s	1642	55	54	1588	105	72	1570
59	8-Apr	s	2050	_	198	1852	450	400	1650
60	25-Apr	s	2170	_	188	1982	239	_	1931
61	25-Apr	s	1996	_	174	1966	_	200	1796
62	25-Apr	w	1670	73	51	1619	110	_	1560
63	25-Apr	w	_	_	110	_	190	_	_
64	25-Apr	w	1990	10	8	1982	20	20	1970
65	26-Apr	s	1760	_	43	1717	54	_	1706
66	26-Apr	s	1760	_	32	1728	200	_	1560
67	26-Apr	w	_	55	60	_	100	_	_
68	26-Apr	s	2083	100	132	1951	210	200	1883
69	1-May	w	2320	_	260	2060	340	_	1980
70	1-May	s	2225	140	217	2008	220	270	1955
71	1-May	w	2150	149	146	2004	200	235	1915
72	1-May	s	_	_	34	_	_	80	_
73	1-May	w	2230	_	228	2002	380	285	1850
74	1-May	w	2151	_	126	2025	_	150	2001
75	14-May	w	2160	_	191	1969	350	_	1810
76	14-May	w	2064	_	121	1943	200	220	1844
77	14-May	w	2185	_	185	2000	_	225	1960
78	15-May	s	1720	_	96	1624	_	130	1590
79	15-May	w	1720	_	93	1627	_	110	1610
80	15-May	s	1782	_	161	1621	_	190	1592
81	17-May	w	2188	_	156	2032	170	240	1948
82	17-May	w	2185	_	187	1998	_	260	1925
83	17-May	s	2310	_	266	2044	_	275	2035
84	17-May	s	2071	101	93	1978	200	204	1867

Table of water levels in wells

Project well #	Date measured (1994)	Windmill (w) Submersible pump (s)	Ground elevation (feet asl)	Depth to water (state data) (feet)	Depth to water (measured) (feet)	Water table elevation (feet asl)	Total depth (state data) (feet)	Total depth (measured) (feet)	Bottom of hole elevation (calculated) (feet asl)
85	17-May	s	2088	225	122	1966	125	206	1882
86	17-May	s	2010?	_	88	1922?	_	250	1760
87	17-May	w	2080	102	97	1983	225	166	1914
88	17-May	w	2194	240	_	1954	225	275	1919
89	17-May	w	2190	_	184	2006	_	205	1985
90	state data	s	2140	155	_	1985	240	_	1900
91	state data	w	1797	183	_	1614	240	_	1554
92	state data	s	1666	66	_	1600	118	_	1548
93	state data	s	1720	96	_	1624	150	_	1570
94	state data	s	1600	46	_	1554	120	_	1480
95	18-Jul	w	2270	280	_	1990	320	_	1950
96	18-Jul	w	2190		178	2012		195	1995
97	18-Jul	w	2209	205	146	2063	220	225	1984
98	18-Jul	w	2165	_	195	1970	254	_	1911
99	18-Jul	w	2135	142	144	1991	200	_	1935
100	18-Jul	w	2064	50	_	2014	200	_	1864
101	18-Jul	w	2070	_	149	1921	220	_	1850
102	state data	w	2253	238	_	2015	250	_	2003
103	state data	w	2250	256	_	1996	_	>280	<1970
104	state data	s	2190	186	_	2004	264	_	1926
105	state data	s	1680	38	_	1642	104	_	1576
106	state data	s	1665	40	_	1625	65	_	1600
107	state data	s	1640	42	_	1598	60	_	1580
108	state data	s	1620	40	_	1580	60	_	1560
109	state data	s	1617	40	_	1577	50	_	1567
110	state data	s	1646	88	_	1558	220	_	1426
111	state data	s	1580	60	_	1520	324	_	1256
112	state data	w	2092	126	_	1966	240	_	1852

Appendix E
Specific capacity and transmissivity calculations

Specific capacity/ transmissivity calculations

(based on driller sc test values used within the Walton (1962) equation)

Edwards Group Formations

Well #	Pump time (days)	Well radius (feet)	Specific capacity= rate of discharge(Q) in gpm/ drawdown(s) in feet	Transmissivity (feet^2/day) assuming the following values of storativity: S = .02	S = .002	S = .0002	S = .00002
56-27-1a	0.0139	0.29	0.0340	1.9	3.3	4.7	6.0
56-27-2	0.0208	0.21	0.1000	9.6	13.6	17.5	21.4
56-19-4a	0.0417	0.25	0.2500	35.5	39.4	49.1	58.6
56-19-4a	0.0833	0.25	0.0667	7.2	9.9	12.6	15.1
56-19-7b	0.0208	0.25	0.1692	16.7	23.5	30.0	36.6
56-19-7b	0.0208	0.25	0.0465	3.5	5.5	7.3	9.2
56-19-7a	0.0208	0.25	0.0543	4.1	6.4	8.5	9.6
56-19-5a	0.0208	0.25	0.1300	12.6	17.9	23.2	28.4
56-19-5b	0.0417	0.25	0.0170	1.2	1.9	2.5	3.2
56-19-7f	0.0313	0.25	0.0400	3.6	5.5	7.2	8.9
56-19-7f	0.0208	0.25	0.1200	10.9	15.9	20.7	25.2
56-19-7e	0.0208	0.25	0.0100	0.4	0.9	1.3	1.7
56-18-6c	0.0313	0.25	0.1000	9.6	13.6	17.6	21.5
56-18-6a	0.0833	0.25	0.1091	12.6	17.0	21.1	25.2
56-18-6a	0.0417	0.25	0.3000	35.0	46.7	58.1	70.1
56-18-9e	0.0208	0.30	0.0667	6.3	8.9	11.7	14.2
56-18-9c	0.0208	0.20	0.0042	0.3	0.4	0.7	0.9
56-18-9c	0.0104	0.25	0.0057	0.1	0.4	0.7	0.9
56-18-9c	0.0104	0.25	0.0042	0.1	0.4	0.5	0.7
56-18-9c	0.0104	0.25	0.0083	0.1	0.1	0.1	0.1
56-18-9b	0.0417	0.25	0.1406	15.1	20.8	26.2	31.5
56-26-3a	0.0417	0.25	0.0571	5.2	7.5	9.7	12.0
56-19-8a	0.0208	0.25	0.1100	9.9	14.4	18.8	23.0
56-19-8g	0.0208	0.25	0.0300	2.0	3.2	4.4	5.6
56-19-8d	0.0208	0.25	0.2300	23.9	33.2	42.2	50.9
56-19-8c	0.0208	0.25	0.0500	3.7	5.9	7.9	9.7
			sums:	231.1	316.3	404.5	490.4
			averages:	**8.9**	**12.2**	**15.6**	**18.9**

Specific capacity/ transmissivity calculations

Hensel Sand Formation

Well #	Pump time (days)	Well radius (feet)	Specific capacity= rate of discharge(Q) in gpm/ drawdown(s) in feet	Transmissivity (feet^2/day) assuming the following values of storativity: S = .02	S = .002	S = .0002	S = .00002
56-27-6j	.0417	.2080	.4167	56.0	72.4	88.6	104.4
56-27-6e	.0208	.2090	.2375	26.6	36.3	45.5	54.8
56-27-6e	.0208	.2090	.2500	28.3	38.4	48.2	57.6
56-27-6e	.0208	.2090	.2368	26.5	36.1	45.4	54.4
56-27-6c	.0208	.2090	.1111	10.9	15.5	19.9	24.1
56-27-6c	.0208	.2090	.1333	13.5	19.0	24.1	29.2
56-27-6b	.0208	.2920	.0615	4.6	7.3	9.7	12.1
56-27-6f	.0104	.2090	.0167	0.8	1.6	2.3	3.0
56-27-6g	.0104	.2090	.0822	6.6	10.0	13.2	16.6
56-27-8l	.0208	.2090	2.0000	298.8	376.9	453.6	530.1
56-28-1d	.0208	.2290	3.3333	516.7	646.8	773.8	900.3
56-28-1d	.0208	.2500	.0909	10.6	11.8	15.3	18.8
56-28-1f	.0208	.2290	2.8571	435.4	546.8	656.1	764.7
56-28-1g	.0417	.2920	5.8333	980.5	1206.6	1428.7	1648.6
56-28-1h	.0833	.2090	5.0000	942.8	1134.6	1324.2	1512.1
56-28-1h	.0417	.2090	10.0000	1886.3	2269.9	2648.6	3024.9
56-28-1k	.0208	.2090	.4000	48.7	64.5	80.1	95.4
56-28-1l	.0208	.2500	1.3330	181.6	233.9	285.2	376.4
56-28-1m	.0104	.2500	.0833	6.1	9.6	12.9	16.2
56-28-1p	.0208	.2500	.1000	9.0	13.2	17.0	23.1
56-28-2b	.0139	.2770	.0781	5.7	9.0	12.1	15.2
56-28-2b	.0139	.2770	.1786	16.0	23.4	30.4	37.4
56-28-4	.0417	.2090	.0247	2.0	3.1	4.0	5.1
56-28-4f	.0208	.2090	.0147	0.9	1.6	2.2	2.7
56-28-4f	.0104	.2090	.0222	1.2	2.2	3.1	3.9
56-28-4h	.0208	.2090	.0400	3.2	4.8	6.5	7.9
56-28-4k	.0208	.2090	.0455	3.6	5.5	7.3	9.0
56-28-4p	.0417	.2090	.0054	0.3	0.5	0.7	0.9
56-27-9c	.0208	.2500	.0079	0.3	0.7	0.9	1.3
56-27-9a	.0208	.2500	1.2000	161.0	208.3	254.8	300.5
56-28-4b	.0417	.2500	.0960	9.7	13.7	17.4	21.1
56-28-4c	.0417	.2500	.1600	24.1	30.4	36.5	42.5
56-28-4	.0208	.2500	.0532	4.2	6.3	8.5	10.6

56-28-7a	.0417	.2500	.8000	111.3	142.8	173.6	204.0
56-28-7c	.0208	.2500	3.0000	450.1	567.3	682.5	796.2
56-28-4q	.0208	.2090	.2778	31.9	43.1	53.8	64.6
56-28-4r	.0208	.2090	.1429	14.7	20.6	26.1	31.6
56-28-4s	.0208	.2090	.0079	0.4	0.8	1.1	1.3
56-28-4	.0208	.2090	.0532	4.4	6.7	8.6	10.8
56-20-6b	.0417	.2500	.5000	65.5	85.3	104.7	123.7
56-20-7a	.0208	.2500	.0800	6.5	9.7	12.8	15.5
56-20-8	.0104	.2500	.0900	7.0	10.9	14.7	18.3
56-20-8	.0069	.2500	3.1300	412.0	535.7	656.7	775.8
56-20-8	.0104	.2500	1.0000	119.0	158.8	197.8	236.1
56-20-4b	.0417	.2500	.8500	119.1	152.6	185.3	217.6
56-20-5t	.0625	.2500	.8600	126.8	160.4	193.5	226.1
56-20-5q	.0208	.2500	.1700	16.8	23.8	30.4	37.0
56-20-5p	.0104	.2500	.0200	0.8	1.7	2.6	3.4
56-20-5m	.0208	.2500	.0500	3.8	5.9	7.9	9.8
56-20-5h	.0208	.2500	.0900	7.8	11.6	15.2	18.7
56-20-5g	.0417	.2500	.7500	91.8	121.7	150.9	179.5
56-20-5g	.0208	.2500	.1900	19.2	27.1	34.5	41.7
56-20-5e	.0208	.2500	.3400	38.0	51.7	65.0	78.1
56-20-5e	.0417	.2500	.7000	95.8	123.4	150.3	177.1
56-20-5d	.0417	.2500	1.3330	196.8	248.9	300.0	350.3
56-20-5c	.0417	.2500	1.0000	143.1	182.4	220.9	258.8
56-20-5a	.0417	.2500	1.3300	196.8	248.9	300.0	350.5
sums:				8001.6	10002.4	11965.4	13952.0
averages:				**140.4**	**175.5**	**209.9**	**244.8**

Appendix F
Aquifer recharge calculations

Calculation of average monthly rainfall and average monthly Llano River discharge during January and December (low-flow months) for the period 1939-1988 for the combined North and South Llano River watersheds west of the study area.

Sources of data:

Rainfall - Dunk family for the National Weather Service
River discharge - USGS river gauge # 08150000

Month	Year	Rainfall (inches)	Llano River Discharge (acre-feet/ month)	High discharge values caused by storm runoff are removed and replaced by the ave. of the remaining monthly discharges. This adjusts the database in a way that allows the ave. river discharge to be more representative of gw discharge only.
JAN	1939	2.51	7210	
DEC	1939	2.29	6600	
JAN	1940	0.58	6280	
DEC	1940	2.27	5500	
JAN	1941	0.45	4820	
DEC	1941	0.78	5610	
JAN	1942	0.00	5270	
DEC	1942	0.85	7360	
JAN	1943	0.32	6650	
DEC	1943	1.90	5330	
JAN	1944	4.10	7860	
DEC	1944	1.55	4830	
JAN	1945	1.78	4920	
DEC	1945	0.36	2890	
JAN	1946	1.91	3640	
DEC	1946	0.41	3590	
JAN	1947	4.18	6060	
DEC	1947	1.60	3560	
JAN	1948	0.98	3490	
DEC	1948	0.07	4800	
JAN	1949	3.46	4840	
DEC	1949	2.23	6380	
JAN	1950	0.62	6310	
DEC	1950	0.00	3850	
JAN	1951	0.00	3730	
DEC	1951	0.33	2380	
JAN	1952	0.09	2370	
DEC	1952	3.02	2280	
JAN	1953	0.00	2200	
DEC	1953	0.30	2040	
JAN	1954	0.46	2050	
DEC	1954	0.00	1920	
JAN	1955	1.43	1990	
DEC	1955	0.41	2980	
JAN	1956	0.31	2850	
DEC	1956	0.80	1560	
JAN	1957	0.65	1610	
DEC	1957	0.47	5800	11140
JAN	1958	2.96	8550	

DEC	1958	0.69	5800	10780
JAN	1959	1.43	9460	
DEC	1959	2.34	6570	
JAN	1960	1.29	7390	
DEC	1960	4.03	5800	14490
JAN	1961	2.44	5800	13360
DEC	1961	0.55	8730	
JAN	1962	0.18	7740	
DEC	1962	0.63	4810	
JAN	1963	0.00	5120	
DEC	1963	0.43	4430	
JAN	1964	1.30	4220	
DEC	1964	0.55	7320	
JAN	1965	2.29	6670	
DEC	1965	1.28	4770	
JAN	1966	0.87	4670	
DEC	1966	0.00	5710	
JAN	1967	0.25	5770	
DEC	1967	1.68	4470	
JAN	1968	6.05	5800	39390
DEC	1968	0.00	5540	
JAN	1969	0.25	5540	
DEC	1969	1.81	5800	12900
JAN	1970	0.39	5800	11810
DEC	1970	0.00	6650	
JAN	1971	0.00	6770	
DEC	1971	1.12	9650	
JAN	1972	0.77	8780	
DEC	1972	0.00	7500	
JAN	1973	2.27	7410	
DEC	1973	0.00	9200	
JAN	1974	0.60	8540	
DEC	1974	1.55	5800	16460
JAN	1975	0.00	5800	13490
DEC	1975	0.41	5800	11310
JAN	1976	0.46	5800	10810
DEC	1976	1.59	5800	12530
JAN	1977	1.17	5800	11300
DEC	1977	0.00	9370	
JAN	1978	0.47	9210	
DEC	1978	1.06	7640	
JAN	1979	0.71	7330	
DEC	1979	1.76	6290	
JAN	1980	1.64	6330	
DEC	1980	1.23	7350	
JAN	1981	0.93	6920	
DEC	1981	0.00	5800	10650
JAN	1982	0.00	5800	10070
DEC	1982	1.47	6880	
JAN	1983	0.82	6840	
DEC	1983	2.02	5600	
JAN	1984	1.18	5440	
DEC	1984	7.48	5800	75560
JAN	1985	1.02	5800	20140
DEC	1985	0.00	6770	
JAN	1986	0.60	6360	
DEC	1986	3.24	5800	14190
JAN	1987	0.00	5800	16580
DEC	1987	0.89	5800	12260
JAN	1988	0.14	5800	11470
DEC	1988	0.54	8880	
	averages =	**2.9 cm (1.14 in.)/ month**	**5686 acre-ft/ month**	

Estimation of average annual ground-water recharge to be used as the initial value for numerical model input

Calculate recharge in the drainage basin above USGS Llano River gauge # 08150000 (drainage basin next to study area which includes drainage from both the North and South Llano Rivers)

area of drainage basin above Llano River stream gauge	1,849 square miles or 1,183,360 acres
average monthly rainfall during the low-flow months of Jan. and Dec. (1939-1988)	1.14 inches or .0950 feet
average monthly rainfall in acre-feet	.0950 feet * 1,183,360 acres = 112,419 acre-feet
average monthly discharge at river gauge (Jan and Dec, 1939-1988). Anomalously high discharge values which are caused by surface water runoff are replaced by the average of the remaining stream gauge values	5,686 acre-feet
% rainfall measured at Llano River gauge	5,686 acre-feet / 112,419 acre-feet = **5.06 %**

5.06 % IS THE PERCENTAGE OF RAINFALL DISCHARGING FROM THE AQUIFER INTO THE LLANO RIVER. BECAUSE THIS AQUIFER IS BEING MODELED AS A STEADY-STATE SYSTEM, DISCHARGE = RECHARGE.

Now transfer this discharge value to the area under study (which has no river gauge downgradient) to be used as the initial estimate of recharge in each cell of the numerical model.

average annual rainfall in study area 1939-1988 (Dunk data for the NWS)	24.15 inches
average annual recharge in study area	24.15 inches * .0506 **=1.22 inches or 3.10 cm**

Appendix G
Table of water chemistry values

Table of water chemistry values

Project well #	Formation	pH	H + (mg/l)	Eh measured (mv)	Eh calculated approxi-mation (mv)	Eh of Zobell standard (mv)	Temp (°C)	O2(probe) (mg/l)	O2 (mg/l)
1	Edwards Limestone	7.34	4.57E-08	315	488	255	21.4	8.6	7.0
2	Edwards Limestone	7.29	5.13E-08	248	414	262	20.3	7.0	7.0
3	Edwards Limestone	7.45	3.55E-08	282	431	279	21.7	8.0	7.0
4	Edwards Limestone	7.29	5.13E-08	195	328	295	22.3	6.3	7.0
5	Edwards Limestone	7.46	3.47E-08	260	416	272	20.5	6.8	6.0
6	Edwards Limestone	7.35	4.47E-08	251	419	260	22.3	2.9	2.0
7	Edwards Limestone	7.52	3.02E-08	235	404	259	20.6	6.0	6.5
8	Hensel Sand	7.10	7.94E-08	101	255	275	20.1	1.3	0.4
9	Hensel Sand	7.17	6.76E-08	235	415	248	21.3	5.6	5.5
10	Hensel Sand	7.30	5.01E-08	45	213	260	22.1	1.1	0.0
11	Hensel Sand	7.16	6.92E-08	325	413	340	21.4	5.0	9.0
12	Hensel Sand	6.95	1.12E-07	310	461	277	22.5	7.1	–
13	Hensel Sand	7.45	3.55E-08	310	413	345	21.5	1.9	0.8
14	Hensel Sand	7.10	7.94E-08	-75	99	254	21.6	1.7	0.0
15	Hensel Sand	7.24	5.75E-08	-30	108	290	22.0	1.2	0.5
16	Hensel Sand	7.07	8.51E-08	-5	151	272	21.6	1.8	0.5
17	Hensel Sand	7.20	6.31E-08	59	193	294	21.4	2.1	1.0
18	Alluvium	7.23	5.89E-08	195	388	235	20.8	1.9	1.5
19	Hensel Sand	7.05	8.91E-08	255	360	323	21.1	6.5	5.5
21	Hensel Sand	7.40	3.98E-08	250	228	400	21.6	1.3	0.3
22	Hensel Sand	7.45	3.55E-08	178	353	367	22.3	1.6	0.3

Table of water chemistry values

Project well #	Formation	O2 % sat.	Fe 2+ (mg/l)	Fe-tot (mg/l)	NH3 (mg/l)	Sulfide (mg/l)	SiO2 (mg/l)	Mn (mg/l)	HCO3 (mg/l)
1	Edwards Limestone	100	.00	.00	0.21	.03	15	.00	269
2	Edwards Limestone	79	.05	.08	0.36	.03	12	.00	319
3	Edwards Limestone	–	.02	.08	0.14	.02	21	.00	302
4	Edwards Limestone	76	.14	.02	0.25	.03	12	.00	299
5	Edwards Limestone	78	.02	.08	0.03	.03	15	.00	236
6	Edwards Limestone	–	.11	.11	0.40	.03	14	.00	328
7	Edwards Limestone	70	.08	.05	0.32	.03	10	.00	275
8	Hensel Sand	15	.14	.14	0.60	.03	14	.00	352
9	Hensel Sand	60	.02	.05	0.36	.04	15	.00	350
10	Hensel Sand	14	.66	.86	1.25	.04	9	.00	338
11	Hensel Sand	–	.05	.11	0.48	.04	12	.00	352
12	Hensel Sand	82	.08	.11	0.40	.03	18	.00	446
13	Hensel Sand	22	.05	.14	0.73	.04	6	.00	345
14	Hensel Sand	20	.51	1.85	1.74	.06	0	.00	386
15	Hensel Sand	14	.05	.74	1.35	.03	9	.00	331
16	Hensel Sand	21	.11	.24	1.46	.04	9	.00	345
17	Hensel Sand	25	.05	.41	1.46	.03	9	.00	327
18	Alluvium	23	.05	.14	0.25	.06	12	.00	266
19	Hensel Sand	77	.14	.27	0.17	.03	20	.00	333
21	Hensel Sand	–	.05	.11	1.70	.03	12	.00	303
22	Hensel Sand	–	.02	.02	1.30	.03	10	.00	368

Table of water chemistry values

Project well #	Formation	HCO3 (meq/l) (mm/l)	F (mg/l)	F (meq/l) (mm/l)	Cl (mg/l)	Cl (meq/l) (mm/l)	NO2 (mg/l)	Br (mg/l)	NO3 (mg/l)
1	Edwards Limestone	4.41	0.49	.03	19.74	0.56	0.21	0.20	1.59
2	Edwards Limestone	5.23	0.72	.04	25.42	0.72	0.20	0.23	11.47
3	Edwards Limestone	4.95	0.80	.04	31.93	0.90	0.20	0.22	4.65
4	Edwards Limestone	4.90	0.40	.02	16.65	0.47	0.00	0.00	2.14
5	Edwards Limestone	3.87	0.59	.03	31.83	0.90	0.24	0.03	2.13
6	Edwards Limestone	5.38	1.39	.07	34.74	0.98	0.42	0.01	1.59
7	Edwards Limestone	4.51	–	–	–	–	–	–	–
8	Hensel Sand	5.77	1.55	.08	61.54	1.73	0.39	0.71	0.62
9	Hensel Sand	5.74	0.50	.03	46.84	1.32	0.44	0.03	9.35
10	Hensel Sand	5.54	1.78	.09	316.73	8.92	0.85	2.17	0.31
11	Hensel Sand	5.77	0.47	.02	38.84	1.09	0.35	0.01	8.13
12	Hensel Sand	7.31	0.00	.00	36.30	1.02	0.43	0.00	21.80
13	Hensel Sand	5.66	1.84	.10	151.01	4.25	0.00	1.05	2.35
14	Hensel Sand	6.33	1.32	.07	156.50	4.41	0.43	0.57	0.26
15	Hensel Sand	5.43	1.72	.09	196.75	5.54	0.53	0.96	0.25
16	Hensel Sand	5.66	1.37	.07	182.05	5.13	0.52	1.45	0.33
17	Hensel Sand	5.36	3.39	.18	242.17	6.82	0.94	1.34	0.74
18	Alluvium	4.36	0.39	.02	32.65	0.92	0.16	0.29	0.53
19	Hensel Sand	5.46	–	–	–	–	–	–	–
21	Hensel Sand	4.97	2.93	.15	104.99	2.96	0.52	0.54	0.30
22	Hensel Sand	6.03	3.16	.17	104.74	2.95	0.55	0.52	0.24

Table of water chemistry values

Project well #	Formation	NO3 (meq/l) (mm/l)	SO4 (mg/l)	SO4 (meq/l)	SO4 (mm/l)	Li (mg/l)	Na (mg/l)	Na (meq/l) (mm/l)	K (mg/l)
1	Edwards Limestone	.026	11.2	0.23	0.12	.017	17.876	0.777	1.520
2	Edwards Limestone	.185	12.4	0.26	0.13	.018	20.640	0.897	0.850
3	Edwards Limestone	.075	13.7	0.29	0.14	.027	22.190	0.965	0.840
4	Edwards Limestone	.035	7.5	0.16	0.08	.000	13.730	0.597	1.520
5	Edwards Limestone	.034	21.5	0.45	0.22	.019	27.910	1.213	1.370
6	Edwards Limestone	.026	56.1	1.17	0.58	.063	41.650	1.811	4.210
7	Edwards Limestone	–	–	–	–	.000	21.640	0.941	1.210
8	Hensel Sand	.010	110.4	2.30	1.15	.000	68.980	2.999	7.820
9	Hensel Sand	.151	40.0	0.83	0.42	.035	30.580	1.330	0.700
10	Hensel Sand	.005	109.6	2.28	1.14	.000	170.360	7.407	12.410
11	Hensel Sand	.131	26.9	0.56	0.28	.027	28.750	1.250	1.310
12	Hensel Sand	.352	24.9	0.52	0.26	.023	47.780	2.077	7.590
13	Hensel Sand	.038	63.2	1.32	0.66	.111	160.100	6.961	10.780
14	Hensel Sand	.004	188.0	3.91	1.96	.082	94.260	4.098	9.890
15	Hensel Sand	.004	181.3	3.77	1.89	.000	131.580	5.721	14.710
16	Hensel Sand	.005	174.9	3.64	1.82	.082	83.100	3.613	9.880
17	Hensel Sand	.012	625.3	13.02	6.51	.203	361.650	15.724	14.310
18	Alluvium	.009	22.0	0.46	0.23	.028	22.570	0.981	1.660
19	Hensel Sand	–	–	–	–	.015	22.450	0.976	3.680
21	Hensel Sand	.005	390.1	8.12	4.06	.143	190.840	8.297	16.380
22	Hensel Sand	.004	389.3	8.10	4.05	.130	196.200	8.530	18.060

Table of water chemistry values

Project well #	Formation	K (meq/l) (mm/l)	Ca (mg/l)	Ca (meq/l)	Ca (mm/l)	Mg (mg/l)	Mg (meq/l)	Mg (mm/l)	Sr (mg/l)
1	Edwards Limestone	.04	48.58	2.429	1.212	30.84	2.538	1.269	0.2
2	Edwards Limestone	.02	83.40	4.170	2.081	24.28	1.998	0.999	0.3
3	Edwards Limestone	.02	61.53	3.077	1.535	32.41	2.667	1.333	0.7
4	Edwards Limestone	.04	59.41	2.971	1.482	31.44	2.588	1.293	0.3
5	Edwards Limestone	.04	43.53	2.177	1.086	27.23	2.241	1.120	0.4
6	Edwards Limestone	.11	57.09	2.855	1.424	42.23	3.476	1.737	4.0
7	Edwards Limestone	.03	50.69	2.535	1.265	33.86	2.787	1.393	0.9
8	Hensel Sand	.20	62.39	3.120	1.557	47.63	3.920	1.959	5.5
9	Hensel Sand	.02	76.80	3.840	1.916	42.20	3.473	1.736	0.5
10	Hensel Sand	.32	91.35	4.568	2.279	72.32	5.952	2.975	10.7
11	Hensel Sand	.03	73.88	3.694	1.843	40.07	3.298	1.648	0.6
12	Hensel Sand	.19	83.90	4.195	2.093	42.08	3.463	1.731	0.8
13	Hensel Sand	.28	44.56	2.228	1.112	24.37	2.006	1.002	2.5
14	Hensel Sand	.25	94.08	4.704	2.347	75.02	6.174	3.086	6.3
15	Hensel Sand	.38	78.30	3.915	1.954	66.22	5.450	2.724	13.9
16	Hensel Sand	.25	93.17	4.659	2.325	77.10	6.346	3.172	10.3
17	Hensel Sand	.37	85.41	4.271	2.131	77.56	6.384	3.190	22.8
18	Alluvium	.04	65.78	3.289	1.641	23.19	1.909	0.954	1.8
19	Hensel Sand	.09	87.86	4.393	2.192	26.91	2.215	1.107	0.9
21	Hensel Sand	.42	72.01	3.601	1.797	57.64	4.744	2.371	17.5
22	Hensel Sand	.46	71.42	3.571	1.782	58.01	4.774	2.386	17.6

Table of water chemistry values

Project well #	Formation	HCO3-2(Ca+Mg-SO4+.5(Na-Cl))	Ca+Mg	(Ca+Mg-SO4+.5*(Na-Cl))	(Ca+Mg-SO4+.5(Na-Cl))/HCO3	Ca+Mg/HCO3	Na/Cl	Ca/SO4	Ca/HCO3
1	Edwards Limestone	-0.540	2.481	2.475	0.561	0.563	1.398	10.413	0.275
2	Edwards Limestone	-0.853	3.080	3.041	0.582	0.589	1.253	16.139	0.398
3	Edwards Limestone	-0.566	2.868	2.758	0.557	0.579	1.073	10.769	0.310
4	Edwards Limestone	-0.622	2.776	2.762	0.563	0.566	1.273	19.047	0.302
5	Edwards Limestone	-0.413	2.206	2.141	0.553	0.570	1.354	4.853	0.281
6	Edwards Limestone	-0.610	3.162	2.994	0.557	0.588	1.851	2.438	0.265
7	Edwards Limestone	_	2.658	_	_	0.589	_	_	0.281
8	Hensel Sand	-0.230	3.516	3.000	0.520	0.609	1.730	1.355	0.270
9	Hensel Sand	-0.745	3.652	3.241	0.565	0.637	1.008	4.606	0.334
10	Hensel Sand	-1.170	5.254	3.356	0.606	0.948	0.830	1.998	0.411
11	Hensel Sand	-0.808	3.492	3.289	0.570	0.605	1.142	6.579	0.319
12	Hensel Sand	-0.874	3.824	4.093	0.560	0.523	2.032	8.080	0.286
13	Hensel Sand	0.037	2.114	2.809	0.497	0.374	1.636	1.689	0.197
14	Hensel Sand	-0.314	5.433	3.321	0.525	0.859	0.930	1.199	0.371
15	Hensel Sand	-0.334	4.678	2.880	0.531	0.862	1.032	1.035	0.360
16	Hensel Sand	-0.181	5.496	2.918	0.516	0.972	0.705	1.277	0.411
17	Hensel Sand	-1.167	5.321	3.264	0.609	0.993	2.305	0.327	0.398
18	Alluvium	-0.433	2.595	2.397	0.550	0.595	1.067	7.168	0.376
19	Hensel Sand	_	3.299	_	_	0.604	_	_	0.402
21	Hensel Sand	-0.587	4.168	2.777	0.559	0.839	2.806	0.442	0.362
22	Hensel Sand	0.221	4.168	2.906	0.482	0.691	2.891	0.440	0.295

Table of water chemistry values

Project well #	Formation	Sr (meq/l)	Sr (mm/l)	Hardness (mg/l)	%Na	SAR	RSC	TDS (mg/l)	Ionic Strength (mm)
1	Edwards Limestone	.005	.002	249	13.4	0.5	-0.6	279	0.008116
2	Edwards Limestone	.007	.004	309	12.7	0.5	-0.9	348	0.009968
3	Edwards Limestone	.015	.007	288	14.3	0.6	-0.8	338	0.009513
4	Edwards Limestone	.006	.003	278	9.6	0.4	-0.7	292	0.008744
5	Edwards Limestone	.008	.004	222	21.4	0.8	-0.5	287	0.007908
6	Edwards Limestone	.090	.045	321	22.0	1.0	-1.0	418	0.011769
7	Edwards Limestone	.019	.010	267	15.0	0.6	-0.8	_	_
8	Hensel Sand	.124	.062	359	29.3	1.6	-1.3	553	0.014851
9	Hensel Sand	.011	.005	367	15.4	0.7	-1.6	435	0.012438
10	Hensel Sand	.245	.122	539	40.6	3.2	-5.0	961	0.024178
11	Hensel Sand	.013	.006	351	15.1	0.7	-1.2	404	0.011708
12	Hensel Sand	.018	.009	384	20.9	1.1	-0.3	502	0.013663
13	Hensel Sand	.057	.029	215	60.7	4.8	1.4	636	0.014243
14	Hensel Sand	.145	.072	552	26.9	1.8	-4.6	815	0.022507
15	Hensel Sand	.316	.158	485	37.0	2.6	-3.9	856	0.022026
16	Hensel Sand	.234	.117	562	24.3	1.5	-5.3	811	0.022231
17	Hensel Sand	.521	.261	559	58.8	6.8	-5.3	1603	0.038414
18	Alluvium	.041	.020	262	15.8	0.6	-0.8	313	0.008856
19	Hensel Sand	.020	.010	332	12.7	0.5	-1.1	_	_
21	Hensel Sand	.399	.200	438	48.6	4.1	-3.4	1014	0.025256
22	Hensel Sand	.403	.201	438	49.2	4.2	-2.3	1050	0.025917

Table of water chemistry values

Project well #	Formation	Sum of Cations (meq)	Sum of Anions (meq)	Charge Balance Error (%)	Na/Cl	Mg/Ca	Ca+Mg-SO4	Na-Cl	.5(Na-Cl)
1	Edwards Limestone	5.79	5.25	4.9	1.398	1.047	2.364	0.221	0.111
2	Edwards Limestone	7.09	6.43	4.9	1.253	0.480	2.951	0.181	0.091
3	Edwards Limestone	6.75	6.25	3.8	1.073	0.868	2.726	0.065	0.033
4	Edwards Limestone	6.20	5.58	5.2	1.273	0.873	2.698	0.128	0.064
5	Edwards Limestone	5.67	5.28	3.6	1.354	1.031	1.982	0.317	0.158
6	Edwards Limestone	8.34	7.62	4.5	1.851	1.220	2.577	0.832	0.416
7	Edwards Limestone	6.31	–	–	–	1.101	–	–	–
8	Hensel Sand	10.36	9.89	2.3	1.730	1.259	2.367	1.266	0.633
9	Hensel Sand	8.67	8.07	3.6	1.008	0.906	3.236	0.010	0.005
10	Hensel Sand	18.49	16.84	4.7	0.830	1.305	4.113	-1.515	-0.757
11	Hensel Sand	8.29	7.58	4.5	1.142	0.894	3.211	0.156	0.078
12	Hensel Sand	9.95	9.20	3.9	2.032	0.827	3.565	1.055	0.527
13	Hensel Sand	11.53	11.36	0.7	1.636	0.902	1.456	2.707	1.353
14	Hensel Sand	15.38	14.72	2.2	0.930	1.315	3.476	-0.310	-0.155
15	Hensel Sand	15.78	14.84	3.1	1.032	1.394	2.791	0.179	0.089
16	Hensel Sand	15.10	14.50	2.0	0.705	1.364	3.676	-1.515	-0.758
17	Hensel Sand	27.27	25.39	3.6	2.305	1.497	-1.187	8.902	4.451
18	Alluvium	6.26	5.77	4.1	1.067	0.581	2.366	0.062	0.031
19	Hensel Sand	7.70	–	–	–	0.505	–	–	–
21	Hensel Sand	17.46	16.20	3.7	2.806	1.320	0.107	5.340	2.670
22	Hensel Sand	17.74	17.26	1.4	2.891	1.339	0.116	5.580	2.790

Bibliography

Bibliography

Abbott, P. L., and C. M. Woodruff, Jr., eds, 1986, The Balcones Escarpment-geology, hydrology, ecology and social development in central Texas: Published for the Geological Society of America Annual Meeting, San Antonio, Texas, November, 1986, 200 p.

Alexander, W. H., Jr., and J. H. Patman, 1969, Groundwater resources of Kimble County, TX, Texas Water Development Board Report 95, 93 p.

American Association of Petroleum Geologists, 1973, Geological highway map of Texas, H. B. Renfro Memorial Edition.

Amsbury, D. L., R. F. Inden, F. E. Lozo, Jr., C. H. Moore, B. F. Perkins, C. I. Smith, and F. L. Stricklin Jr.,1974, Shallow marine sediments of the early Cretaceous (Trinity) platform of central Texas, a field guide: Society of Economic Paleontologists and Mineralogists, Forty-eighth Annual Meeting, April 4-6, 1974, San Antonio, TX, p. 1-15.

Anderson, M. P., and W. W. Woessner, 1992, Applied Groundwater Modeling, Simulation of Flow and Advective Transport: Academic Press, 379 p.

Ardis, A. F., and R. A. Barker, 1993, Historical saturated thickness of the Edwards-Trinity aquifer system and selected contiguous hydraulically connected units, west-central Texas: U. S. Geological Survey Water Resources Investigations Report 92-4125, 2 plates.

Ashworth, J. B., 1983, Ground-water availability of the Lower Cretaceous formations in the Hill Country of south-central Texas: Texas Department of Water Resources Report 273, 173 p.

Back, W. H., 1966, Hydrochemical facies and groundwater flow patterns in the northern part of the Atlantic coastal plain: U. S. Geological Survey Professional Paper 498-A, 42 p.

Bain, J. S., 1973, The nature of the Cretaceous-pre-Cretaceous contact in north-central Texas: Baylor Geological Studies Bulletin 25, 44 p.

Barker, R. A., P. W. Bush, and E. T. Baker, Jr., 1994, Geologic history and hydrogeologic setting of the Edwards-Trinity aquifer system, west-central Texas: U. S. Geological Survey Water Resources Investigations Report 94-4039, 51 p.

Barker, R. A., and A. F. Ardis, 1992, Configuration of the base of the Edwards-Trinity aquifer system and hydrogeology of the underlying pre-Cretaceous rocks, west-central Texas: U. S. Geological Survey Water Resources Investigations Report 91-4071, 25 p.

Barnes, V. E., 1981, Geologic Atlas of Texas, Llano sheet: The University of Texas at Austin, Bureau of Economic Geology.

Bay, T. A., Jr., 1977, Lower Cretaceous models from Texas and Mexico, in D. G. Bebout, and R. G. Loucks, eds., Cretaceous carbonates of Texas and Mexico, applications to subsurface exploration: The University of Texas at Austin, Bureau of Economic Geology Report of Investigations 89.

Bear, J., M. S. Beljin, and R. R. Ross, 1992, Fundamentals of ground-water modeling, EPA/540/S-92/005: Superfund Technology Support Center for Ground Water, Robert S. Kerr Environmental Research Lab, U. S. Environmental Protection Agency, 11p.

Bebout, D. G., and R. G. Loucks, eds, 1977, Cretaceous carbonates of Texas and Mexico, applications to subsurface exploration: The University of Texas at Austin, Bureau of Economic Geology Report of Investigations 89, 332 p.

Blum, E., 1982, Soil survey of Kimble County, U. S. Department of Agriculture, Soil Conservation Service, 99 p.

Bluntzer, R. L., 1992, Evaluation of the ground-water resources of the Paleozoic and Cretaceous aquifers in the Hill Country of central Texas: Texas Water Development Board Report 339, 130 p.

Boone, P. A., 1968, Stratigraphy of the basal Trinity Sands (Lower Cretaceous) of central Texas: Baylor Geological Studies Bulletin 15, 64 p.

Bush, P. W., A. F. Ardis, and K. H. Wynn, 1993, Historical potentiometric surface of the Edwards-Trinity aquifer system and contiguous hydraulically connected units, west-central Texas: U. S. Geological Survey Water Resources Investigations Report 92-4055, 3 sheets.

Bush, P. W., 1986, Planning report for the Edwards-Trinity regional aquifer-system analysis in central Texas, southeast Oklahoma, and southwest Arkansas: U. S. Geological Survey Water Resources Investigation Report 86-4343, 15 p.

Campbell, D. H., 1962, Petrography of the Cretaceous Hensell Sandstone, central Texas: M.A. thesis, The University of Texas at Austin, 180 p.

Cartwright, L. D. Jr, 1932, Regional structure of the Cretaceous on the Edwards Plateau of southwest Texas: American Association of Petroleum Geologists Bulletin, v. 16, no. 7, p. 691-700.

Chebotarev, I. I., 1955, Metamorphism of natural waters in the crust of weathering: Geochim. Cosmochim. Acta., 8, p. 22-48, 137-170, and 198-212.

Darcy, H., 1856, Les fontaines publiques dela ville de Dijon: Paris, Victor Dalmont, 647 p.

Dixon, W., and B. Chiswell, 1992, The use of hydrochemical sections to identify recharge areas and saline intrusions in alluvial aquifers, southeast Queensland, Australia: Journal of Hydrology, v. 135, p. 259-274.

Dugan, J. T., 1986, Hydrologic characteristics of soils in parts of Arkansas, Colorado, Kansas, Missouri, Nebraska, New Mexico, Oklahoma, South Dakota, and Texas: U. S. Geological Survey Hydrologic Investigations Atlas HA-678, three sheets.

Dugas, W. A., and R. A. Hicks, 1994, Effect of removal of juniperus ashei on evapotranspiration and runoff in the Seco Creek watershed: 1994 Annual Report of the Seco Creek Demonstration Project, Texas Agricultural Experiment Station Blackland Research Center, September 1994, 12 p.

Dunk, W., 1994, rainfall data recorded in the years 1939-1993 by the Dunk family in the Junction area for the National Weather Service.

Fetter, C.W., 1988, Applied Hydrogeology, 2nd. ed., Columbus, Ohio, Merrill Publishing Co., 592 p.

Fisher, W. L., and P. U. Rodda, 1969, Edwards Formation (Lower Cretaceous),Texas, dolomitization in a carbonate platform system: American Association of Petroleum Geologists Bulletin, v. 53, no. 1, p. 55-72.

Fogg, G. E., 1989, Architecture and interconnectedness of geologic media, role of the low-permeability facies in flow and transport, in Hydrogeology of Low Permeability Environments, Special Symposium of the Twenty-Eighth International Geological Congress, July 9-19, 1989: International Association of Hydrogeologists, Verlag Heinz Heise, p 19-40.

Freeze, R.A., and J.A. Cherry, 1979, Ground Water, Englewood Cliffs, New Jersey, Prentice-Hall, 604 p.

Golden Software, Inc., 1988, SURFER manual, vers. 4., Golden, Colorado.

Hall, D W., and J. L. Turk, 1975, Aquifer evaluation using depositional systems, an example in north-central Texas: Ground Water, v. 13, no. 6, p 472-483.

Hammond, W. W., G. Longley, D. J., Pavlicek, and G. B. Ozuna, 1986, Hydrogeology of the Edwards Aquifer: Field Trip Guidebook, Geological Society of America Annual Meeting, San Antonio, TX, 45 p.

Heath, R. C., 1983, Basic ground-water hydrology, U. S. Geological Survey Professional Paper 2220, 84 p.

Hendricks, L., ed., 1967, Comanchean (Lower Cretaceous) stratigraphy and paleontology of Texas: Permian Basin Section, Society of Economic Paleontologists and Mineralogists Publication 67-8, 410 p.

Henningsen, R. E., 1962, Water diagenesis in Lower Cretaceous Trinity aquifers of central Texas: Baylor University, Baylor Geological Studies Bulletin 3, 38 p.

Hill Country Underground Water Conservation District, 1994, Gillespie County regional water management plan, prepared in association with Blackwell, Lackey and Associates Inc., McGinnis, Lockridge and Kilgore LLP.

Hill, R. T., 1901, Geography and geology of the Black and Grand Praries, Texas, with detailed descriptions of the Cretaceous formations and special reference to artesian waters: U. S. Geological Survey, Twenty-First Annual Report, pt. 2, 1899-1900, 666 p.

Hill, R. T., and T. W. Vaughan, 1898, Geology of the Edwards Plateau and Rio Grande Plain adjacent to Austin and San Antonio, Texas with reference to the occurence of underground waters, U. S. Geological Survey Eighteenth Annual Report pt. 11, p. 193-321.

Holland, P. H., and H. B. Mendieta, 1965, Base-flow studies, Llano River, Texas, quantity and quality: U. S. Geological Survey, March, 1965, 20 p.

Hughes, R. J. Jr., 1948, A study of the Lower Cretaceous section near Junction, TX: MA thesis, The University of Texas at Austin, 32 p.

Inden, R. F., 1974, Lithofacies and depositional model for a Trinity Cretaceous sequence, central Texas: Louisiana State University, Geoscience and Man 8, p. 37-52.

Konikow, L. F., and J. Bredehoeft, 1992, Ground-water models cannot be validated: Advances in Water Resources v. 15, p. 75-83.

Larkin, T. J., and G. W. Bomar, 1983, Climatic atlas of Texas, Texas Department of Water Resources Publication LP-192, 151 p.

Lattman, L. H., and R. R. Parizek, 1964, Relationship between fracture traces and the occurance of groundwater in carbonate rocks: Journal of Hydrology, v. 2, p. 73-91.

LeGrand, H. E., and V. T. Stringfield, 1971, Water levels in carbonate rock terranes: Ground Water, v. 9, no. 3, p 4-10.

LeGrand, H. E., and V. T. Stringfield, 1971, Development and distribution of permeability in carbonate aquifers: Water Resources Research, v. 7, no. 5, p. 1284-1295.

Lloyd, J. W., and J. A. Heathcote, Natural Inorganic Hydrochemistry in Relation to Groundwater, An Introduction: Oxford, Oxford Press, 295 p.

Lozo, F. E., and others, 1959, Symposium on the Edwards Limestone in central Texas: The University of Texas at Austin, Bureau of Economic Geology Publication 5905, 235 p.

Lozo, F. E., and F. L. Stricklin Jr., 1956, Stratigraphic notes on the outcrop basal Cretaceous, central Texas: Transactions, Gulf Coast Association of Geological Societies, v. 6, p. 67-78.

Lozo, F. E., 1949, Stratigraphic relations of Fredricksburg limestones, northwest Texas: Shreveport Geological Society Seventeenth Annual Field Trip Guidebook, p 85-91.

Maclay, R. W., and L. F. Land, 1989, Simulation of flow in the Edwards aquifer, San Antonio region, Texas, and refinement of storage and flow concepts: U. S. Geological Survey Water Supply Paper 2336, 47 p.

Maclay, R. W., and T. A. Small, 1984, Carbonate geology and hydrology of the Edwards aquifer in the San Antonio area, Texas: U. S. Geological Survey Open File Report 83-537, 72 p.

Mazor, E., 1991, Applied Chemical and Isotopic Groundwater Hydrology, New York, N. Y., Halsted Press, 274 p.

McDonald, M. G., A. W. Harbaugh, B. R. Orr, and D. J. Ackerman,1991, A method of converting no-flow cells to variable-head cells for the U.S. Geological Survey modular three-dimensional finite-difference ground-water flow model: U.S. Geological Survey Open File Report 91-536, 99 p.

McDonald, M. G., A. W. Harbaugh, 1988, A modular three-dimensional finite-difference ground-water flow model: U. S. Geological Survey Techniques of Water Resources Investigations, Book 6, Chapter A1.

Menard, J. A., 1995, Bibliography of the Edwards aquifer, Texas, through 1993: U. S. Geological Survey Open File Report 95-336, 75 p.

Moore, C. H., Jr., and D. G. Bebout, 1989, Carbonate rock sequences from the Cretaceous of Texas: Field Trip Guidebook T376, American Geophysical Union, Washington D. C.

Moore, C. H., Jr., 1969, ed., Depositional environments and depositional history, Lower Cretaceous shallow shelf carbonate sequence, west-central Texas: Dallas Geological Society, Annual Meeting of the American Association of Petroleum Geologists and the Society of Economic Paleontologists and Mineralogists, Dallas, Texas, April, 1969, 135 p.

Moore, C. H., Jr., 1964, Stratigraphy of the Fredricksburg Division, south-central Texas: The University of Texas at Austin, Bureau of Economic Geology Report of Investigations 52, 48 p.

Murray, C. R., and E. B. Reeves, 1972, Estimated use of water in the United States in 1970: U. S. Geological Survey Circular 676, 37 p.

Myers, B. N., 1969, Compilation of results of aquifer tests in Texas, Texas Water Development Board Report 98, 532 p.

Payne, J. Hopkins, 1982, Sedimentation and pedogenesis of the Lower Cretaceous Hensell Formation, central Texas: M.A. thesis, The University of Texas at Austin, 136 p.

Pearson, F. J., and P. L. Rettman, 1976, Geochemical and isotopic analysis of waters associated with the Edwards limestone aquifer, central Texas: U. S. Geological Survey and the Edwards Underground Water District, 34 p.

Piper, A. M., 1953, A graphic procedure in the geochemical interpretation of water analysis: American Geophysical Union Transactions, v. 25, p. 914-923.

Rapp, K. B., 1988, Groundwater recharge in the Trinity aquifer, central Texas: Baylor Geological Studies Bulletin 46, Baylor University, 34 p.

Reddi, L. N., 1990, Potential pitfalls in using groundwater models, transferring models to users: American Water Resources Association, Nov. 1990, p. 131-140.

Rose, P. R., 1972, Edwards Group, surface and subsurface, central Texas: The University of Texas at Austin, Bureau of Economic Geology Report of Investigations 74, 198 p.

Sami, K., 1992, Recharge mechanisms and geochemical processes in a semi-arid sedimentary basin, Eastern Cape, South Africa: Journal of Hydrology, v. 139, p. 27-48.

Sharp, J. M. Jr., 1990, Stratigraphic, geomorphic, and structural controls on the Edwards Aquifer, Texas, USA, in E. S. Simpson and J. M. Sharp Jr., eds., Selected papers on hydrogeology: International Association of Hydrogeologists, Heise, Hannover, v. 1, p. 67-82.

Stiff, H. A., Jr., 1951, The interpretation of chemical water analysis by means of patterns: Journal of Petroleum Technology 3, no. 10, sec. 1, and no. 15-16, sec. 2, 3.

Stricklin, F. L. Jr., C. I. Smith, and F. E. Lozo, 1971, Stratigraphy of Lower Cretaceous Trinity deposits of central Texas: The University of Texas at Austin, Bureau of Economic Geology Report of Investigations 71, 63 p.

Texas Natural Resources Information Service (TNRIS), 1994, Streamflow data for U. S. Geological Survey stream gauge # 08150000, Llano River at Junction.

Toth, J., 1963, A theoretical analysis of groundwater flow in small drainage basins, Journal of Geophysical Research v. 67, p. 4795 - 4812.

Toth, J., 1962, A theory of groundwater motion in small drainage basins in Central Alberta, Canada: Journal of Geophysical Research v. 67, p. 4375- 4387.

U. S. Geological Survey, 1989, National Water Summary 1988-89, Floods and Droughts, Texas, U. S. Geological Survey Water Supply Paper 2375, p. 513-520.

Walker, L., 1979, Occurence, availability and chemical quality of ground water in the Edwards Plateau region of Texas: Texas Department of Water Resources Report 235, 337 p.

Walton, W. C., 1962, Selected analytical methods for well and aquifer evaluation, State of Illinois Water Survey Bulletin 49, 81 p.

Wang, H. F., and M. P. Anderson, 1982, Introduction to Groundwater Modeling, Finite Difference and Finite Element Methods, San Francisco, CA, W. H. Freeman and Co., 237 p.

Wermund, E. G., J. C. Cepeda, and P. E. Luttrell, 1978, Regional distribution of fractures in the southern Edwards Plateau and their relationship to tectonics and caves: The University of Texas at Austin, Bureau of Economic Geology Geological Circular 78-2, 15 p.

Wood, W.W., 1981, Guidelines for collection and field analysis of ground-water samples for selected unstable constituents, U.S. Geological Survey Techniques of Water Resources Investigations, Chapter d2, 24 p.

Woodruff, C. M., 1975, Land capability in the Lake Travis vicinity, Texas, a practical guide for the use of geologic and engineering data: The University of Texas at Austin, Bureau of Economic Geology Report of Investigations 84, 37 p.

Woodruff, C. M., and R. M. Slade Jr., 1985, Hydrogeology of the Edwards Aquifer, Barton Springs segment, Travis and Hays Counties, Texas: Austin Geological Society Guidebook 6, 96 p.

Yelderman, J. C. Jr., coordinator, 1987, Hydrogeology of the Edwards Aquifer, northern Balcones and Washita Prarie segments: Austin Geological Society Guidebook 11, 91 p.

The vita has been removed from the digitized version of this document.